ACS OMEGA

Open Access

This article is licensed under CC-BY-NC-ND 4.0

http://pubs.acs.org/journal/acsodf

Review

A Comprehensive Review on the Boosted Effects of Anion Vacancy in the Heterogeneous Photocatalytic Degradation, Part II: Focus on Oxygen Vacancy

Mahdieh Rezaei,* Alireza Nezamzadeh-Ejhieh,* and Ahmad Reza Massah*

Cite This: *ACS Omega* 2024, 9, 6093−6127

Read Online

ACCESS | Metrics & More | Article Recommendations | Supporting Information

ABSTRACT: Environmental problems, including the increasingly polluted water and the energy crisis, have led to a need to propose novel strategies/methodologies to contribute to sustainable progress and enhance human well-being. For these goals, heterogeneous semiconducting-based photocatalysis is introduced as a green, eco-friendly, cost-effective, and effective strategy. The introduction of anion vacancies in semiconductors has been well-known as an effective strategy for considerably enhancing the photocatalytic activity of such photocatalytic systems, giving them the advantages of promoting light harvesting, facilitating photogenerated electron−hole pair separation, optimizing the electronic structure, and enhancing the yield of reactive radicals. This Review will introduce the effects of anion vacancy-dominated photodegradation systems. Then, their mechanism will illustrate how an anion vacancy changes the photodegradation pathway to enhance the degradation efficiency toward pollutants and the overall photocatalytic performance. Specifically, the vacancy defect types and the methods of tailoring vacancies will be briefly illustrated, and this part of the Review will focus on the oxygen vacancy (OV) and its recent advances. The challenges and development issues for engineered vacancy defects in photocatalysts will also be discussed for practical applications and to provide a promising research direction. Finally, some prospects for this emerging field will be proposed and suggested. All permission numbers for adopted figures from the literature are summarized in a separate file for the Editor.

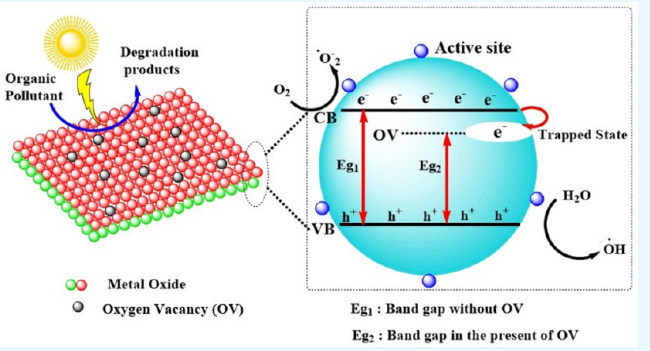

1. INTRODUCTION

The critical global population and environmental pollution have severely affected human health in recent decades. More profound attention has been paid to environmental pollution by several developing industries because of discharging their effluents, especially untreated industrial wastewater, into the environment. Discharging untreated effluents releases numerous organic molecules as pollutants into the river, severely threatening the ecological environment.[1−3]

The remaining excellent challenge for worldwide researchers is the construction, introduction, and development of a novel/appropriate technology, catalyst, or adsorbent to remove these pollutants.[4] Accordingly, semiconducting-based photocatalysis technology has been considered as a green and benign method for eliminating most environmental pollutants due to its environmentally friendly nature, high efficiency for mineralizing organic pollutants to less hazardous materials, and natural ability to utilize sunlight depending on the semiconductor's band gap energy.[5−7] A promising photocatalyst should have other characteristics, such as high stability, low cost, earth abundance, and attractive catalytic activity. Commonly used semiconductors have these advantages.

Unfortunately, some bare photocatalysts suffer from an ineffective absorption of visible light and, thus, low numbers of photoexcited electrons and holes (e/h pairs).[8] This limited photocatalytic activity for these bare systems is due to the rapid recombination of the photoproduced e/h pairs. This recombination process, as a significant drawback of heterogeneous semiconductor photodegradation, drastically reduces the overall efficiency of the photocatalytic process.[9] To improve the overall photocatalytic efficiency, the essential factors are the effective harvesting of solar light and the effective separation of e/h pairs. Thus, a crucial photocatalytic issue is the optimal design of photocatalysts with high photocatalytic activity.[10] A challenge in enhancing photocatalytic activity is regulating the semiconductor's band structure to harvest sunlight photons. To achieve this, different strategies, including doping with metals/

Received: September 29, 2023
Revised: January 10, 2024
Accepted: January 11, 2024
Published: February 5, 2024

ACS Publications

© 2024 The Authors. Published by American Chemical Society

https://doi.org/10.1021/acsomega.3c07560
ACS Omega 2024, 9, 6093−6127

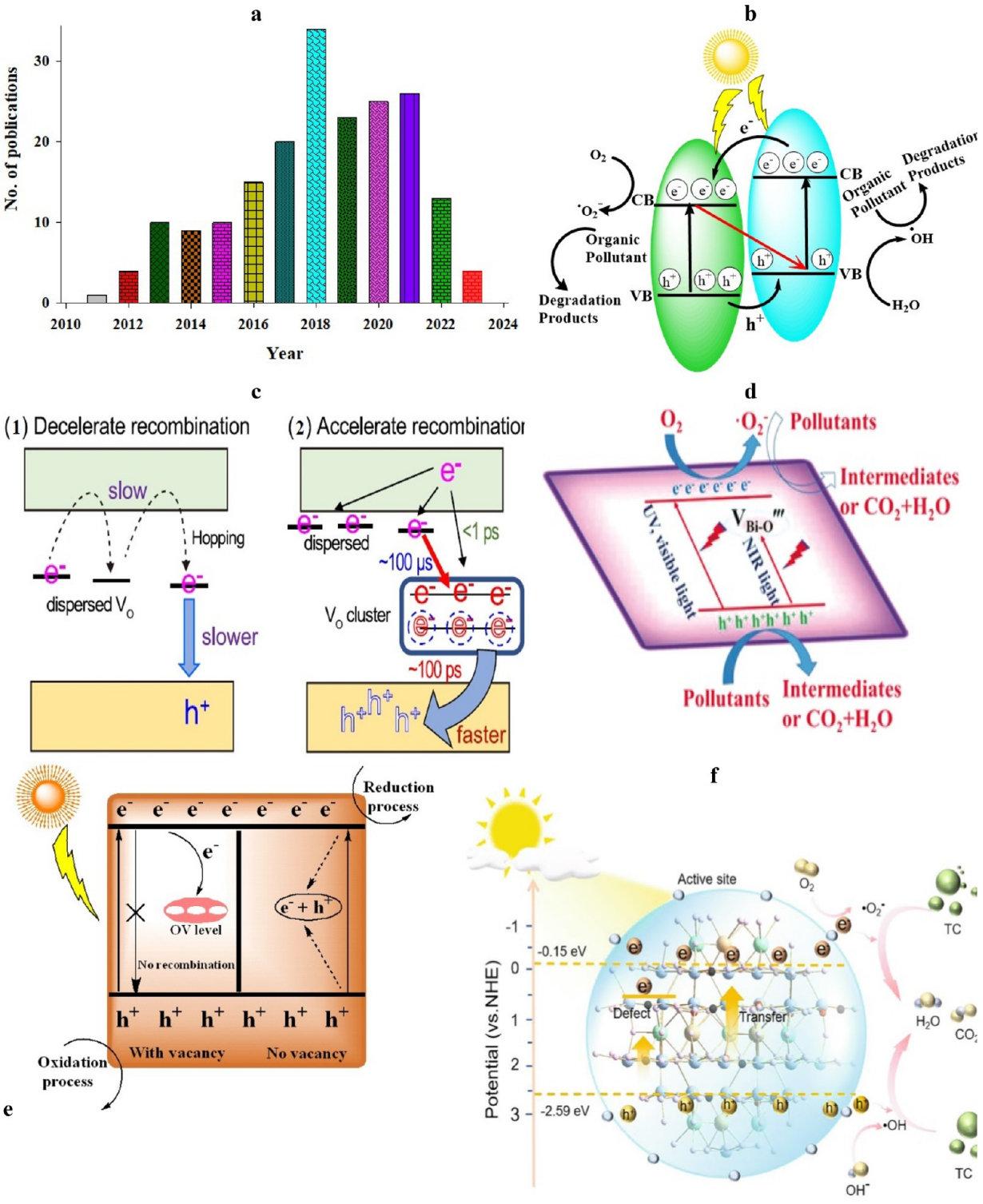

Figure 1. (a) Number of publications per year in vacancy-engineered photocatalysts used in this Review. (b) Schematic representation of the mechanism of photocatalysis by a heterojunction structure. (c) (1) Decelerated recombination by dispersed OVs and (2) accelerated recombination by an aggregated OV.[115] Reprinted with permission from ref 115. Copyright 2022 ACS. (d) The photocatalytic activity of BiO_{2-x} monolayer under UV/vis and NIR illumination.[133] Reprinted with permission from ref 133. Copyright 2018 Wiley. (e) The e/h separation by OVs. (f) TC photocatalytic degradation.[102] Reprinted with permission from ref 102. Copyright 2022 Elsevier.

nonmetals,[11] controlling phase and morphology,[12] engineering crystal facets and defects, modulating the microelectronic structure, constructing homojunctions and heterojunctions, and loading of noble metals, have been applied.[13]

An effective strategy is defect engineering, which regulates the atom coordination number and electronic structure. This improves the carriers' mobility and conductivity and tunes the surface futures, such as the interaction between vacancy sites, reactants, or intermediates. Finally, enhanced photocatalytic

https://doi.org/10.1021/acsomega.3c07560
ACS Omega 2024, 9, 6093−6127

activity would be obtained. Vacancy engineering manipulates the catalyst composition without any introduction of impurities. Its ease of use, precise control capability, and high efficiency are other characteristics of this strategy that have attracted significant attention.[9,14−18] The advantages of vacancy defects in semiconductors can be summarized as light absorption, facile separation of e/h pairs, optimization of the electronic structure, activation of reactant molecules, acceleration of product desorption on the photocatalyst, and promotion of the production of reactive radicals.[19] Recently, the relationship between photocatalytic activity and vacancy defects in various materials has been evaluated.[20,21] The conclusion of such studies proves that tuning a semiconductor's electronic structure using vacancy defects improves visible light harvesting. This strategy broadens the absorbance spectrum of the investigated semiconductor. Vacancy defects prohibit e/h recombination via the semiconductor's newly formed energy level.[22−24]

The performance of photocatalyst nanomaterials depends on light harvesting to produce photogenerated electron−hole pairs (charge carriers), their separation efficiency and transfer to the surface, and interfacial redox reactions on the active site of photocatalysts' surfaces.[25] To boost the activity of semiconductor photocatalysts, these drawbacks should be overcome by applying suitable strategies, like modification of their structure, control of their morphology, the plasmonic effect, engineering of their surface and interface, and engineering of their facets and defects.[26−29]

Due to the critical roles of semiconductors' microstructural properties, including dimensions, morphologies, effective surface area, and pore dispersion, on the overall photocatalytic efficiency, a significant issue is rational semiconductor design and synthesis with well-designed structures.[30] In this regard, dramatically altering of the rate of the surface reactions and electron transport pathways improves the charge transfer kinetics and light harvesting. For example, the close CB bottom of $BiVO_4$ to the H_2 formation potential causes a deficient driving force for H^+ reduction. However, this negative shift of the CB edge can be overcome by the quantum-sized $BiVO_4$ (quantum confinement effect).[31]

Among the various strategies, heterojunction-engineered photocatalysts (including common type II, p-n, surface, direct Z-scheme, and semiconductor-graphene heterojunctions) are some of the most common systems to enhance spatial e/h separation and thus the overall photocatalytic efficiency.[32] The facet, as a typical microstructure aspect of crystal, separates more e/h pairs to different crystal facets because of the subtle distinction of coupled facets,[33] for example, the high activity of the rutile with (111)−(110) facet couples in TiO_2 polymorphs under visible light.[34]

In the doping process, such as the common method of element doping, doped species change the lattice structure of substrates, increase the density of the main carriers, and decrease the semiconductor electrical resistivity, consequently enhancing the overall photocatalytic performance. For example, I^- self-doping in BiOI,[35] and CO_3^{2-} self-doping in $Bi_2O_2CO_3$[36] broadened absorption harvesting to the visible light region.

In general, "defect engineering" is one of the most economically effective E_g-narrowing methods to boost visible light absorption, separate charge separation, and transfer energy.[37] In particular, intrinsic defect engineering regulation is more effective than the extrinsic approach for fine-tuning electronic and structural features. Depending on their atomic structure (size) and location, various defects have been defined as point defects (vacancies and doping), line defects (helical and edge dislocations), planar defects (grain and twinning boundaries), and bulk defects (lattice disorder and voids).[38] A point defect is considered the core of defect photodegradation research; thus, it gets special attention in this Review. In general, missing a cation or anion from a definite location in the perfect crystal lattice forms a vacancy commonly used for structural modulation because of its high feasibility and controllability.[39] The created surface vacancy creates lattice disorder that induces increased surface energy, acting as additional reactive sites for catalyzing surface photoreactions.[40] To date, despite the publication of many reviews to illustrate the role of point defects, especially vacancies, for in-depth understanding of the photocatalytic mechanism, the intrinsic defect's role in photodegradation remains a problem that should be overcome.[41]

Thus, several reviews on oxygen-vacancy-defect photocatalysts have been published, including OV-based metal oxides in photoelectrochemical water splitting;[42] OV-Ce_2O in photocatalytic water oxidation;[43] OV-ZnO;[44] engineered OV photocatalysts for water splitting, CO_2 reduction, nitrogen fixation, and generating reactive oxygen species;[45] engineered OV photocatalysts in hydrogen evolution and N_2 fixation applications;[46] the structure−function relationship of OVs in OV photocatalytic applications in air purification, H_2 production, and CO_2 reduction;[47] OVs systems in the degradation of gaseous pollutants;[48] and OV-BiOCl in water splitting, H_2O_2 dissociation, and solar ammonia synthesis.[49] Based on our studies, no review has been published on the role of oxygen vacancies in the photodegradation of organic pollutants. Figure 1a shows the roles of the defects in the material and their effects on various physicochemical features. The preferential roles of defects in materials chemistry, which give them some exceptional features compared to pristine materials, emphasize the importance of their further investigation.

This Review introduces and summarizes the recent advances in oxygen vacancies. This part is a continuation of the first part that focused on other anion vacancies such as sulfur, nitrogen, and halogen vacancies. It focuses on the formation chemistry of this anion vacancy and its principal benefits in the photocatalytic the degradation process. Understanding these features of the anion vacancy helps researchers advance the main theories of the photocatalytic process and offer novel guidelines for designing advanced and more efficient photocatalysts. The synergistic effect of these anion vacancies in photocatalysis can be confirmed by presenting some multicomponent catalytic platforms. Finally, some engineering defect opportunities will summarize the future directions of this research field. The importance of this revision can be emphasized by considering the high number of published works in defect engineering in recent years, as shown in Figures 1a and S1.

2. PHOTODEGRADATION OF ORGANIC POLLUTANTS

A critical health issue in modern times is the lack of clean drinking water because the final goal of the above-mentioned industrial waste effluent is the aquatic environment. Thus, drinking water resources may be polluted and contained by various hazardous chemicals, including pharmaceuticals,[50−54] organic synthetic dyes,[55−59] insecticides, detergents, herbicides, and pesticides.[55,60−63] For example, introducing antibiotics, as a class of pharmaceutical pollutants, into aquatic resources has some adverse effects on human health and marine life due to their potentially toxic and hazardous products and persistence.[64]

https://doi.org/10.1021/acsomega.3c07560
ACS Omega 2024, 9, 6093−6127

Their long-term presence in the environment can cause the occurrence of resistant genes.[65] Unfortunately, traditional wastewater treatment plants are unable to eliminate antibiotics effectively. Azo dyes, and in general organic synthetic dyes, are other environmental pollutants with carcinogenicity depending on their structural characteristics and degradation mechanism.[64,66,67] For example, common degradation intermediates of azo dyes are aromatic amines with a common carcinogenic future. Further, azo dyes can alter biochemical markers, provoking allergic reactions.[56,66,68−71]

With the increased environmental awareness, some effective methods must be introduced to remove organic pollutants from wastewater before they are discharged into the environment. The most effective methods for this goal are advanced oxidation processes (AOPs) based on the production of hydroxyl radicals ($^{\bullet}OH$) that act as nonselective high-oxidation-potential species toward the degradation of organic pollutants at high reaction rates (between 10^8 -10^{11} M^{-1} s^{-1}).[9,72] For example, peroxydisulfate (PDS) and peroxymonosulfate (PMS) can generate different reactive oxygen species (ROS), including sulfate radicals ($SO_4^{\bullet-}$), hydroxyl radicals ($^{\bullet}OH$), singlet oxygen ($^1O_2$), and superoxide radicals ($^{\bullet}O_2^-$) in the general PMS-based AOPs. These ROSs can critically degrade various organic pollutants.[73,74] Some common AOPs have many drawbacks, as illustrated in the literature.[75] For example, Fenton and photo-Fenton processes are economically dependent on the solution pH and remain secondary sludge. Some AOPS create secondary pollution, and some transfer the pollutant to a secondary phase that needs secondary treatment.[75]

Thus, especial attention has been paid to heterogeneous photocatalysis based on the illumination of a semiconducting compound under UV or visible light irradiation.[76−78] This AOP strategy is an environmentally friendly, low-cost technology with high efficiency for degrading/mineralizing various organic pollutants without secondary pollution. Its overall efficiency (including the adsorption and photodegradation of the pollutant molecules) depends on the operational parameters.[79−81]

The photocatalytic degradation process is the chemical breakdown of organic pollutants induced by light. Under the system's illumination, several reactant species, including singlet oxygen, superoxide, hydroxyl radicals, and hydrogen peroxide, may produce powerful centers toward the degradation of organic pollutants.[82−85] The following steps can be considered to happen in a typical heterogeneous process[86,87] (Figure 1b):

- Under the irradiation of the semiconductor by UV or visible photons with energy $\geq E_g$, VB electrons get excited into the CB of the semiconductor (production of e/h pairs).
- The induced VB holes can oxidize donor molecules directly. Further, the reaction of VB holes with water produces hydroxyl radicals as robust oxidizing species toward the degradation of pollutants.
- The photoexcited electrons in the semiconductor CB reduce the dissolved oxygen species, and the produced superoxide anion radicals act as another center for oxidizing the pollutants. The redox reactions can also be facilitated by the CB electrons.[86,88−93]

As mentioned in section 1, e/h recombination critically decreases the overall efficiency of a typical heterogeneous photocatalysis reaction.[93−96] As also mentioned, one way to reduce this drawback is to blend various semiconductor materials to fabricate heterojunction systems[86,97,98] that involve two stacked semiconductors with different E_g values (with the E_g in the visible region). The heterostructure term is used for the blend of multiple heterojunctions. Moreover, the preferred E_g in heterostructures is the direct band gap compared to the indirect ones. In the direct band gap, the highest VB energy level aligns with the lowest CB energy level concerning momentum.[99] As mentioned in section 1, another effective strategy for reducing e/h recombination is defects, of which anion vacancies will be reviewed below as this Review's goal.

Photocatalyst separation from the reaction solution is also essential, which can be be easily done by an external magnetic field when a magnetic compound is used. In other cases, centrifugation on an experimental scale[100] or special filters on an industrial scale must be used to separate the photocatalyst. In the loaded catalyst on the bed like FTO, removing the bed from the reaction mixture easily separates the photocatalyst.

As a critical practical application issue, the catalyst's stability can be investigated by testing the reusability of recovered catalyst from the reaction mixture and reusing it in the next degradation run with the same conditions as the previous run. An increased cycle test shows the photocatalyst's high stability.[101] The mean contact angles of fresh and reacted Ba^{2+}-doped $SrBi_2B_2O_7$ in three different sites are 11.76° and 40.20°, respectively, proving the sample's tendency to become a hydrophobic powder after the reaction. Moreover, the lack of an apparent change in the XRD of the doped sample after four recycling runs proves the high stability of the sample.[102] Generally, a common way to test the photocatalyst stability is to perform characterization techniques, such as XRD, DRS, FTIR, SEM, TEM, and photoluminescence, on the catalyst before and after use in the photodegradation process. Smaller changes in the results before and after using the catalyst show more stable photocatalysts.[10]

3. VACANCY ENGINEERING

Depending on the defect type, its exerted effects on the photocatalytic activity and their intrinsic relationship can vary.[103−105] Depending on the dimensions and vacancy, material defects can be classified as point, line, planar, volume, and manifold.[106−109] To manage the optical and electronic futures of semiconductors to achieve improved phtocatalytic activity, a common frequently used strategy is point defects, including vacancies and doping. Vacancy defects are commonly used to achieve the desired photocatalytic action and selectivity due to their easier creation and precise semiconductor tuning concentrations.[110]

In general, the transfer and recombination of charge carriers in photocatalysts are closely related to their defects because the induced new defect level (or "trap state") can change the migration pathway for the photoinduced carriers, influencing their dynamics. To date, the various contradictory effects of defects on carrier trapping, separation, transfer remain an open question.[111] Generally, some researchers believe that the roles of defects as both recombination and trapping centers toward charge carriers may decrease the photocatalytic efficiency.[112] In contrast, some believe their positive role in the enhanced catalytic activity is because they can preferentially improve the e/h separation.[113,114] For example, the effects of OVs on WO_3 powder photocarrier dynamics were studied via broadband transient absorption spectroscopy. In contrast to TiO_2 and $SrTiO_3$, where increasing OVs increases the carrier lifetime, here the increase in OVs (as recombination centers) via H_2 reduction in WO_3 accelerated the decay of deeply trapped electrons. This

https://doi.org/10.1021/acsomega.3c07560
ACS Omega 2024, 9, 6093−6127

difference is related to the difference in the distance between OVs. In dispersed defects, trapped electrons should migrate over long distances by sequence hopping and tunneling between defects to combine with holes, decelerating the recombination. In contrast, in the case of connected defects or defects located close together, the ready migration of trapped electrons among defects enhances recombination. Thus, an important factor for enhanced photocatalytic activity is control of the distance between defects (figure. 1c).[115]

Desaturated periodic atomic arrangements widespread through the semiconductor act as deep trapping and e/h recombination centers, impairing the native photocatalytic performance.[116] Nevertheless, it has experimentally and theoretically confirmed that the defect in the engineered materials can maximize photocatalytic activity by breaking the thermodynamic and photogenerated carrier dynamics limitations in the redox process.[117] Despite the increased photocatalytic activity in the presence of an optimal OV dose, reduced activity can be achieved in the presence of excessive OVs that trap electrons and restrain electronic mobility, decrease the photocatalyst crystallinity, and serve to recombine e/h pairs.[118,119] Generally, the type of defect (bulk and surface defects) plays a crucial role in the positive or negative effect in boosting photocatalysis efficiency. The surface defects improve e/h separation and dissociate adsorbed molecules, thus increasing the overall photodegradation activity, while the bulk defects recombine e/h pairs, resulting a negative effect in the overall process efficiency.[120−123] Thus, the absolute role of defects in photocatalytic processes is still unclear, requiring a bridge to be established between the engineering of defects and the controllable features of nanomaterials.

3.1. Cationic Vacancies. Nowadays, various cation vacancies, such as Ti, Zn, Bi, In, etc., have been created in semiconductors to optimize the band gap configurations and surface futures of photocatalysts to achieve improved photocatalytic activity. For example, in the facile one-pot hydrothermal synthesis of SnO_2−Zn_2SnO_4/graphene, as a visible-light-responsive photocatalyst, graphene causes the production of SnO_2 and the formation of Sn vacancies, resulting in a visible-light-responsive system.[124] Some metal vacancies, such as Ti vacancies (VTi), have been readily demonstrated in undoped oxides. The presence of VTi in TiO_2 induced some novel physiochemical properties because it changed the TiO_2 charge density and valence band edge. Compared to common n-type TiO_2 with nonferromagnetic properties, Ti-defected TiO_2 (VTi-TiO_2) is a native p-type system with high charge mobility. Further, it has room-temperature ferromagnetism that is stronger than Co-doped TiO_2 nanocrystalline. Moreover, the photocatalytic performance of VTi-TiO_2 is much better than normal TiO_2 toward degradation of organic pollutants (7.0-fold for phenol). This enhanced activity has been related to the more efficient e/h charge carrier separation via faster transfer in the bulk and reaching the semiconductor−electrolyte interface;[14] compared with anion vacancies, the relatively higher energy required for fabricating cation vacancies resulted in some obstacles in their production and control.[14,125,126]

Cationic vacancies (the controlled removal of metal cations from transition metal compounds) are shallow migration acceptors and usually induce p-type conductivity. As a more attractive method, metal cation vacancies result in multifarious electron configurations and orbits concerning nonmetal cation vacancies with considerable essential achievements. Cationic defects give the catalyst novel properties, like the modulated energy band structure, via upward shifting of the VB maximum and downward shifting of the CB minimum with no new intermediate states. Further, cationic defects easily segregate and quickly migrate the photogenerated carriers, optimizing E_g configurations and surface features.[127] However, the higher fabrication energy of cationic vacancies compared to the anionic ones limited the roles of metal vacancies in photocatalysis.[128] Cation defect engineering alters the semiconductor's electronic structure and boosts photocatalytic features by adjusting surface properties, improving electrical conductivity, and optimizing the adsorption energy of intermediates.[129] For example, inducing Ti vacancies in TiO_2[14] appeared to have some benefits, such as (1) enhancing the electrical conductivity of ionic components; (2) increasing e-mobility and interfacial charge carrier transfer, suppressing their recombination; (3) generating room-temperature ferromagnetism; and (4) enhancing water splitting by providing water adsorption surface active sites and the formation of active complexes.[14,130] VTi in TiO_2 nanosheets shifted the VB maximum slightly downward with a considerable downward shift of the CB minimum, resulting in a net narrowing of E_g.[131]

Figure 1d illustrates the possible photocatalytic mechanism in vanadium vacancy $BiVO_4$, which creates new defect levels in the forbidden band of single-unit-cell layers of $BiVO_4$ to increase the number of holes near the Fermi level.[132] By decreasing the thickness of the BiO_{2-x} nanoplates to monolayer, the induced new VBi-O‴ defect states dominant the transfer of VB electrons to the CB under UV−vis illumination, whereas quick capture of the photoexcited electrons under NIR illumination by VBi-O‴ defect states separates the carriers. The more negative E_{CB} in monolayer BiO_{2-x} compared to the $O_2/{}^{\bullet}O_2^-$ redox potential facilitates this reduction and the production of superoxide radicals.[133]

3.2. Anionic Vacancies. Anionic vacancies (AVs) are commonly limited to oxygen, nitrogen, sulfur, carbon, and halogen atoms. Due to the low formation energy, they have been widely applied in transition metal oxides to enhance their photocatalytic activity.[134,135] Anion vacancies in semiconductors promote light absorption and facile photoinduced e/h carrier separation, optimize the electronic structure, and produce reactive radicals, promoting photocatalytic activity.[49]

The enhanced photocatalytic efficiency of AV-rich catalysts is because of the following features: (i) induced broadened light absorption to the visible−NIR region, (ii) improved adsorption of organics and gas (O_2, CO_2 and N_2) by AV sites, and (iii) enhanced carrier separation by the middle-gap AVs (Figure 1e). The vacancy-induced midgap state and broadening E_g can narrow E_g (bring a new defect level within the E_g), enhancing the light harvesting. The shallow trapping effect of AV sites to facilitate the separation and transfer of carriers improves these processes' kinetics. Moreover, the defect regulation induces both acceptor and donor sites, giving semiconductors unique electron/hole separation pathways.

The mismatched energy levels and incompact interface contact problems in the heterogeneous junction can be overcome by inducing suitable defect levels. The defect sites with plentiful localized carriers and unsaturated coordination sites can appear as cocatalytic features intrinsic to the fast reaction process. These defect sizes tune the reaction path with high selectivity and efficient photocatalytic activity by promoting the adsorption/activation of small molecules (O_2, CO_2, H_2O, and N_2). Here, the surface activation by AVs is a challenge.[111] As shown in Figure 1f, doped Ba^{2+} is conducive to OV production, in which surface OVs act as reacting sites for

https://doi.org/10.1021/acsomega.3c07560
ACS Omega 2024, 9, 6093−6127

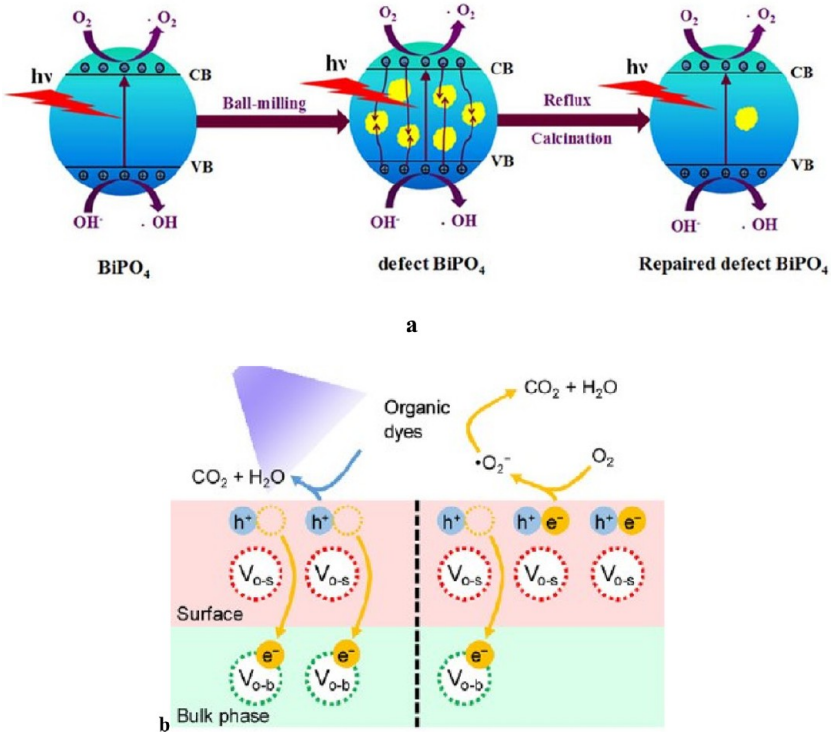

Figure 2. (a) The e/h separation and photocatalytic mechanisms in $BiPO_4$ under UV activation.[146] Reprinted with permission from ref 146. Copyright 2016 Elsevier. (b) The effects of various surface/bulk OV ratios.[154] Reprinted with permission from ref 154. Copyright 2021 Elsevier.

adsorbed molecules, while bulk OVs act as capture centers to separate e/h pairs.[102]

Anion vacancies act as shallow donors, while cation vacancies act as shallow acceptors and commonly induce p-type conductivity.[136] Due to the various electron configurations and orbital distributions, both anion and cation vacancies greatly moderate electronic structure and physicochemical characteristics of metal compounds.[137] Because of the considerable formation energy, engineering and manipulating metal cation vacancies is more complex than engineering and manipulating anion vacancies. Thus, a more significant challenge is determining the function of cation vacancies.[134]

4. INFLUENCE OF SURFACE/BULK DEFECTS ON PHOTOCATALYTIC ACTIVITY

A promising strategy for enhancing light absorption for e/h production and e/h charge carrier separation in photocatalysts is defect engineering, including the surface and bulk defects. Despite the extensive research on these phenomena, their exact roles are still unclear.[110,122,138,139] The synergistic role of these defects in promoting the absorption of light and donor density in photocatalytic processes has been studied in detail.[140] The surface defects affect the physicochemical properties and photocatalytic performance because they can effectively tune the local atomic structure, optical property, electronic structure, or electrical conductivity of materials. Thus, defect engineering can enhance the surface catalytic reactions on photocatalysts. Surface defects are associated with dangling bonds and coordinately unsaturated atoms at terraces, steps, kinks, adatoms, and vacancies. These are thermodynamically unstable and thus favor the adsorption and activation of reactant molecules.[141] Some surface defects may induce positive or negative charges in the surface, which electrostatically promote the adsorption of negatively charged or positively charged reactants.[142,143]

Some point defects (such as vacancies and dopants) may directly participate in the response in surface activation reactions. Further, the activation of the adsorbed molecules may also be facile due to the abundant charge carriers localized at the surface defects.[144] Different surface defects may result in different reaction pathways depending on the further adsorption and dissociation modes. This enhances the selectivity toward specific products.[145]

The bulk defects can trap the photogenerated charge carriers, and the trapped holes may act as new recombination centers, as the latter are no longer available for the photocatalytic reaction. Alternatively, the captured photogenerated holes by the surface defects can favor the electron/hole separation efficiency. Further, due to the ready availability of these captured photogenerated holes for redox reactions, they enhance the photocatalytic activity.[43,122] The trapping role of bulk defects for photogenerated charge carriers causes electronic delocalization, decreased reactivity, and lower photocatalytic efficiency. For example, the VBi and OVs (as the bulk defects) were formed during the ball-milling preparation of $BiPO_4$. These defects can be repaired by reflux and calcination. These induced bulk defects in $BiPO_4$ resulted in a critical decrease in the e/h separation and thus reduced photocatalytic activity. The overall mechanistic pathways for charge separation and the photocatalytic process (under UV light irradiation) in this $BiPO_4$ system are shown in Figure 2a.[146]

One effective strategy for accelerating charge carrier transfer and improving the photoelectrochemical performance in semiconductor photoanodes is the introduction of oxygen vacancies based on the creation of excess surface oxygen vacancies. Here, surface recombination will also be aggravated. It has been reported that ozone treatment of two-dimensional

https://doi.org/10.1021/acsomega.3c07560
ACS Omega 2024, 9, 6093−6127

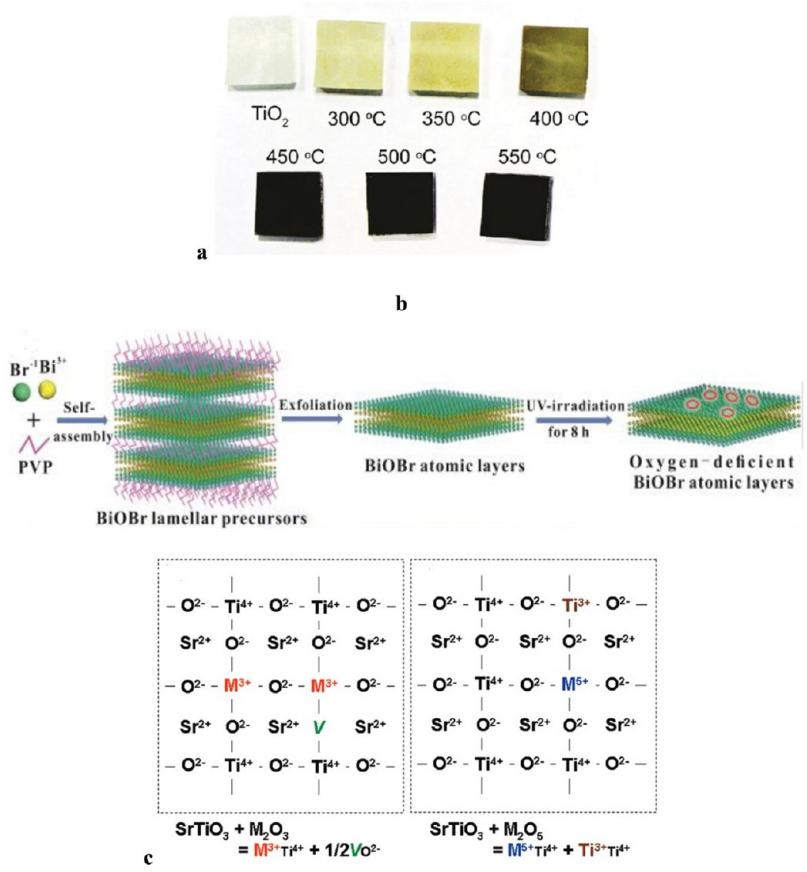

Figure 3. (a) Pictures of H_2-annealed pristine TiO_2 and H:TiO_2 nanowires at various temperatures.[184] Reprinted with permission from ref 184. Copyright 2011 American Chemical Society. (b) Illustration OVs formed in BiOBr atomic layers.[190] Reprinted with permission from ref 190. Copyright 2018 Wiley. (c) Schematic illustration of doping of the trivalent cation and the pentavalent cation in aliovalent-doped $SrTiO_3$.[199] Reprinted with permission from ref 199. Copyright 2009 American Chemical Society.

WO_3 nanoflakes results in the effective formation of surface oxygen vacancies and suppresses the e/h recombination on the surface. Ozone oxidation of the W^{5+} on the photoanode surface decreases the number of surface oxygen vacancies. This critically shifts the cathodic onset potential of about 150 mV relative to the pristine WO_3 photoanode. The hydrogen- and ozone-treated WO_3 sample shows a photocurrent of 2.25 mA cm^{-2} at 1.23 V (vs reversible hydrogen electrode). This treated sample is critically stable over 10 h with an overall water-splitting Faradaic efficiency of about 90%.[147] A new insight into the surface localization of defects and the liquid−solid interface has been presented by Zhang et al. Based on this insight, photocatalytic performance critically depends on controlling the bulk (charge transport) and surface (chemical reaction) recombination processes.[148] In another work, evacuating WO_3 at different temperatures has been used to synthesize WO_{3-x} with varying concentrations of surface oxygen vacancy defects. The sample treated at 150−350 °C showed more surface oxygen vacancies, high photocurrent density, and high photocatalytic activity relative to the pristine WO_3. In contrast, more bulk defects were observed for WO_{3-x} treated at 450 and 550 °C, which may decrease the e/h separation, leading to lower photocurrent density and photocatalytic activity relative to the pristine WO_3.[149]

The effects of defect distribution on TiO_2's energy band structure and photocatalytic activity have been studied by Zhang et al. The surface defects induced a tail of TiO_2's CB above the H^+/H_2 redox potential, resulting in photocatalytic activity. In contrast, a band tail below the H^+/H_2 potential was generated by TiO_2 bulk defects, inhibiting H_2 production. Thus, a major factor determining TiO_2's photocatalytic activity is the change in the band gap structure by defects.[140] In another work, hydrogenation of an anatase TiO_2 nanosheet under an H_2 gas flow in the temperature range of 500−700 °C changed its size, shape, bulk phase, band gap, and concentration and distribution of defects. Among these, a nonuniform distribution of defects between the surface and the bulk played a vital role in controlling the photoactivity. Many Ti^{3+} defects were formed at the beginning of hydrogenation at 600 °C. Eventually, O^- is a significant species on the surface with hydrogenation elongation. This varied distribution of surface/bulk defects produces dramatically enhanced photoactivity.[150] Also, the surface defects of TiO_2 enhanced e/h separation, and the photocatalytic activity of TiO_2 in photocatalytic methanol reforming and the photocatalytic oxidation of α-phenethyl alcohol was the sole effect of surface/bulk defects.[122] In another study, Wu and co-workers investigated the acute effects of bulk and surface defects on the photoactivities of four kinds of uniform TiO_2 NPs. Moreover, the synergistic effect of bulk defects on the photoactivity was observed for particles larger than 10 nm, while the that of surface defects was observed for particles less than 10 nm.[151]

In another research, the solid solution Zn−Cd−S with surface defects was prepared in a hydrazine hydrate with a narrower band gap, more comprehensive light absorption range, and better photocatalytic activity. Based on the theoretical

https://doi.org/10.1021/acsomega.3c07560
ACS Omega 2024, 9, 6093−6127

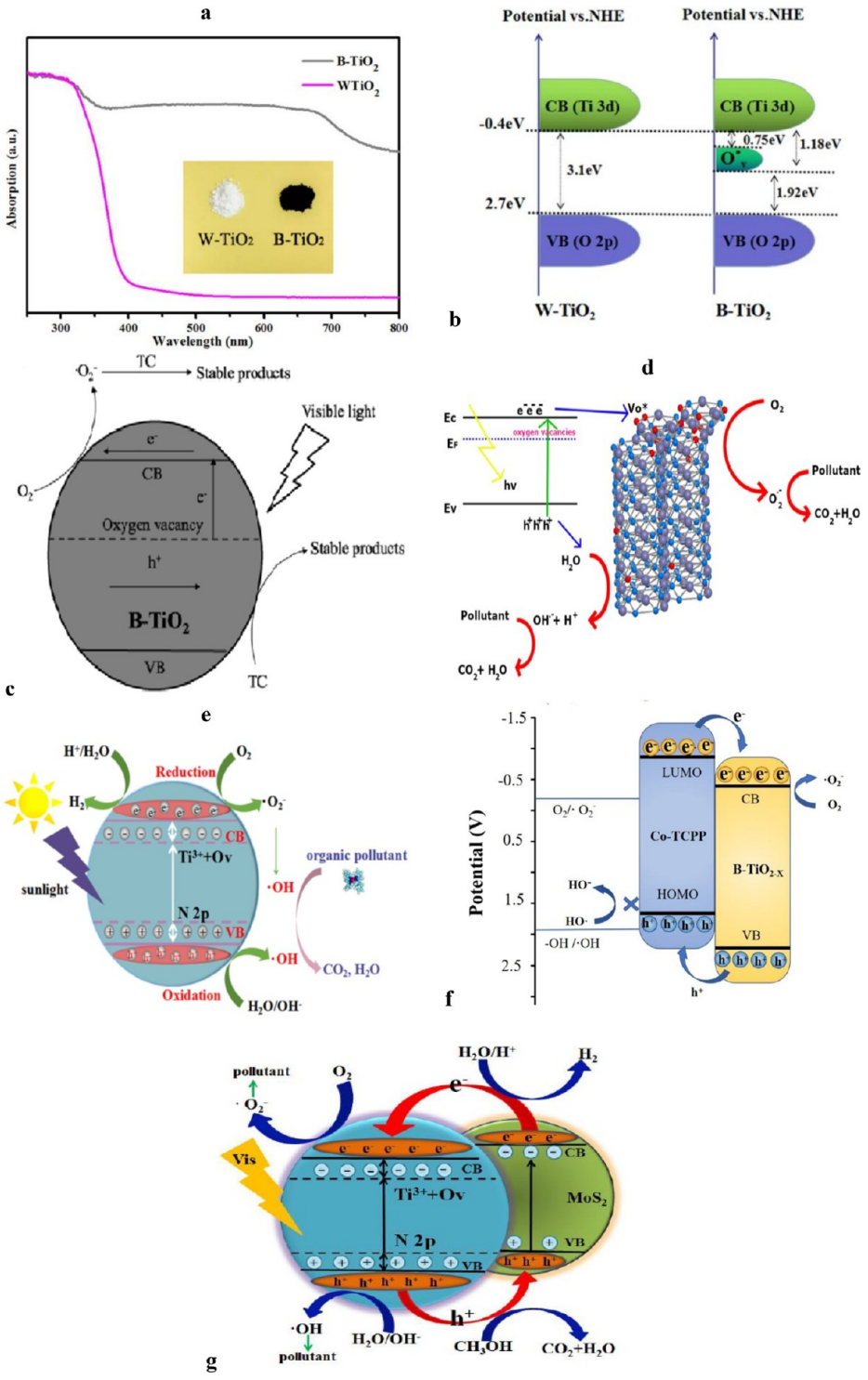

Figure 4. (a) UV−vis absorption spectra of black B-TiO_2 and W-TiO_2 NPs.[211]. (b) Energy band diagram of B-TiO_2 and W-TiO_2 NPs.[211] Reprinted with permission from ref 211. Copyright 2018 The Authors. (c) Visible light TC degradation by black TiO_2.[213] Reprinted with permission from ref 213. Copyright 2021 Elsevier. (d) The e/h formation and transfer mechanism in g-C_3N_4@C-TiO_2.[216] (e) The b-N-TiO_2 solar-driven photocatalytic mechanism.[223] Reprinted from ref 223. Copyright 2017 Elsevier. (f) The visible light photocatalytic activity of BTC-10% toward BPA.[10] Reprinted with permission from ref 10. Copyright 2021 Elsevier. (g) Schematic of the energy band structure for the N-TiO_{2-x}@MoS_2 heterostructure and the e/h transfer mechanism.[229] Reprinted with permission ref 229. Copyright 2017 Elsevier.

calculation, the surface defects cause the CB minimum and VB maximum to shift downward and upward, respectively. Thus, a type I junction was formed between the bulk and surface of the solid solution, promoting the e/h migration toward the nanostructure surface and leading to enhanced photocatalytic activity.[152]

Jiang and co-workers have studied the effects of well-defined crystal facets of CeO_2 nanocrystals (NCs) in the photocatalytic oxidation of volatile organic compounds (VOCs). The surface

https://doi.org/10.1021/acsomega.3c07560
ACS Omega 2024, 9, 6093−6127

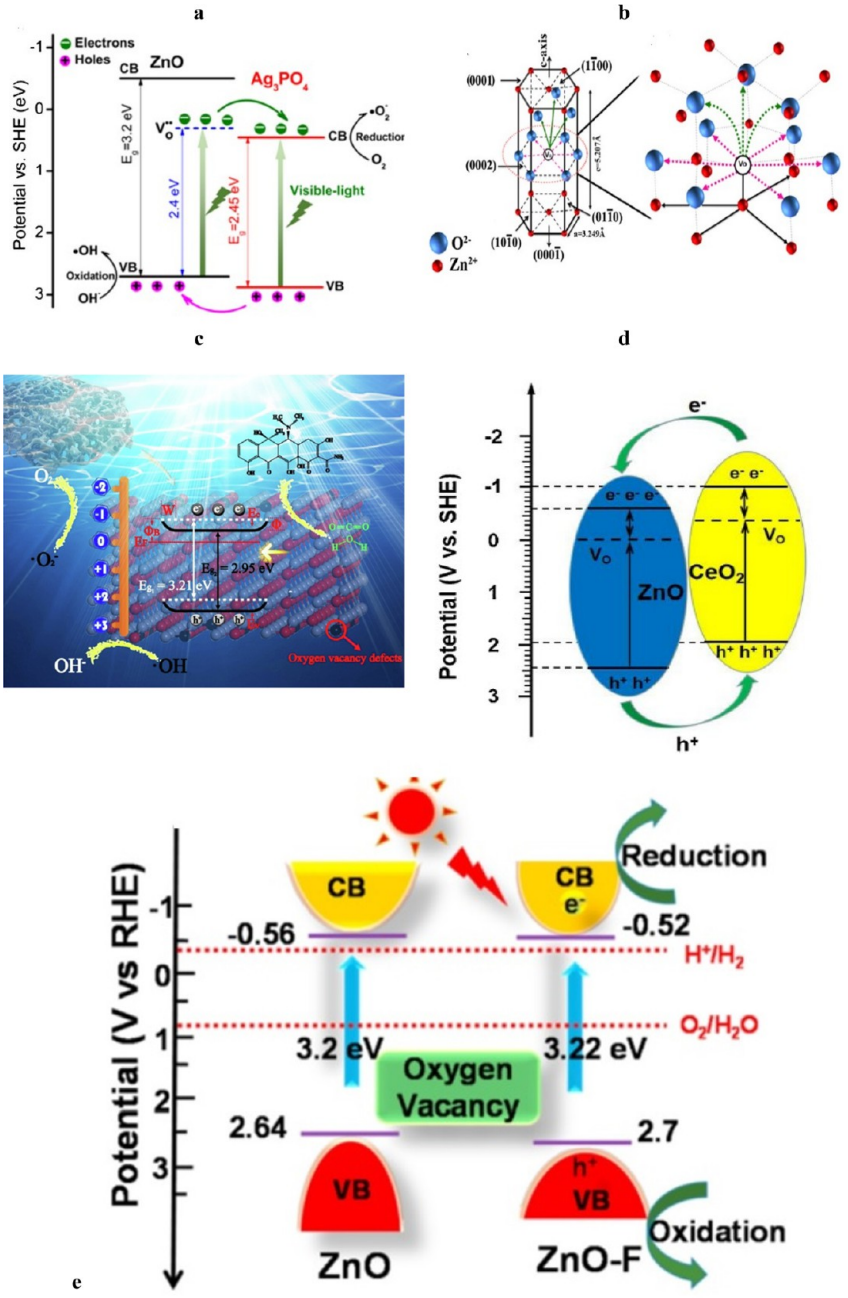

Figure 5. (a) The band structure and e/h transfer of OV-enriched ZnO/Ag_3PO_4 under visible light illumination.[37] Reprinted with permission from ref 37. Copyright 2016 Elsevier. (b) In-plane and out-of-plane diffusions of OVs in the ZnO wurtzite crystal and its unit cell structure expanded view and defect migration (pink arrows, in-plane diffusion; green arrows, out-of-plane diffusio)n.[209] Reprinted with permission from ref 209. Copyright 2017 Elsevier. (c) Proposed defective ZnO photocatalytic mechanism, CB minimum (E_C), VB maximum (E_V), Fermi level energy (E_F), surface band bending (Φ), surface barrier height (Φ_B), and width of the surface band bending region (W).[245] Reprinted with permission from ref 245. Copyright 2020 Elsevier. (d) The e/h separation and production of oxidation groups over a CeO_2/ZnO photocatalyst.[247] Reprinted with permission from ref 247. Copyright 2020 Elsevier. (e) The pristine ZnO and ZnO-F energy band structures.[252] Reprinted with permission from ref 252. Copyright 2021 Elsevier.

defect structure (e.g., Ce^{3+} ions and O vacancies) critically influenced the surface properties, including the activation of reactants and the mobility of surface lattice oxygen.[153] In an easy hydrothermal synthesis of 1D CeO_2 nanorods, the extent of surface oxygen vacancies (OV-s) can be tuned relative to bulk oxygen vacancies (OV-b). The highest OV-s/OV-b ratio led to more efficient utilization of photogenerated electrons in the CeO_2 nanorod due to their faster transfer to the surface for the photodegradation process. This also reduced the probability of photogenerated recombination of electrons and OV-b in the bulk, as shown in Figure 2b.[154]

5. PHOTODEGRADATION ON ANION VACANCIES

Experimental and theoretical calculation results have evidenced the low formation energy of anion vacancies. Thus, it has been widely investigated among photocatalysts, including the O, N, C, S, and halogen vacancies as the most frequent anion vacancies.[43,155] The reduced band gap in metal oxides is formed

https://doi.org/10.1021/acsomega.3c07560
ACS Omega 2024, 9, 6093−6127

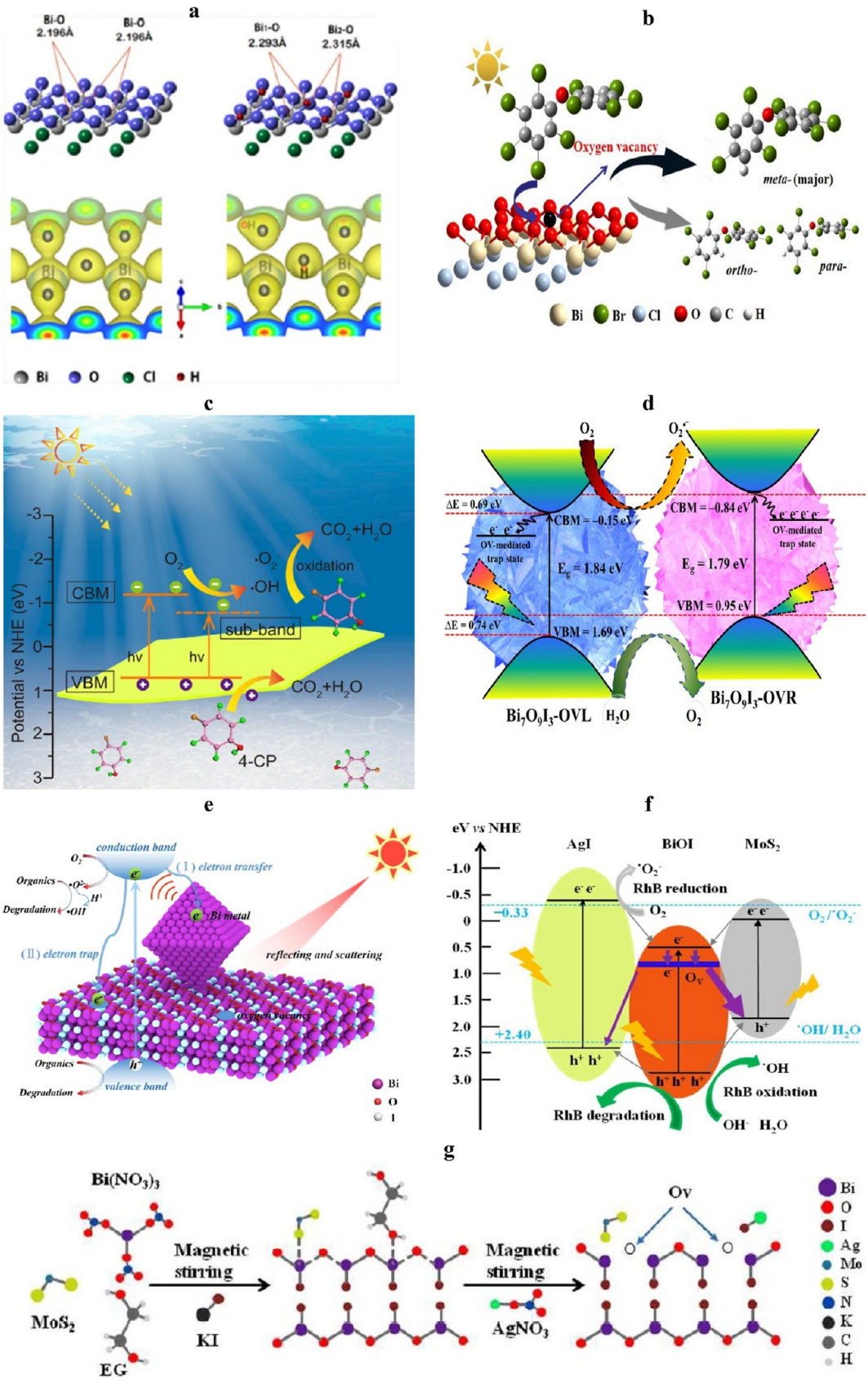

Figure 6. (a) The Bi−O bond length and charge density distribution along the O-terminated (001) surface of BiOCl: clean surface (left) and hydroxyl-rich surface (right).[260] Reprinted with permission from ref 260. Copyright 2017 American Chemical Society. (b) Schematic diagram for a position-selective multielectron reduction of BDE209 over BOC001 with OVs.[262] Reprinted with permission from ref 262. Copyright 2021 Elsevier. (c) Visible light 4-CP photocatalytic degradation by OV-rich ultrathin BB-5S nanosheets.[272] Reprinted with permission from ref 272. Copyright 2019 Elsevier. (d) Schematic illustration of the photocatalytic process of as-prepared $Bi_7O_9I_3$−OVR and $Bi_7O_9I_3$−OVL microspheres.[280] Reprinted with permission

https://doi.org/10.1021/acsomega.3c07560
ACS Omega 2024, 9, 6093−6127

Figure 6. continued

from ref 280. Copyright 2019 Elsevier. (e) The proposed mechanism for the degradation of organics over the Bi/BOI-2 catalyst under visible light irradiation.[281] Reprinted with permission from ref 281. Copyright 2017 Royal Society of Chemistry. (f) Schematic mechanism of a Z-scheme photocatalyst with OV states.[282] (g) Schematic for the proposed OV formation.[282] Reprinted with permission from ref 282. Copyright 2016 RSC.

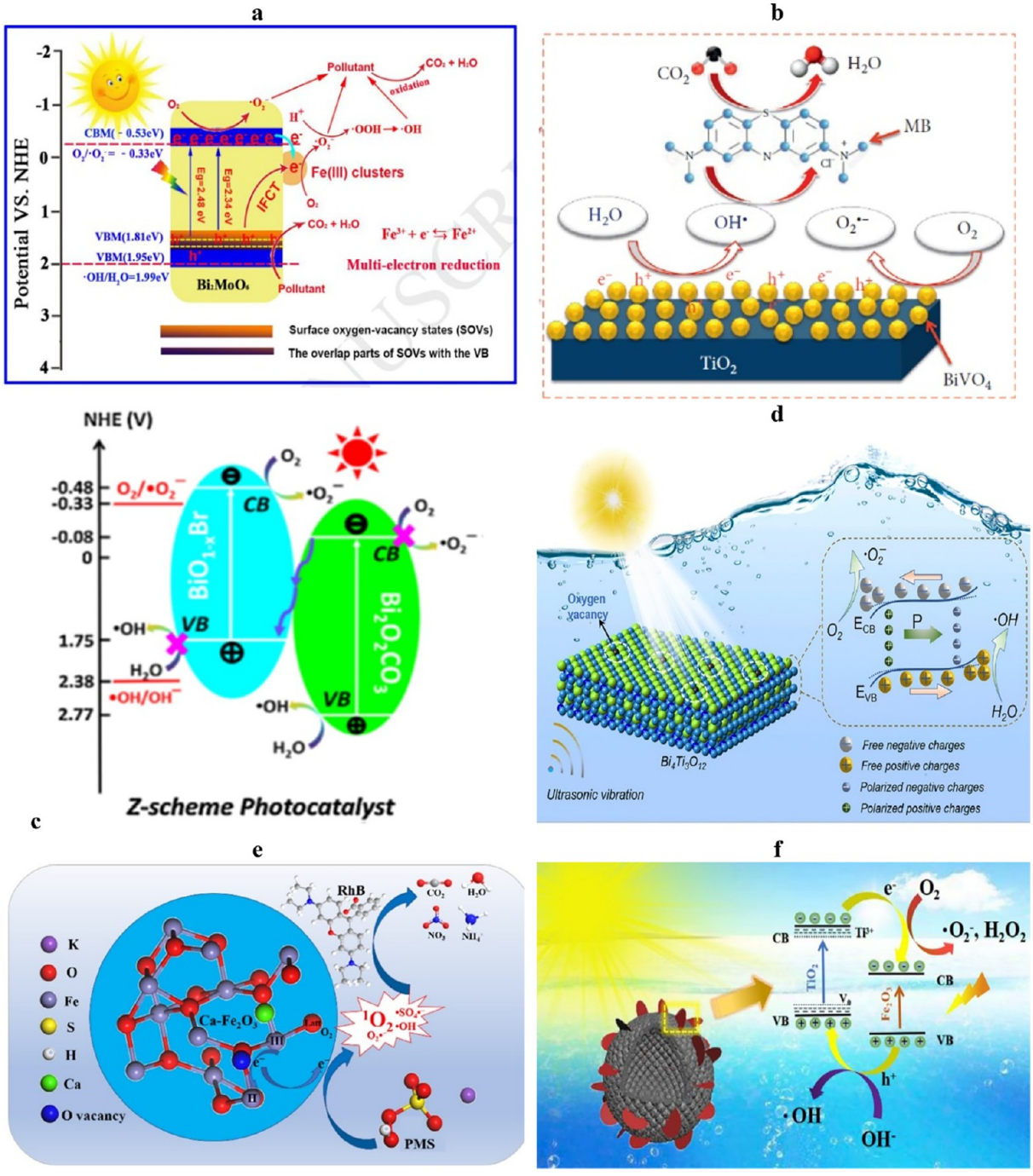

Figure 7. (a) The degradation mechanism of organics over 15% Fe(III) cluster-grafted Bi_2MoO_6 photocatalysts under visible light irradiation.[284] Reprinted with permission from ref 284. Copyright 2019 Elsevier. (b) Schematic for MB degradation.[286] Reprinted with permission from ref 286. Copyright 2020 Sahar Mansour et al. (c) The Z-scheme photocatalytic mechanisms.[290] Reprinted with permission from ref 290. Copyright 2017 Elsevier. (d) Schematic for the piezo-photocatalytic mechanism of $Bi_4Ti_3O_{12}$ OV.[299] Reprinted with permission from ref 299. Copyright 2023 Elsevier. (e) Proposed PMS activation in RhB degradation by 5%Ca−Fe_2O_3.[300] Reprinted with permission from ref 300. Copyright 2020 Elsevier. (f) Illustration of the energy band structure for γ-Fe_2O_3/b-TiO_2 heterojunctions and the proposed e/h transfer mechanism[301] Reprinted with permission from ref 301. Copyright 2019Elsevier.

by vacancy energy states, broadening the light absorption edge. Further, the electron sink effect of anion vacancies prevents the e/h recombination. Both light harvesting and the photoinduced charge carrier separation can be enhanced due to coordinated

https://doi.org/10.1021/acsomega.3c07560
ACS Omega 2024, 9, 6093−6127

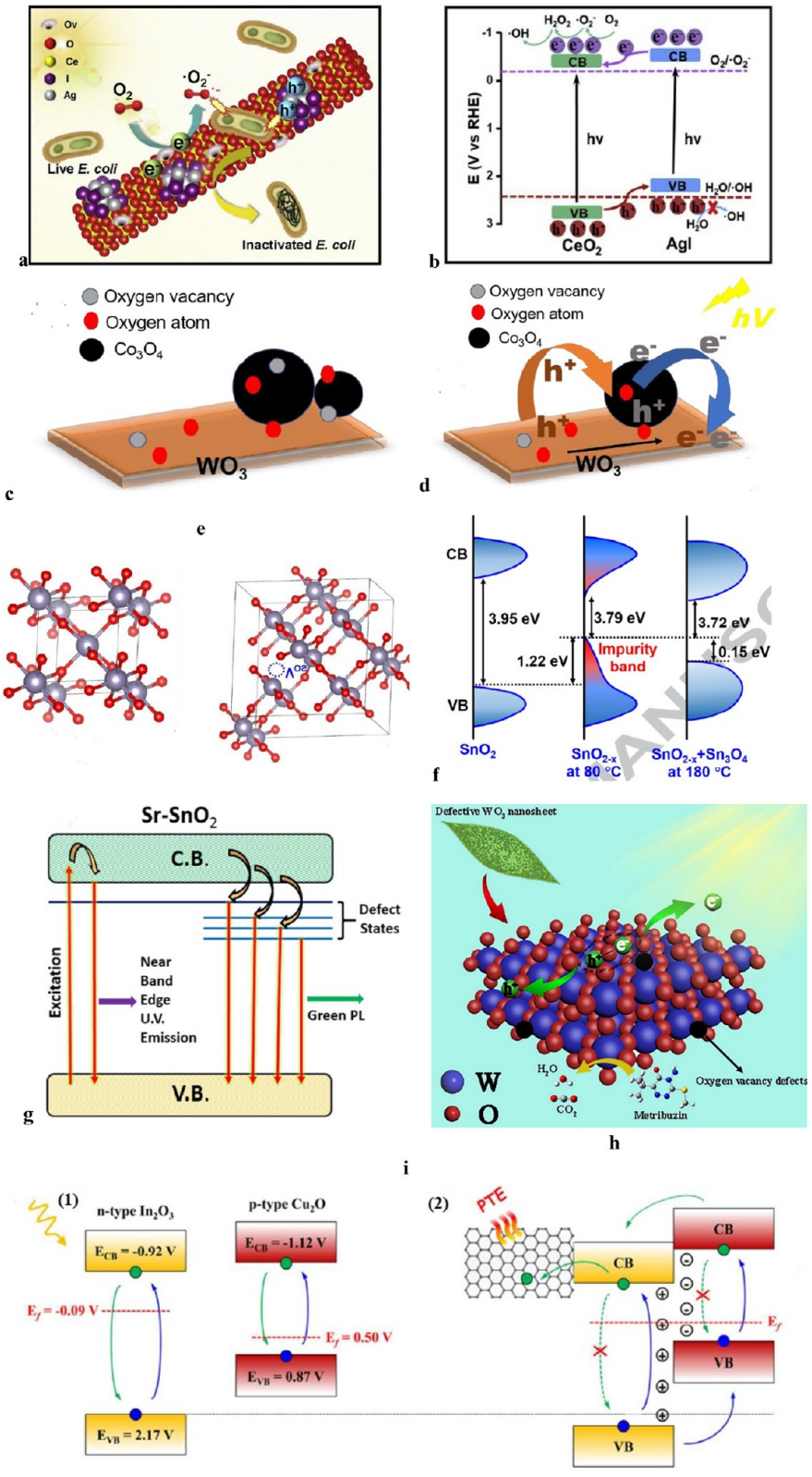

Figure 8. (a and b) The photocatalytic O_2 activation mechanism in a AgI/CeO_2 heterojunction.[308] Reprinted with permission from ref 308. Copyright 2021 Elsevier. (c) Interaction and (d) charge transfer mechanism in a CW_2 composite.[311] Reprinted with permission from ref 311. Copyright 2020 Elsevier. (e) Crystal structures and (f) schematic diagrams for SnO_{2-x} at various reaction temperatures.[313] Reprinted with permission from ref 313. Copyright 2018 Elsevier. (g) The possible transitions in Sr-SnO_2 NPs.[314] Reprinted with permission from ref 314. Copyright 2019 Elsevier. (h) The photocatalytic mechanism of solar-driven defective WO_3 ultrathin nanosheets.[315] Reprinted with permission from ref 315. Copyright 2019 Elsevier. (i) (1) The formation and transfer of e/h pairs over pure In_2O_3 and Cu_2O samples and (2) the proposed enhanced e/h separation mechanism on a Cu_2O/RGO/In_2O_3 hybrid.[318] Reprinted with permission from ref 318. Copyright 2017 American Chemical Society.

https://doi.org/10.1021/acsomega.3c07560
ACS Omega 2024, 9, 6093−6127

Table 1. Summary of the Roles of Defects in Different Photocatalysts

photocatalysts	OV introduction method	role of OV in photodegradation	application	ref
black anatase TiO_2	hydrogen-treated white anatase-TiO_2	OV narrows E_g, enhancing light absorption/active sites	tetracycline photodegradation	213
TiO_2-OV	one-step molten salt method	OV shifts light absorption toward the visible light region	RhB photodegradation	217
black TiO_2	high-temperature surface hydrogenation	OV extended response to the visible light region and solar-driven photocatalytic activity, increasing long-term stability of e/h pairs	RhB, thiobencarb, atrazine, phenol, and hexadecane photodegradation	218
iodine-doped TiO_2-OV	two-step hydrothermal/modified by HIO_3	OV increases the optical response in the visible light region	MB photodegradation	219
black Ti^{3+}/N-TiO_2	in situ hydrogenation	OV improves charge separation, light absorption, and active sites	MO photodegradation	223
TiO_2-OV/graphene	solvothermal/thermal treatment	OV inhibits e/h recombination	photodegradation of MO and RhB	224
N-TiO_{2-x}@MoS_2	hydrothermal/chemical reduction	OV narrows E_g, restraining the e/h recombination	MO photodegradation	229
black TiO_2	hydrogen treatment	OV extends light absorption	Photocatalytic activity	232
ZnO nanorods	high-temperature quenching method	OV suppresses e/h recombination	RhB photodegradation	242
black ZnO	hydrogen treatment	OV enhances visible light absorption	MB photodegradation	243
ZnO hexagonal plates	hydrothermal method/high-temperature $NaBH_4$ reduction	OV improves the e/h separation	TC photodegradation	245
CeO_2/ZnO	thermal method by controlling the air/N_2 ratio	Ssynergistic effect of OVs and CeO_2/ZnO heterojunction, enhanced light absorption	RhB photodegradation	247
CdS QDs/ZnO_{1-x}-TiO_{2-x}	chemical reduction	OV narrowed E_g	bisphenol A photodegradation	248
NiO-ZnO	homogeneous precipitation	OV promotes adsorption and activation of PMS and formation of $SO_4^{\bullet-}$	bisphenol A photodegradation	249
OV-BiOCl	solvothermal method	OV favored the activation of adsorbed O_2 for pollutant oxidation	RhB photodegradation	253
BiOCl	UV light irradiation	OV activates molecular oxygen to produce $^{\bullet}O_2^-$ and $^{\bullet}OH$ radicals under visible light	pentachlorophenol sodium photodegradation	261
BiOCl	sulfuric acid corrosion of Bi_2O_3−B_2O_3−ZnO−SrO−Na_2O (BBZSN) glass containing OVs	OV inhibited the e/h recombination and adjusted the band structure	RhB photodegradation	267
S-doped BiOBr	one-step solvothermal method	OV enhanced the visible light absorption and suppressed the e/h recombination	4-chlorophenol photodegradation	272
Bi/BiOBr	combustion method	OVs and surface plasma resonance, narrowing the E_g and increasing visible light absorption	RhB photodegradation	273
BiOBr/$Bi_4O_5Br_2$	calcination treatment	promoting the photoelectric and ultrahigh photocatalytic activities	tetracycline and ciprofloxacin photodegradation	185
BiOBr	solvothermal method	higher visible light photodegradation, narrowing E_g, excellent chemical stability of BiOBr-OV	real oil field-produced wastewater	277
$Bi_7O_9I_3$	postcalcination treatment	OV boosted the holes mobility and electrons reduction of $Bi_7O_9I_3$, increased charge carrier separation and ROS concentration	photodegradation of phenols	280
Bi_2MoO_6	wet chemical synthesis	OV improves light harvesting and increases the number of reactive sites and e/h separation	phenol, MO, MB, and *p*-nitrophenol photodegradation	191
Ba^{2+} doped $SrBi_2B_2O_7$	high-temperature solid-phase method	OV promotes e/h separation and transport and visible light absorption	tetracycline photodegradation	102
Bi_2WO_{6-x}	controllable hydrogen reduction	OV extends the photoresponse range	photodegradation of phenols	288
Bi/Bi_2WO_{6-x}	one-step hydrothermal	OV improves the ability of Bi/Bi_2WO_{6-x} to generate $^1O_2$	bisphenol A photodegradation	289
BiO_{2-x}	liquid exfoliation	OV decreases the E_g, promoting e/h separation	RhB photodegradation	133
$BiO_{1-x}Br$/$Bi_2O_2CO_3$	solvothermal method	OV electron mediator promoted e/h separation; due to the increase of the redox ability, it produced high amounts of superoxide radical ($^{\bullet}O_2^-$) and hydroxyl radical ($^{\bullet}OH$)	photodegradation of antibiotics (CIP, 4-MAA etc.)	290
$Bi_4Ti_3O_{12}$	modified molten salt method	OV increases the adsorption energy, facilitating the activation of ROS, such as $^{\bullet}O_2^-$, $^{\bullet}OH$, and H_2O_2, and enhances the charge transfer between O_2/H_2O and BIT	RhB photodegradation	299
Ca-doped α-Fe_2O_3	a scalable precipitation-calcination method	OV increases $^1O_2$ and $^{\bullet}O_2^-$ generation, specific surface area, and electrical conductivity.	RhB photodegradation	300
γ-Fe_2O_3	metal ion mediated hydrothermal method/high-temperature hydrogenation	OV favors the e/h diffusion and transportation	retracycline photodegradation	301
$CoFe_2O_4$	a simple thermal aging strategy	OV increases the active sites	bisphenol A photodegradation	302
$CoFe_2O_{4-x}$	hydrogen calcination	promote e-transfer and participate in the redox cycle, along with $^1O_2$ and $^{\bullet}O_2^-$ production$^-$	bisphenol A photodegradation	303

https://doi.org/10.1021/acsomega.3c07560
ACS Omega 2024, 9, 6093−6127

Table 1. continued

photocatalysts	OV introduction method	role of OV in photodegradation	application	ref
α-Fe_2O_3	thermal treatment	OV on the α-Fe_2O_3 surface active site responsible for $^1O_2$ generation	sulfamethoxazole photodegradation	306
CeO_2	one-step hydrothermal method	OV dominates O_2 adsorption sites to accelerate its chemisorption, inhibiting the e/h recombination	practical wastewater photocatalysis	308
Co_2O_3/WO_3 p-n	coprecipitation method	high e/h separation, strong visible light absorption	diclofenac sodium degradation	311
$Cu_2O/RGO/In_2O_3$	surfactant-free hydrothermal method	OV reduces E_g by forming new energy levels and serves as an e/h trapper to inhibit their recombination	photodegradation of methylene blue and Cr^{6+} solutions	318

unsaturated metal centers and excess electrons in these anion vacancies.[135] In the following sections, we will focus on oxygen vacancies among the above-mentioned anion vacancies.

5.1. Oxygen Vacancy (OV). OVs, the most frequent anion vacancy approach in photocatalytic applications, were first proposed in the 1960s by Tompkins,[156] in which OVs were supposed to be a species in solid superficial chemistry. Researchers found that OVs act as active sites in catalytic reactions to adsorb substrates; thus, extensive studies on them started in 2000.[157,158] OVs in metal oxides can change their local atomic and electronic structures and native chemical/physical properties.[45] Accordingly, the change in the location and concentration of OVs can modulate the electronic structure, charge generation, and surface sorption of photocatalysts.[49,159]

Based on the experimental and theoretical reports, OVs will form abundant localized electrons and affect the physicochemical futures of metal oxides (e.g., optical characteristics, electron transport, surface structure, etc.), providing active centers for catalysis. In addition, the surface OVs critically attract reactive molecules, changing their state. All improve the catalytic performance of metal oxides containing OVs.[38]

Modulating the composition and stoichiometry of classic wide-bandgap photocatalysts like TiO_2 is essential for narrowing their bandgap for a strong visible light absorption band. So far, the bands obtained commonly suffer from low absorbance and a narrow range.[48] For example, an influential absorption band, unlike the ordinary tail-like absorption band, has been observed in hydrogen-free oxygen-deficient TiO_2. This impressive band spans the visible light spectrum achieved in anatase TiO_2 by intentionally introducing atomic hydrogen-occupied OVs. The atomic hydrogen-occupied OVs form a new subvalence band in the original band gap, acting as vital absorption sites. Combined experimental data and theoretical calculations confirmed the excitation of a new subvalence band associated with atomic hydrogen-filled OVs as the origin of such a band. Subsequently, this leads to visible light photoelectrochemical activity.[160] An OV may act as a shallow donor for inducing defect states in the forbidden band of photocatalysts that enhance the conductivity and potentially create active centers.[118161−] Both bulk (e.g., conductivity and energy level) and surface (e.g., molecular absorption and surface component) properties can be significantly changed by OVs. Thus, the engineering of OVs plays critical roles in various fields such as supercapacitors,[163] electrocatalysis,[164] and photo(electro)catalysis,[165] including photoelectrochemical (PEC) water splitting[166] and photodegradation.[167]

5.1.1. Strategies for Creating Vacancies. Among the various ways to create vacancies, vacancies may built-in during the crystal growth or activated via post-treatment processes such as annealing and redox reaction reactions. The most straightforward vacancy creation method is controlling the ratio of starting materials. The formation of cationic defects is more challenging because of the higher energy requirements,[168] and thus does not have the same level of importance as the formation of anionic defect in photocatalysts. In the deposition process of oxide thin films, oxygen pressure can tailor the cationic vacancies, which is an obvious drawback because of the difficulty in predicting/controlling the precise vacancy distribution.

Another cationic vacancy generation method is elemental doping by elements like Al, Bi, Cd, Co, Cu, Fe, In, Li, Mn, Mo, Nb, Ni, Sb, Sn, Ti, W, V, and Zn. An effective method of inducing cationic defects at the atomic scale in metals is acid or alkali etching, which selectively removes acid-soluble or alkali-

https://doi.org/10.1021/acsomega.3c07560
ACS Omega 2024, 9, 6093−6127

soluble metal atoms from definite sites, respectively. An effective way to induce metal cation defects in some layered materials is to tempt small organic molecules following thermal calcination or sonication. The plasma technology for constructing defect-rich catalysts can be well controlled by manipulating the discharge medium, power intensity, and etching time;[169] this method has advantages including rapidity, nondestructive processing, time-saving operation (compared to chemical or high-temperature heat treatments), flexibility, cleanliness (eco-friendly), and scalability, with various applications in areas such as environmental science.[170] In the plasma etching strategy, etching of the material's surface produces a high number of surface defects. Hydrothermal methods, electrochemical exfoliation, chemical reduction, and heat treatment are other strategies for inducing cationic vacancies.

In general, the most popular strategies can be classified as low-frequency ultrasound,[171] ion doping (e.g., N-doping),[172] construction of two-dimensional ultrathin materials,[173] reduction of the solid-state chemical by $NaBH_4$,[174−176] plasma treatment,[177] the addition of chelation precursors with carboxylic acids,[178] hydrothermal reduction with graphene oxide,[179] and annealing in inert[180] or vacuum conditions,[149] all of which facilitate the escape of O atoms. Here, some of these strategies will be briefly discussed.

5.1.1.1. Thermal Treatment in the Gas Phase. Annealing a pure metal oxide in an oxygen-free environment enriched by pure N_2, Ar, and He in a vacuum condition[149] can create OVs in it at high temperatures (>400 °C).[181−183] For example, black TiO_2 NPs consisting of OVs have been synthesized by Chen et al. through TiO_2 thermal treatment in a H_2 atmosphere.[17] The thermal treatment of some metal oxides in the H_2 atmosphere has been suggested by Wang et al. as a general way to control the formation of OVs in their nanomaterials. Air-annealing titanium dioxide at 550 °C for 3 h, followed by additional H_2 annealing, resulted in the construction of oxygen-deficient TiO_{2-x} nanowires. This process has studied the effects of various temperatures of 300, 350, 400, 450, 500, and 550 °C. For example, the sample's morphology change as a function of the annealing temperature (SEM pictures) is depicted in Figure 3a.[184]

The vacancy can also be induced under an inert atmosphere or vacuum during annealing. Generally, a widely used OV-creating approach uses an oxygen-free environment during photocatalyst synthesis, in which control of the annealing temperature tunes the vacancy concentration.[149] For example, heat treatment cracks a fraction of W−O bonds in the fabrication of oxygen-defected WO_{3-x} samples under vacuum deoxidation at various temperatures.[164] Thus, OVs from at the surface the escape of surface lattice oxygen atoms, while W^{6+} reduces to W^{5+} via the following reactions (the Kroger−Vink notation). Accordingly, each induced OV reduced two W^{6+} ions.

$$O_O^{\times}(\text{lattice O}) \rightarrow OV + \frac{1}{2}O_2(g) + 2e^- \quad (1)$$

$$2W^{6+} + 2e \rightarrow 2W^{5+} \quad (2)$$

Furthermore, an unstable Bi−O bond with low bond energy is a notable case for creating OV for Bi-based compounds.[49] In synthesizing the OV-induced 3D flower-sphere BiOBr/$Bi_4O_5Br_2$ heterojunction in the presence of CTAB as a Br source, the effects of calcination temperature, stirring time, and −OH concentration were studied in the synthesis mechanism. Based on the results, temperature and stirring time optimized the sample's composition and structure. NaOH, as a structure-driving agent, also acted as an OV midwifery agent.[185]

5.1.1.2. OVs Induced by $NaBH_4$ Reduction. A common and robust reducing reagent for creating OVs in metal oxides is $NaBH_4$. A mass of OVs has been induced in TiO_2 nanotube arrays by low-cost $NaBH_4$ reductant in a liquid phase by Zhang et al. Adjusting the reduction time (0−24 h, can control the saturation of the doping concentration of the oxygen vacancy.[186,187] Xing et al. fabricated reduced TiO_2 NPs using $NaBH_4$ at a lower temperature in a liquid phase. The following reaction shows the quick hydrolysis of $NaBH_4$ to release the reductive H_2 and atomic hydrogen under hydrothermal conditions:

$$8Ti^{4+} + NaBH_4 + 2H_2O \rightarrow 8Ti^{3+} + NaBO_2 + 8H^+ \quad (3)$$

Under the applied conditions, atomic hydrogen favors the reduction of Ti^{4+} to Ti^{3+}, which can improve the conductivity. Consequently, the $NaBH_4$ liquid-phase treatment may reduce the preparation cost and enhance photocatalytic performances.[188]

The $NaBH_4$, CaH_2, and N_2H_4 reducing agents help reduce material via active hydrogen production during the reaction. In this method, annealing of the semiconductor and a particular reducing agent mixture at various temperatures engineers the induced vacancies. In general, this low-cost and straightforward method needs no equipment, critical thermal annealing treatment, or environment (occurs at room temperature or moderate heating conditions), making it a cheaper and easier mass production method for vacancy defects compared thermal reduction. Unfortunately, the requirement of a hazardous (carcinogenic) reducing agent (like hydrazine, $NaBH_4$) is the main drawback of the reduction reaction.[189]

5.1.1.3. Construction of Ultrathin Metal Oxides. A well-known strategy for forming defects is the fast escape of atoms from the interior atoms exposed in ultrathin materials. Construction of OVs in ultrathin structures needs many surfactants in the synthesis procedure and relatively challenging conditions.[42] As revealed in Figure 3b, a high number of OVs have been induced on the surface of BiOBr via the construction of an atomic layer. This has been confirmed by TEM and AFM results.[190] Atomically thin Bi_2MoO_6 nanosheets have been constructed by Wang et al. using a facile and scalable synthesis procedure. These atomically thin Bi_2MoO_6 nanosheets exhibited critical photocatalytic activity toward phenol degradation, with excellent cycling stability.[191]

A critical shortened charge diffusion path from the bulk to the surface can result from the intrinsic ultrathin architecture, which can critically reduce the recombination of e/h pairs. Moreover, interfacial redox reactions could be facilitated by the exposed plentiful coordination-unsaturated surface atoms as the surface active sites.[192]

5.1.1.4. Doping. Another efficient strategy for inducing OVs is metal or nonmetal doping. For example, codoping of F^- and Ag^+ ions into a Bi_2MoO_6/rGO nanocomposite caused OVs in its structure to be created due to the substitution of F^- with surface oxygen atoms. The OVs trapped the photogenerated electrons, resulting in a decreased e/h recombination rate and a synergistic effect of the photocatalyst toward rhodamine B (RhB). The insertion of Ag^+ and F^- into Bi_2MoO_6 led to surface plasmon resonance and surface OVs, respectively, and finally a red-shift in the absorption edge of nanocomposite was observed.[193] The effect of Ba^{2+} doping on $Sr_{1-x}Ba_xBi_2B_2O_7$ ($0 \le x \le 0.6$) in the

https://doi.org/10.1021/acsomega.3c07560
ACS Omega 2024, 9, 6093−6127

enhanced photocatalytic degradation of tetracycline (TC) induced OVs that caused enhanced ferroelectricity. The boosted activity of the doped catalyst was about 6.8× and 2.6× greater than those of the undoped one and $BaTiO_3$, respectively, due to the formation of a strong built-in electric field and OVs.[102] It further introduced foreign atoms into the lattice of samples with induced OVs via the substitution of larger atoms, causing lattice expansion. Also, the defect level reduces E_g, a practical reason for enhanced light absorption with a broader wavelength.[194]

The oxygen vacancies and IO_3^- doping have been induced in BiOI nanosheets by adding NaH_2PO_2. This improved the BiOI charge carrier dynamics, such as excitation, e/h separation, trapping, and transfer, resulting in an improved activity toward methyl orange degradation under visible light irradiation.[195] Additionally, incorporating Mg into magnesium-doped hematite (Mg/Fe_2O_3) as a cost-effective and environmentally friendly catalyst via a facile precipitation method followed by calcination induced OVs in its structure. Maximum OVs and specific surface area were achieved for $5\%Mg/Fe_2O_3$, leading to higher RhB degradation through peroxymonosulfate (PMS) activation.[196]

Bulk iodine doping in BiOCl has been reported through a convenient molten salt method that introduced iodine atoms and induced rich OVs in the system. The doped BiOCl catalyst showed a higher visible light harvesting range and photocatalytic activity than the pure BiOCl.[197] Crystal facet engineering and nonmetal doping strategies have effectively improved semiconductors' e/h separation and photocatalytic activity. Thus, the oxygen-deficient Br-doped BiOCl nanosheets have been hydrothermally manufactured with dominating (001) facets to explore the impact of the Br doping and specific facets on carrier separation and photocatalytic activity. Br doping induced a large number of OVs, as well as the formation of impurity energy levels. These energy levels enhance light absorption. Both effects are beneficial for enhancing photocatalytic activity.[198]

In an N-doped TiO_2 anatase matrix, the formation of localized states in the band gap has been confirmed by DFT calculations. Substitutional N states lie just above the VB, while interstitial N states lie higher in the gap. Excitations from these localized states to the CB in N-doped TiO_2 are a probable reason for the shift of the absorption edge wavelength toward the visible region compared to pure TiO_2 (UV region). This N-doping leads to the formation of OVs in bulk TiO_2, a reduced-cost energy procedure. This proves that N-doping probably assists OV formation.[172]

Based on the works of Takata et al., the low valence cation dopant will occupy the Ti^{4+} sites and form OVs, as displayed in Figure 3c.[199] This cation doping process introduces OVs and decreases Ti^{3+}, effectively enhancing photocatalytic activity.[199] However, it is worth mentioning that not all dopants can form OVs; for creating OVs, the doped ions should be matched with the metal oxides' ions.[42]

Cl-doped $Bi_2O_2CO_3$ was fabricated via a new ionic-liquid-assisted solvothermal method and used in RhB degradation because the ionic liquid can do no Cl doping. The induced OVs, via Cl-doping, can result in a narrower band gap and improve the e/h separation.[200]

In the doped semiconductors, replacing the existing lattice ions/atoms or occupying the interstitial positions of the lattice with foreign elements creates point defects. To prevent any structural alteration and secondary phase formation, the ionic radius of substitutional dopants must be comparable to that replacing atoms/ions.[201] In some cases, such as doping Eu,[202] Bi,[203] and Mn[204] into Cu_2O, the larger ionic radii of the incorporating ions compared the host Cu^+ ions led to the formation of secondary phases and noticeable structural changes. For example, the critically larger radius of Eu^{3+} (0.109 nm, as the largest ionic radius among all the lanthanides) compared to that of Cu^+ (0.077 nm) relatively increased the crystallites size, which exposed more photoelectrode surface area and decreased the grain-boundary recombination degree.

In general, doping can negatively and positively affect the e/h transfer and separation. The temporary trapping of photogenerated e/h by doped species is conducive to effective e/h separation.[205] In contrast, the dopant has an e/h recombination role this is detrimental to the e/h transfer and separation if the impurities are located at a deep level near the E_g center or acts as an electron trap center if it located near the Fermi level based on the classical theory of semiconductor physics.[206] Thus, a substantial electron trap effect can only be expected if the impurity level is relatively higher than or equal to the Fermi level.

5.1.1.5. Comparison among Methods. Due to the advantages and disadvantages of each OV creation strategy in semiconductors, it is very difficult to conclude which is better. For example, the most common thermal treatment usually has long processing times, high energy consumption, and complicated processes. In some cases, chemical reduction is another common strategy that needs some toxic reducing reagents. The new and clean plasma defect-inducing method needs expensive equipment, and it is not as readily available.

Some approaches, including post-treatment methods, only facilitate the removal of surface atoms from photocatalysts. However, simultaneous induction of bulk and surface vacancies can be done via in situ reduction methods.[43] Nevertheless, the facile repair of surface OVs can be related to their poor stability, requiring them to increase their stability and prevent self-repairing.[41] For example, different strains have been achieved under external heat and light energy actions between strong in-plane bonding and weak out-of-plane interactions, resulting in easier removal of the lattice outer atoms than the inner atoms.[207,208] Due to the limited penetration depth of reductants in the subjected materials, chemical reduction prefers to induce surface vacancies.[38] In general, the stability of the substance is a critical key to choosing the methods used to generate defects. For example, for a substance unstable at high temperatures, hydrothermal reduction is a preferential approach for defect creation over heating at a reducing gas atmosphere. Different ways to induce the generation of simultaneous defects cannot precisely control the defect type yet.[111]

5.1.2. Oxygen Vacancy-Mediated Photocatalysis of TiO_2. Despite the urgent need for novel visible-light-active photocatalysts,[209] the application of titanium dioxide (TiO_2) as the most popular, abundant, and highly chemically stable photocatalyst under visible light illumination has been limited mainly due to its absorption edge wavelength in the UV spectrum, which accounts for only 5% of solar radiation. Further, its high electronic energy band gap and e/h recombination are other limitations of it as a photocatalyst. One strategy to overcome these problems is producing an oxygen-deficient surface,[167] which critically changes the band gap position and the color of catalysts, resulting in an extended absorption wavelength range.[160,210] For example, inducing OVs in black TiO_2 (B-TiO_2) via a facile approach introduced by Chen and co-workers significantly improved its visible−IR light absorption efficiency. The decrease in e/h recombination is due to the localized states in the bandgap induced by OVs, which act as trap centers (Figure 4a). The valence band maximum (VBM) and CB

https://doi.org/10.1021/acsomega.3c07560
ACS Omega 2024, 9, 6093−6127

minimum (CBM) of TiO_2 are the O 2p and the Ti 3d orbitals, respectively. Based on Figure 4b, better photocatalytic activity can be observed for B-TiO_2 NPs compared to the white TiO_2 (W-TiO_2) NPs.[211] Oxygen-deficient brookite TiO_2 (BT) nanorods exhibit better photocatalytic activity than the anatase TiO_2 NPs or other visible light-active metal oxides.[212] This synergistic photocatalytic activity of BT is related to the OV concentration.[212] In a similar work, Wu and co-workers treated white anatase TiO_2 (W-TiO_2) with hydrogen to synthesize OV-induced anatase-TiO_2 (B-TiO_2) with a boosted TC photodegradation activity against visible light. As shown in Figure 4c, this boosted effect is related to the unique narrow energy gap between the OV state and the CB, resulting in excellent visible light harvesting to produce e/h pairs in TiO_2. Both h^+ and $^{\bullet}O_2^-$ played critical relative roles in TC photodegradation.[213] Hydrothermally synthesized TiO_2 NPs[214] were further sintered at 200, 300, 500, and 800 °C, and the catalyst sintered at 300 °C showed higher photocatalytic activity toward rhodamine-B under UV illumination. The quenched photoluminescence intensity of this sample at a wavelength of 475 nm confirms the induced OVs result in a higher charge separation rate. Thus, the trapped e/h pairs in the vacancy sites form various oxidizing agents for decomposing RhB molecules. Both OVs and generated Ti^{3+} ions are responsible for producing these oxidizing agents mentioned above, like hydroxyl ions, oxygen species, hydrogen peroxides, etc.[214] Similarly, improvements in the nanostructures, OVs, and photocatalytic activity of electrospun TiO_2 fibers have been reported by Li et al. via a combined heat treatment (500 to 800 °C) and plasma surface modification methods. A boosted degradation rate was observed at higher calcination temperatures up to 700 °C (about 2.5−4.5× that of the other heat-treated fibers).[215]

A two-step anodization process has been used by Hernandez et al., to synthesize TiO_2 nanosheets on TiO_2 nanocavities, TiO_2 nanobowls on TiO_2 nanocavities, and TiO_2 nanocavities containing single-ionized OVs, while a three-step process was used in the synthesis of TiO_2 nanotubes. The single-ionized OVs are the main source of defect states of these TiO_2 films. The number of singly ionized OVs was increased by the decrease in the length of the tubular nanostructure and the thickness of the self-assembled nanostructures. With the increased number of OVs, a narrower band gap was obtained for self-assembled nanostructures and nanocavities due to overlapped localized states at the CB level. The highest number of single-ionized OVs in the TiO_2-ns/TiO_2-nc hybrid structures increased the chemisorption of the molecular oxygen and photoinduced charge carriers. Thus, increased superoxide radical anion production increased methylene blue photodegradation (Figure 4d).[216]

In an induced stable OV-TiO_2 (P25) sample produced via a one-step molten salt procedure (by Zou et al.), a red shift in optical adsorption edge toward the visible light region has been observed, accompanied by a color change from white to dark blue. Accordingly, the highest photocatalytic activity toward RhB and the highest selectivity toward the benzyl alcohol oxidation under visible light irradiation were obtained by the blue TiO_2 with rich OVs.[217]

Self-floating amphiphilic black TiO_2 foams with 3D macro-mesoporous architectures have been prepared by Zhang et al. via a freeze-drying method followed by cast molding technology and subsequent high-temperature surface hydrogenation. These black TiO_2 foams with a water-floating capability, an excellent solar-driven photocatalytic response, and long-term stability have been used to completely mineralize floating insoluble hexadecane and many pesticides.[218]

Another strategy for creating OVs on TiO_2 is doping. Accordingly, Li et al. used a two-step hydrothermal procedure to synthesize TiO_2 nanomaterials in the presence of iodic acid (HIO_3) as a dopant. The reduction of iodic acid caused the formation of multivalent iodine that induced OVs and 3d state Ti^{3+} species in the TiO_2 lattice, resulting in the visible light TiO_2 nanomaterials with an enhanced photocatalytic activity due to existing OVs, multivalent iodine in I−O−Ti bonds, and 3d state Ti^{3+} sites in the TiO_2 lattice. The sample exhibited more methylene blue (MB) photodegradation (10 ppm MB) (K_{ap}, of 7.92×10^{-3} min^{-1}) than commercial P25 (3.87×10^{-4} min^{-1}) and pristine TiO_2 nanowires (4.18×10^{-4} min^{-1}).[219]

The hydride reducing reagents like $NaBH_4$, NaH, and $Ca(H)_2$ create oxygen vacancies. For example, Wang et al. synthesized brown-color TiO_2 with the absorption edge in red light in a facile one-step treatment in a NaH solution. The Ti(III) species and OVs induced by NaH shifted the TiO_2 absorption edge from the UV region to the red end of the visible spectrum, resulting in critically enhanced photocatalytic activity in phenol degradation.[220] The OVs induced in TiO_2 NPs by sodium borohydride treatment caused a lower energy band gap, smaller pore sizes, and improved photocatalytic activity in orange II sodium salt degradation.[221] In another work, OVs were induced in TiO_2 films by CaH_2 as a reducing agent, resulting in a 340% photodegradation enhancement toward benzene under UV light. A band-bending model as a p−n junction between the bulk and the surface layer with OVs was confirmed by the density functional theory (DFT) calculations. This inhibited e/h recombination and oxygen transport at different depths, improving the photocatalytic prospects.[222]

Mesoporous black Ti^{3+}/N-TiO_2 spheres were fabricated by Cao et al. via an EISA approach by using urea as the nitrogen source and an in situ reduction by $NaBH_4$. The prepared samples with high effective surface areas showed a critical e/h separation, a remarkable harvesting of visible light and near-infrared photons, excellent MO photodegradation efficiency, and a small band gap of about 2.11 eV due to the Ti^{3+} self-doping and N species. In a proposed mechanism illustrated in Figure 4e, N-doped species create a new impurity level above the TiO_2 VB. In other words, the induced Ti^{3+} and OV generate intermediate energy levels below the TiO_2 CB, critically narrowing the integrated E_g with N species to harvest visible light energy.[223]

Various oxygen vacancies have been induced in the ultrathin TiO_2 nanolayer-grafted graphene nanosheets (TiO_2/graphene oxide) in an H_2 atmosphere (Ti/RGO(H_2)) by Xie et al. This H_2 treatment induced OVs and a large surface area in the sample. At the same time, the TiO_2/graphene oxide reduced by solid $NaBH_4$ (Ti/RGO($NaBH_4$)) showed the generation of bulk vacancies, a larger crystal size, and significantly decreased surface area and pore volume. Thus, the activity of treated Ti/RGO(H_2) is higher than that ofTi/RGO($NaBH_4$) due to the facilitated interfacial electron transfer and enhanced electronic conductivity. This is because of the favorable surface vacancy that suppressed the e/h recombination, elongating the electron lifetime and transport compared with the bulk vacancy.[224]

The induced OVs in the hydrothermally synthesized two-dimensional (2D) porphyrin Co-TCPP MOF-decorated 2D B-TiO_{2-x} nanosheet (by Li et al.) showed critically enhanced the harvesting of visible light photons and bisphenol A (BPA) photocatalytic degradation (7.3× and 19.3× higher than the individual Co-TCPP MOF and B-TiO_{2-x}, respectively). This is

https://doi.org/10.1021/acsomega.3c07560
ACS Omega 2024, 9, 6093−6127

due to the reduced interface resistance for charge migration, elongation of the photoelectron lifetime, and facilitated e/h separation induced by the intimate contacting of B-TiO_{2-x} and the Co-TCPP MOF (Figure 4f).[10] Similarly, the TiO_{2-x}/g-C_3N_4 nanorod array photoelectrode was fabricated by Qi et al. via urea drop calcination and $NaBH_4$ reduction. The induced OVs promoted the photodegradation efficiency of the Z-scheme mechanism (between TiO_2 nanorods/g-C_3N_4 nanosheets) toward phenol under visible light illumination.[225]

Oxygen vacancy-mediated sandwich-structured TiO_{2-x}/ultra-thin g-C_3N_4/TiO_{2-x} showed a direct Z-scheme photocatalytic mechanism with an excellent TC photodegradation efficiency (87.7% for 90 min) employing $^{\bullet}O_2^-$, h^+ and $^{\bullet}OH$ reactive species (by Ni et al.). This excellent activity is related to the special 3D structure, the Z-scheme heterojunction expediting charge transfer, and enhanced active species formation. Meanwhile, the OVs enhanced the spatial e/h separation.[226] The induced OVs critically enhanced the activity of (010)-faceted TiO_2 toward sulfamethoxazole (SMX). Qi et al. confirmed that vacuum-treated samples generated bulk defects and surface hydroxyl groups, improving the extract of the photoinduced holes for photooxidation reactions. In contrast, air-calcined samples resulted in the formation of surface OVs.[227]

A novel oxygen vacancy-modified TiO_2 (TiO_{2-x})/Ti_3C_2 (A-TOTC) photocatalyst has been fabricated by Miao et al. The enhanced e/h separation observed is due to the in situ growth of Ti_3C_2 to construct a Schottky barrier. Meanwhile, the induced OVs enhanced the BPA adsorption. They strengthened the photocatalytic interfacial reaction, so the photocatalytic activity of A-TOTC was nearly 5.1× and 4.0× greater than those of TiO_2/Ti_3C_2 and TiO_{2-x}, respectively.[228] Some TiO_2-containing mixed metal oxides have been fabricated as photocatalysts. For example, in the 3D black N-TiO_{2-x}@MoS_2 core−shell nanostructures synthesized by Liu et al. via the hydrothermal method, followed by an in situ solid-state chemical reduction and 350 °C calcination process under an Ar atmosphere, N and Ti^{3+} doping and simultaneous formation of the core−shell heterojunction nanostructure have occurred. N and Ti^{3+} codoping and hybrid heterostructures improved visible light harvesting toward MO photodegradation by about 92% (Figure 4g).[229] B-doped anatase-TiO_2/rutile-TiO_2 (A-TiO_2/R-TiO_2) with an adjustable band structure via B-doping was constructed by forming a Z-scheme transfer path between the B-doped A-TiO_2/R-TiO_2. It showed an optimized band structure with critical positively shifted band potentials and a high content of OVs. The amount of B-dopant tailored the band structure and content of surface OVs. Furthermore, e/h separation was enhanced via the Z-scheme transfer path, whih improve the sample's redox ability by retaining the higher redox potential.[230]

A novel one-step hydrothermal Zn-assisted synthesis procedure has been used by Fang et al. to prepare a reduced TiO_2 (TiO_{2-x}) photocatalyst using HF to prevent air oxidation of TiO_{2-x} (for stabilizing the Ti^{3+} and OVs). The obtained TiO_{2-x} with the ability to harvest visible and NIR photons, due to the boosted effect between doped Ti^{3+} and dual-facet exposure, showed excellent activity in RhB and formic acid photodegradation.[231] In the chemical hydrogen-reduced TiO_2, the surface and subsurface OVs created shallow and deep sub-band gap Ti (III) states below the CB. Both the defect-to-CB transitions and the VB-to-defect transitions caused and enhanced visible light photocatalytic activity up to 440 nm. The photoinduced charge carriers from the defect states to the CB have enough short lifetimes to drive photocatalysis. The Ti(III) deep and shallow trap states below the CB also shorted the lifetime of the photogenerated charge carriers under UV light irradiation.[232]

In mixed-phase titania, the phase-ratio-dependent OV was vital in determining the materials' band gap and photocatalytic activity. Another critical factor is the interface of the two materials with different band gap/OV levels. Some gradient intrinsic to the material, as in mixed-phase titania, played the most crucial role in e/h separation. The correlation of interfacial behavior and OVs in mixed-phase titania NPs leads to enhanced photoactivity under UV−vis illumination compared to their pristine counterparts.[233] OVs enhanced the absorption ability of catalysts toward the aqueous dissolved oxygen, increasing the formation of more strong oxidizing species (SOSs).[234,235]

5.1.3. Oxygen Vacancy-Mediated ZnO in Photodegradation. The photocatalytic application of the widely used ZnO photocatalyst has been limited due to its poor tendency to absorb visible light photons, poor charge transport, and low conductivity. One recent effective strategy for inhibiting these drawbacks is inducing oxygen or zinc vacancies in ZnO. Recent progress in oxygen vacancy ZnO compounds in the photodegradation of organic compounds degradation will be reviewed here.

Hybridization of ZnO nanosheets with Ag_3PO_4 NPs enhanced its photocatalytic activity toward RhB under visible light illumination due to the matched energy levels for efficient charge transfer between ZnO and Ag_3PO_4. This suggests a boosted effect of rich surface OVs and Ag_3PO_4 coupling (Figure 5a).[37] In ZnO nanocrystals containing OVs, the deep donor OVs have defect energy levels at E_V = +0.76 eV and shallow acceptor zinc vacancies have defect energy levels at 0.12 eV above the maximum VB, resulting in effective MO photodegradation under visible light illumination. The induced oxygen vacancies in the lattice of ZnO allow ZnO to harvest more visible light photons.[236] Deoxidizing ZnO powder under a vacuum drying process reduced the size of ZnO NPs while increasing the concentration of surface OVs. OVs reduced e/h recombination via the electron capture process, which boosted MB photodegradation activity under UV illumination.[237]

A porous ZnO nanosheet with a near-rectangular morphology was synthesized via the solvothermal-annealing method (annealed at 500 °C, ZnO-500 °C). The photocatalytic activity toward phenol under UV light irradiation can be critically affected by the relative concentration ratio of surface defects to bulk defects, crystallization performance, and effective surface area.[238]

The modulated surface defects in zinc oxide nanorods (ZnO NRs) resulted in the visible light absorption enhancement.[209] The annealing of the NRs up to 250 °C increased the surface defect states, primarily the surface OVs, while higher annealing temperatures could passivate the surface defects. The enhanced visible light of these ZnO NRs is due to the surface defects, which enhances e/h pair production through sub-bandgap absorption of visible light (Figure 5b).[209]

In the dark and light treatment of well-designed micro-, nano-, and capped nano-ZnO in an antibacterial study,[239] surface defects played a vital role in the production of reactive oxygen species (ROS) like $^{\bullet}OH$, $^{\bullet}O_2^-$, and H_2O_2 in a ZnO aqueous suspension even in the dark (17% dark activity). The high activity for ZnO NPs, the low activity for micro-ZnO, and the moderate value for capped ZnO emphasize the critical role of surface defects in ROS generation.[239] One-step thermal heating of metallic zinc powder at 1000 °C in a small oxygen

https://doi.org/10.1021/acsomega.3c07560
ACS Omega 2024, 9, 6093−6127

concentration prepared oxygen-defected ZnO.[240] A red shift in the band gap energy of the sample toward a visible light region relative to that of the commercial sample (with an E_g value of 3.07 eV) and the boosted photocatalytic activity toward methyl green decolorization are related to the oxygen defects in ZnO material.[240]

In the oxygen-deficient ZnO_{1-x} nanosheets prepared by Guo et al., hydroxyl radicals played a vital role in the photodegradation of methyl orange under visible light illumination. The induced OVs induced an increase in the activity of ZnO_{1-x} nanosheets compared to that of defect-free ZnO.[241]

Various defects like zinc interstitial (Zn_i), OV, and zinc vacancy (V_{Zn}) defects have been induced in ZnO nanorods with a controllable surface defects by Fang et al. The defect concentration and the e/h recombination can be controlled by the quenching temperature and cooling rate, so the quenched ZnO nanorods showed improved light harvesting and an efficient retarded e/h recombination toward the degradation of organic dyes.[242] Hydrogenated black ZnO nanoparticles have been synthesized by Xia et al. and exhibit long-wavelength harvesting and excellent photocatalytic activity. This improved activity has been related to a higher optical absorption effect, better e/h separation from the disordered structure, and high Zn-vacancy defects created by hydrogenation.[243]

The controllable surface OVs in ZnO induced by the controllable H_2 reduction process resulted in a narrowed band gap of the visible-light-active ZnO_{1-x}. The overlap of the VB of the surface OVs with O 2p increased the e/h separation efficiency and the photoactivity. Under visible light illumination, the photoinduced hole was vital to MO degradation. Further, the bulk oxygen vacancy formed via depth reduction at 700 °C for 5 h resulted in a photoactivity loss.[244] High-temperature $NaBH_4$ reduction and hydrothermal methods induced OVs in ZnO-prepared porous defective ZnO cellular hexagonal plates with surface OVs (OVZCHPs). The sample showed an enhanced solar-driven photocatalytic TC degradation rate (up to ∼99.9%) three times greater than that of the ZCHPs. As shown in Figure 5c, OVs critically prevent e/h recombination, narrowing E_g to locate in the visible light region; when these effects are accompanied by the unique porous cellular structure that shortens the transmission distance, a high TC photodegradation efficiency can be achieved under AM 1.5 illumination.[245] An increase in oxygen vacancies has also been induced by doping or using a composite. For example, in a dual-reaction-center (RDC) Fenton-like catalyst with the enriched surface electron-rich and electron-poor areas containing OV-rich Co-ZnO microparticles (OV-CoZnO MPs), electron-rich OVs (containing unpaired electrons) and electron-deficient Co^{3+} sites have formed via the lattice-doping of Co into ZnO wurtzite. Based on both experimental and theoretical calculations, the electron-rich OVs capture and reduce hydrogen peroxide to generate powerful hydroxyl radicals. At the same time, the electron-deficient Co^{3+} sites adsorb high amounts of pollutants and act as electron donors for the system, accompanied by their oxidative degradation.[246] In a similar work, a facial calcination process with a controlled OV concentration has been used by Zhang et al. in the synthesis of CeO_2/ZnO nanocomposites by the changing air/N_2 ratio. CeO_2/ZnO nanostructures showed richer OVs than the unmixed ZnO, which reached maximum value when the calcination atmosphere air/N_2 ratio was 2:8 or 4:6. Due to the CeO_2/ZnO nanoparticles prepared at air/N_2 = 2:8 having the highest number of OVs, the highest RhB photodegradation efficiency was obtained under visible light illumination (Figure 5d).[247]

In another work, hydrothermal/calcination combination methods have been applied to synthesize the ZnO-TiO_2 solid solution as a Z-scheme heterojunction of surface OVs and CdS QDs. Among the different samples, the highest phenol degradation was achieved by CdS QDs/ZnO_{1-x}-TiO_{2-x} due to the formation of OVs and Z-scheme heterojunctions.[248] A homogeneous precipitation method has also been used to synthesize a composite NiO/ZnO catalyst, which activated peroxymonosulfate (PMS) in the removal of BPA (95.26% BPA removal and 67.11% total organic carbon (TOC) removal). Based on the characterization and theoretical calculations (DFT), an electron rearrangement process occurred in OVs that modified heterojunction catalysts. This induced surface NiO acidic sites and alkaline OV sites, thus enhancing both PMS adsorption and activation.[249]

As another example of the preparation of mixed oxide composites, a simple universal route, simply heating an MO NC mixture with potassium (K), has been applied to induce continuous internal energy levels in MO semiconductors like TiO_2, ZnO, and In_2O_3 NCs. The prepared black NCs are capable of absorbing nearly full solar spectrum. A MB photodegradation efficiency about 300× greater than those of their conventional counterparts was demonstrated by as-prepared black TiO_2 NCs under visible light irradiation. The surface-disorder-induced OVs and metallic phases likely formed during the reaction process with K have been determined as the main reason for this boosted catalytic activity.[250] Modified OV-rich zinc oxide (VO-ZnO) with graphitic carbon nitride (g-C_3N_4), prepared by Liu et al., showed enhanced visible light photoactivity compared to pure OV-ZnO and g-C_3N_4. A high OV concentration was induced by introducing g-C_3N_4 into OV-ZnO, a promoting factor for visible light absorption. Additionally, an improved e/h separation was induced by the formed strong coupling interface between g-C_3N_4 and OV-ZnO, a factor for high visible light photocatalytic activity.[251]

The oxygen-deficient ZnO single-crystal nanosheets were prepared by adding trace fructose (ZnO−F) with high large-scale phenol photodegradation efficiency. Interestingly, ZnO−F showed a more favorable surface valence band maximum than pristine ZnO, resulting in the easier formation of $^{\bullet}OH$ by ZnO−F and higher photocatalytic activity. The CBM positions of ZnO-F and pristine ZnO are located at −0.52 and −0.56 eV, respectively, while the VBM position of ZnO-F is relatively increased from 2.64 eV for pure ZnO to 2.7 eV (Figure 5e). The more positive VBM position of ZnO-F produces substantial oxidative holes during photocatalysis.[252]

5.1.4. Oxygen Vacancy-Mediated Photocatalysis of Bismuth-Based Oxides. In recent years, some bismuth-contained oxides like BiOX,[253] Bi_2O_3,[254] $BiVO_4$,[255] $BiPO_4$,[256] Bi_2WO_6,[257] and Bi_2MoO_6[193] have been widely used as excellent heterogeneous catalysts. This application has related to their unique advantages, including the simple composition, a relatively narrow bandgap (2.2−2.8 eV), and a high oxidation ability with deep valence band levels. Recently, inducing OVs in bismuth-based composite oxides have been well-known as an emerging promising strategy to improve their photocatalytic performance.[258] This will be summarized in the below sections.

5.1.4.1. BiOX (Cl, Br, and I). Among the bismuth oxides, bismuth oxyhalides are the most famous applied photocatalysts in the degradation of various organic pollutants. In the following

https://doi.org/10.1021/acsomega.3c07560
ACS Omega 2024, 9, 6093−6127

sections, a brief of recent progress in their application will be reported.

5.1.4.2. BiOCl. As visible light photocatalysts, a synergistic efficiency was obtained in RhB and BPA photodegradation by h-BN/OV-BiOCl composites (h-BN = hexagonal boron nitride). An improved e/h separation efficiency has been related to negatively charged h-BN, a promoting factor for the expected migration of positively charged holes to the photocatalyst surface. Moreover, the presence of h-BN increased the number of OVs in OV-BiOCl, a favored factor for activating more adsorbed O_2 toward the oxidation of pollutants.[253] A novel OV-rich 2D/2D BiOCl-*g*-C_3N_4 ultrathin heterostructure nanosheet (CN-BC) was synthesized by Wang et al. Density functional calculations proved the induced OVs bring a new defect level for the increased photoabsorption under visible light irradiation. The photocatalytic activity of the OV-rich optimum ratio of CN-BC (50CN-50BC) toward 4-chlorophenol (4-CP) was about 12.5×, 5.3×, and 3.4× greater than those of pure BiOCl, g-C_3N_4, and an OV-poor heterostructure, respectively.[259]

Based on Wu et al.'s work, the hydroxyl group is the critical center for photoinducing OVs in BiOCl. The hydroxyl-rich BiOCl containing OVs appear black under UV light irradiation. The photoinduced surface OVs dissociate adsorbed water molecules via coordination with hydroxyl groups, leading to the regeneration of BiOCl under a water-rich atmosphere. The DFT calculations of the structure, energy, and charge density distribution of BiOCl and BiOCl−OH have been used to understand better the hydroxyl-dependent evolution of OVs in BiOCl (Figure 6a).[260] Ge et al. show that by tuning the exposed ratio of (001) and (010) facets of BiOCl plates and their surface OV content, the amounts of $^{\bullet}OH$ and $^{\bullet}O_2^-$ can be relatively adjusted under visible light illumination. The activation of molecular oxygen on OVs of BiOCl under visible light is a feasible and controllable approach to produce $^{\bullet}OH$ and $^{\bullet}O_2^-$ reactive species for effective degradation of pentachlorophenol sodium (PCPNa). Also, under a certain amount of $^{\bullet}O_2^-$, it plays a significant role in PCPN degradation depending on whether the content of $^{\bullet}OH$ is higher or lower.[261]

Xu et al. reported the facet dependence of BiOCl with OVs for the photocatalytic decabromodiphenyl ether (BDE209) removal under irradiation (>360 nm) based on the 4.4× faster debromination of BDE209 on the (001) BiOCl reaction compared to that on (010) BiOCl under an oxygen-free environment. This is due to the abundant OVs on the (001) facet of BiOCl, which act as adsorption sites for BDE209 to achieve C−Br bond activation efficiently. The debromination of BDE209 on BOC with OVs is a position-selective reduction process because BDE207 showed the highest proportion in the first debromination products (Figure 6b).[262] The OV-tunable BiOCl nanosheets were synthesized by Song et al. via a facile hydrolysis approach. Under UV illumination, a linear relationship was achieved between the increased number of OVs in BiOCl and the photocatalytic degradation and defluorination of PFOA (TOC removal was 53% after 8 h). The OVs trapped photogenerated e/h carriers and provided sites benefiting direct h^+ oxidation.[263]

Bulk iodine-doped BiOCl was prepared via a convenient molten salt method by Xu et al. by introducing iodine atoms and rich OVs in the bulk iodine-doped crystal structure BiOCl. It showed excellent visible light activity toward ciprofloxacin hydrochloride photodegradation (12× greater than pristine BiOCl). The photoelectrochemistry results have also confirmed higher e/h separation in $BiOCl_{1-3x}I_{3x}$.[197]

Li et al. have fabricated OV-tunable and flower-like CNFs/BiOCl (BOC) composites with excellent visible light-driven photoactivity. The OVs produce defect energy levels, which optimize the energy band structure and accelerate the e/h separation. Superoxide radicals are the main radicals in the photocatalytic degradation based on radical quenching experiments under visible light illumination. Rate constants of BOC-0.5 toward RhB, TC, and phenol were 2.5×, 4.3×, and 5.6× greater than those of BOC, respectively, while they were 60.6×, 4.5×, and 5.8× those of the commercial TiO_2 (P25).[264] The high oxygen density of BiOCl (001) facets resulted in fast OV generation in ethylene glycol under MW irradiation. The resulting BiOCl single-crystalline nanosheets with selectively deposited Ag showed much reactivity and stability on visible light Cr(VI) reduction and sodium pentachlorophenate oxidation compared to their randomly deposited counterparts. These are due to the tight contact between Ag and the BiOCl-(001) facets arising from OV-induced selective silver deposition.[265] The OVs on the BiOCl-(001) facets nanosheets can activate more molecular oxygen for removing organic pollutants under solar light compared to their the TiO_2 counterparts. These OVs can be effectively refreshed by UV light and serve as the efficient absorption of visible light for activating molecular oxygen, accounting for their long-term stability and high efficiency.[266] In another work, the Bi_2O_3−B_2O_3−ZnO−SrO−Na_2O (BBZSN) glass route was used to synthesize OV-enriched 3D BiOCl hierarchical structures with low e/h recombination and an adjustable band structure. They satisfactory degraded RhB under both ultraviolet light and visible light conditions.[267]

5.1.4.3. BiOBr. Solvothermally synthesized BiOBr microspheres containing OVs showed an excellent adsorption and photocatalytic prospects for TC removal in aqueous solutions using superoxide radicals as major reactive species produced in the BiOBr-OV suspension.[268] In the presence of urea, hierarchical BiOBr microflowers containing OVs were solvothermally prepared by Song et al. The amount of urea was used as a tuning factor to control surface OVs. The hierarchical BiOBr microflower-OV system showed a higher RhB photodegradation extant than the BiOBr without oxygen vacancies.[269]

The excitonic effects mediated by Coulombic interactions in the photoinduced e/h pairs cause critical roles in photoinduced processes in heterogeneous semiconducting-based systems. Based on the results from Wang et al., dissociating excitons into charge carriers in BiOBr with the incorporation of OVs led to excellent futures in charge-carrier-involved photocatalytic reactions, like the production of superoxide radicals for selective organic synthesis under visible light irradiation.[270]

There are some reports of OV-containing BiOBr composites in photocatalytic reactions. For example, CC/BiOBr composite (CC = conductive carbon-modified) photocatalysts with a high surface area and high levels of induced OVs promoted e/h charge separation and superoxide production. Under simulated sunlight, these CC/BiOBr composites showed excellent RhB photodegradation compared to the BiOBr blank sample.[271] Also, a facile one-step solvothermal synthesis procedure has been used by Wang et al. to fabricate a novel OV-rich ultrathin sulfur-doped BiOBr nanosheet (BB-xS) as an active visible light system with an excellent degradation efficiency toward 4-chlorophenol (4-CP), as that of the optimal BB-5S sample was 4.9× and 18.0× greater than those of bare BiOBr and OV-poor sulfur-doped BiOBr, respectively. In its photocatalytic mechanism in Figure 6c, after the photoexcitation of electrons into the CB and the sub-band induced by the synergistic effect of S

https://doi.org/10.1021/acsomega.3c07560
ACS Omega 2024, 9, 6093−6127

doping and rich OVs (narrowed the intrinsic E_g for visible light absorption), the electrons on the CB would also transfer into the sub-band and then to the surface to reduce the surface O_2 adsorbed (e^- is more negative than $E(O_2/O_2^-)$ (−0.33 eV vs NHE, pH = 7)). Meanwhile, the photoexcited holes (h^+) remain on the VB. In such a way, a spatially separated e/h can be obtained, leading to an enhanced separation efficiency for e/h. After that, the $^\bullet OH$ is generated from $^\bullet O_2^-$ with the assistance of e^- because the h^+ cannot directly oxidize hydroxyl anions from H_2O molecules to hydroxyl radicals due to the lower potential of h^+ compared to $E(^\bullet OH/OH^-)$ (+1.99 eV vs NHE, pH = 7). Meanwhile, 4-CP can be directly oxidized by the holes to carbon dioxide and water.[272] Compared with pure BiOBr, Bi/BiOBr composites with OVs synthesized via a simple combustion method showed a critically improved RhB photodegradation extent under visible light irradiation due to the surface plasma resonance effect, the electron sink effect of metallic Bi nanoparticles, and the narrowed band gap caused by the induced OVs.[273] Among a novel series of oxygen vacancy-rich ultrathin two-dimensional $BiOBr_xI_{1-x}$ solid solution nanosheets (BBI-x) constructed in a one-step solvothermal process by Wang et al., the optimal $BiOBr_{0.85}I_{0.15}$ sample (BBI-0.85) showed excellent visible light activity toward (4-chlorophenol, 4-CP,)) which was 4.4×, 10.9×, and 5.9× greater than those of pure BiOI nanosheets, pure BiOBr nanosheets, and oxygen vacancy-poor $BiOBr_{0.85}I_{0.15}$ nanoplates, respectively. This improved efficiency is due to the synergistic effect of solid solution and OVs.[274]

The critical enhancement in the visible light-driven photocatalytic future of a novel layered black phosphorus (BP)/BiOBr nanoheterojunction photocatalyst, which has unique band structures and chemically bonding interface, is related to the S-scheme formed between two-dimensional nanoheterojunctions with matched band structures, strong interfacial interactions, high redox, increased spatial e/h charge separation capability.[275] A novel 3D flower-sphere $BiOBr/Bi_4O_5Br_2$ with proper-OV has been synthesized from 3D BiOBr as a self-sacrificing template, NaOH as a structure-driving reagent, and the midwifery agent of OV. The concentration of OVs can be controlled via atmospheric conditions (N_2 or air). The synergistic enhancement of the $BiOBr/Bi_4O_5Br_2$−OV photoelectric activity due to the 3D hierarchical architectures, the optimal heterojunction composition, and proper OV concentrations, three positive factors, caused its ultrahigh photocatalytic activity toward antibiotic photodegradation (tetracycline (TC) and ciprofloxacin (CIP)).[185]

In the solvothermally synthesized Bi-modified BiOB, surface OVs were produced after annealing under an H_2 atmosphere. Both deposited Bi and OVs enhanced the photocatalytic activity of H-1.0 Bi@BiOBr samples toward the degradation of RhB. The introduced impurity level by OVs between the CB and VB narrows E_g, and the OV's role as the electron trapper improves the charge transport. Under the H200−1.0 Bi@BiOBr illumination, the photoexcited e^- from the VB to CB or OV states of BiOBr can be preferably transferred to the metallic Bi and OVs rather than participating in recombination with holes.[276]

Few-layered structural BiOBr-OV showed improved photocatalytic activity for decomposition and oilfield-produced wastewater under visible light due to the ultrathin BiOBr-OV structure and expanded interlayers that generate rapid ROS.[277]

The hydrothermally prepared Bi-metal-modified defective Bi_5O_7Br nanotubes (Bi/Bi_5O_7Br−OV) showed boosted phenol degradation, 3× higher than that of pristine Bi_5O_7Br. Based on DFT results, OVs in Bi_5O_7Br could form an intermediate level, allowing the electron transfer to a new intermediate level and finally to the CB. Good solar light harvesting is related to the defects and Bi, while the enhanced electronic conductivity and the e/h separation are related to the increased and more dispersed charge density allowed. Furthermore, generating more $^\bullet OH$ radicals improved the photocatalytic performance.[278]

5.1.4.4. BiOI. Another example of bismuth oxyhalide photocatalysts is bismuth oxyiodine. Huang et al. have reported an electroreduction strategy for improving the solar absorption and donor density of BiOI nanosheets by inducing OVs. These OVs caused an unexpected redshift of about 100 nm in the electronic band gap and a boosted photocatalytic activity 10× greater than that of the untreated BiOI nanosheets toward MO under visible light irradiation.[279] In another work, the charge carrier dynamics of BiOI, like excitation, separation, trap, and transfer, have been improved by inducing OVs and IO_3^- doping in BiOI nanosheets via adding NaH_2PO_2. This oxygen-deficient catalyst showed excellent boosted visible light photoactivity attractive toward gaseous formaldehyde degradation and MO (5× and 3.5× greater than the activity of the BiOI sample, respectively).[195] An ionic liquid [Emim]I-assisted solvothermal method has been used by Ji et al. to synthesize OVs-rich $Bi_7O_9I_3$ microspheres; compared with the fewer oxygen vacancies in $Bi_7O_9I_3$−OVL, the up-shifted VBM position and more negative CBM potential of $Bi_7O_9I_3$−OVR caused better photo-oxidation power of photoinduced holes, stronger reduction power of transferred electrons, and higher e/h separation efficiency. The mechanism of boosted photocatalyst action is shown in Figure 6d.[280]

A facile one-pot solvothermal method was used by Liu et al. to fabricate metallic Bi-modified $Bi_4O_5I_2$ nanocomposites with OVs with a dramatically increased photocatalytic activity for degrading BPA and MO under visible light irradiation. The synergistic effect of Bi metal and OVs caused their efficient light harvesting and excellent e/h separation abilities (Figure 6e).[281]

An OV-enriched BiOI-based Z-scheme 3D hierarchical $MoS_2/BiOI/AgI$ ternary nanocomposite was synthesized via a simple precipitation process in ethylene glycol and water by Islam et al. The composite's OVs in BiOI and the MoS_2 2D-dimensional nature elongate the e/h lifetime via a Z-scheme pathway, enhancing the RhB photodegradation efficiency. The formation of OVs has been confirmed by electron spin resonance (ESR) analysis (Figure 6f and g).[282]

5.1.4.5. Bi_2MoO_6. The boosted RhB photocatalytic degradation performance of a solvothermally synthesized Z-scheme-based heterojunction Ag and F codoped Bi_2MoO_6/reduced graphene oxide (Ag,F@BMO/rGO) photocatalysts have been related to codoping of F^- and Ag^+ ions, which also caused a redshift in the absorption edge of nanocomposite and decreased the E_g from 2.78 to 2.6 eV due to the synergetic effects of surface plasmon resonance and surface OVs induced by Ag^+ and F^-.[193] In the facile and scalable wet chemical synthesis of atomically thin Bi_2MoO_6 nanosheets (by Huang et al.), OVs were inevitably introduced into the nanosheets as the thickness of the nanosheets exposed interior atoms (large surface area), enhancing charge transport and the photocatalytic activity toward phenol under visible light.[191] In a similar work, plasmonic silver nanoparticles were deposited onto the Bi_2MoO_6 surface with surface OVs to fabricate a heterostructure Ag/Bi_2MoO_{6-x} (Ag/BMO_{6-x}) photocatalyst for RhB photodegradation. Compared to BMO, Ag/BMO, and BMO_{6-x}, its

https://doi.org/10.1021/acsomega.3c07560
ACS Omega 2024, 9, 6093−6127

boosted catalytic activity illustrates the increased effect of the SOVs, the SPR of Ag NPs, and the unique metal−semiconductor junction.[283]

A novel heterostructured composite of Fe(III) cluster-grafted Bi_2MoO_6 nanosheets with surface OVs (F/BMO-SOVs) was synthesized by calcination and impregnation approaches as a visible-light-active system for phenol degradation. The dramatically enhanced activity (80× greater than that of pure Bi_2MoO_6) is due to the synergistic effect between the SOVs, Fe(III) clusters, and Bi_2MoO_6. These factors, in addition to the created narrow band gap, facilitate the direct interfacial charge transfer (IFCT) from the SOVs to the surface Fe(III) clusters, promoting the efficient e/h separation (Figure 7a).[284]

5.1.4.6. $BiVO_4$. A reduced dimension $BiVO_4$ nanosheet with sufficient OV concentration and exposed (001) crystal facets has been fabricated Xu et al. for oxytetracycline removal. The highest OVs density with the best photocurrent (1.083 mA/cm^2 in the LSV) belongs to the $BiVO_4$ lamella within a thickness of 10 nm (tBV200), which showed better OTC degradation (95.8%) and TOC removal (89.55%) compared with hBV200.[285] In MB photodegradation by the visible-light-active $BiVO_4/TiO_2$ heterojunction composites, the catalyst with 2 wt % $BiVO_4$ loading showed higher photocatalytic activity than both pure $BiVO_4$ and TiO_2. The surface OV concentration created by the constructed junction creates an acceptor energy level into the TiO_2 VB (Figure 7b).[286]

5.1.4.7. Bi_2WO_6. Some Bi_2WO_6 visible-light-active photocatalysts with gradient OV concentrations have been constructed by Yang et al. for degrading decabromodiphenyl ether BDE209. Among the BWO-x (x = 0, 250, 400, and 550) materials, the highest BDE209 degradation rate was exhibited by BWO-250 with good light stability even after four reusing runs.[287] OV-controllable hydrogen reduction-prepared Bi_2WO_{6-x} nanoplates have been introduced by Lv et al., with a wide range of visible photoresponses from 450 nm to more than 600 nm. Bi_2WO_{6-x} showed increased photocatalytic activity, 2.1× greater that of pristine Bi_2WO_6, because generated surface OV states above and partly overlapping with the VB will result in the increase of the VB maximum, thus broadening the VB width and enhancing the photoactivity.[288] In another work, hydrothermally prepared Bi-doped Bi_2WO_{6-x} with sufficient OVs were synthesized by Huang et al. OVs and metallic Bi were selectively induced in Bi_2WO_6 nanostructures by adjusting the reaction time and Bi/W molar ratio of the precursors. The boosted activity of Bi/Bi_2WO_{6-x} in the photodegradation of BPA and its analogs has been related to its capability to generate a high amount of singlet oxygen ($^1O_2$) as the main reactive oxygen species. The $^1O_2$ concentration depended on the content of OVs and metallic bismuth.[289]

5.1.4.8. BiO_{2-x}. Compared to bulk BiO_{2-x}, The vacancy-rich monolayer BiO_{2-x} (monolayer BiO_{2-x}) showed an enhanced PhB and phenol photocatalytic degradation extent in UV−vis and NIR regions of light due to the associated VBi-O‴ vacancy, as proved by the positron annihilation spectra.[133] In other work, a Z-scheme OV-right $BiO_{1-x}Br/Bi_2O_2CO_3$ photocatalyst has been prepared via a facile time-dependent procedure and used for visible light photodegradation of some antibiotics like CIP, 4-MAA, etc. The electron mediator OVs significantly promoted the e/h separation, and the increased redox ability produced a superoxide radical ($^\bullet O_2^-$) on the CB of $BiO_{1-x}Br$ and a hydroxyl radical ($^\bullet OH$) on the VB of $Bi_2O_2CO_3$. In a direct Z-scheme mechanism shown in Figure 7c, both $BiO_{1-x}Br$ and $Bi_2O_2CO_3$ phases could be photoexcited to form e/h pairs. Via the OVs intermediate (electron mediator), excited electrons in the CB of $Bi_2O_2CO_3$ transfer to holes in $BiO_{1-x}Br$, preserving the strong electron reducibility in the CB of BiO1-xBr and the substantial oxidant holes in the VB of $Bi_2O_2CO_3$.[290]

5.1.4.9. $BiPO_4$. The N-doped carbon quantum dots (N-CQDs)/$BiPO_4$ materials were synthesized by Di et al. by an ionic liquid-assisted solvothermal procedure, which showed increased activity for degrading four kinds of antibiotics, including ciprofloxacin, enrofloxacin, tetracycline, and phenol 4-chlorophenol. This is due to the molecular oxygen activation ability of N-CQDs induced by the surface OVs of N-CQDs.[291] In a similar work, highly dispersed $BiPO_4$ with surface OVs synthesized by Wei et al. via a solvothermal−calcination method showed enhanced activity more than twice that of Degussa P25 due to the OVs. It is uniformly distributed in water for over 3 days due to the formation of an organic layer on the $BiPO_4$ surface via the solvothermal approach. This results in maintaining good contact between $BiPO_4$ and the pollutants. The induced OVs, at 450 °C, separated e/h pairs in the photoexcited $BiPO_4$ and improved the photocatalytic activity.[292]

5.1.4.10. Bi_2O_3. Recently, the enhanced photoelectrochemical properties of an infrared rapid thermal annealing-synthesized MOF-derived Bi_2O_3@C with rich OVs prepared by by Zou et al. have been related to the increased number of effective reactive sites and rich OVs, high harvesting of light energy, and excellent electron transfer. It showed 88% TC photodegradation efficiency after irradiation of 5 W LED for 120 min.[293] A large-scale porous Bi_2O_3 has been prepared by Wang et al. via etching commercial BiSn powders, followed by an air thermal treatment, and the sample has excellent stability in MB photocatalytic degradation process. The suitable band structure of porous Bi_2O_3 generated $^\bullet O_2^-$ and $^\bullet OH$ reactive species toward MB photodegradation.[294] The surface-rich OV Bi/α-Bi_2O_3 NPs loaded on g-C_3N_4 nanosheets via a calcination−photoreduction technique (Bi/α-Bi_2O_3/g-C_3N_4, labeled as BBC) also showed a boosted visible light photocatalytic activity (TC, 90.2%; RhB, 95.6%) because of the synergistic effect of surface OVs and Bi NPs.[295]

An oxygen-vacancy-rich MoS_2/Bi_2O_3 Z-scheme heterojunction catalyst (2-BO-MS) has been used for crystal violet photocatalytic degradation. The XPS, XRD, and HRTEM results confirmed the vital roles of OVs, enhanced strong MoS_2−Bi_2O_3 interfacial interaction, and specific surface area in the enhanced activity of the system compared to the individual systems.[296] In another study, novel mesoporous ternary hybrids comprised of Bi_2O_3/V_2O_5 photocatalysts anchored on g-C_3N_4 nanosheets (denoted as BiV) have been synthesized by Vattikuti et al. via an in situ copyrolysis approach and used in the visible light photodegradation of phenol red (PR). The improved efficiency was 1.2× and 1.8× greater than those of binary BiV and pristine Bi_2O_3, respectively, due to the highly dispersed V_2O_5 and Bi_2O_3 NPs, mesoporous structure, and high specific surface area.[297]

A core−shell heterostructured $CdWO_4/Bi_2O_2CO_3$ photocatalyst fabricated in a two-step hydrothermal procedure by Yang et al. in a facile process showed much superior RhB, MB, methyl orange (MO), and phenol photodegradation efficiencies compared with individual $CdWO_4$ and $Bi_2O_2CO_3$. The defect levels in the band gap induced by OVs, which increase the visible light harvesting intimate interfacial core−shell heterostructure interactions, and the formation of n−n junction between the $CdWO_4$ and $Bi_2O_2CO_3$ are the main factors for this boosted catalytic effect.[298]

https://doi.org/10.1021/acsomega.3c07560
ACS Omega 2024, 9, 6093−6127

$Bi_4Ti_3O_{12}$ nanosheets with tunable OV concentrations were fabricated via a modified molten salt procedure and used to investigate the effect of OVs on piezo-photocatalytic RhB dye degradation. OVs induced increased adsorption energy, and Bader charges caused an enhanced charge transfer between O_2/H_2O and $Bi_4Ti_3O_{12}$. The facilitated catalytic process by the piezo-photocatalytic degradation mechanism is presented in Figure 7d.[299]

5.1.5. Oxygen Vacancy-Mediated Photocatalysis of Iron-Based Oxides. Some iron-based composites with various Fe loadings have been widely used as catalysts in the degradation of various organic pollutants. For example, OV-rich calcium-doped α-Fe_2O_3 (Ca−Fe_2O_3) was synthesized by the Wang research group via a scalable precipitation−calcination procedure as a cost-effective and eco-friendly photocatalyst to activate peroxymonosulfate (PMS) for wastewater purification. 5% Ca−Fe_2O_3 showed sound RhB degradation compared to the pure α-Fe_2O_3 due to its increased effective surface area, OV content, and better electrical conductivity (Figure 7e).[300] Similarly, metal-ion-involved hydrothermal and high-temperature hydrogenation techniques were used by Ren et al. to fabricate the defect-engineered magnetic γ-Fe_2O_3 ultrathin nanosheet/mesoporous black TiO_2 hollow sphere heterojunctions (γ-Fe_2O_3/β-TiO_2), which showed a faster TC degradation rate with an apparent rate constant (k) ∼3× higher than that of α-Fe_2O_3/b-TiO_2. The narrow bandgap and unit cell thickness of the γ-Fe_2O_3 nanosheets, the hollow structure, and defect engineering are the main factors for the sample's solar-light-harvesting property, rapid electron transport, and spatial e/h separation (Figure 7f).[301]

Recently, the thermal-aging-synthesized MOF-derived $CoFe_2O_4$ nanomaterial series with tuned OVs were used for peroxymonosulfate (PMS) activation with a boosted activity regarding the large surface OV and $CoFe_2O_4$ functional groups.[302] In a similar work, the role of OVs in $CoFe_2O_{4-x}$ in activating persulfate (PS) toward BPA degradation was investigated. OVs enhanced electronic transfer and the redox cycle from Co^{3+}/Fe^{3+} to Co^{2+}/Fe^{2+} to generate $^1O_2$ and $^\bullet O_2^-$.[303]

Hollow sphere $CuFe_2O_4$ with OVs, as a novel heterogeneous Fenton-like catalyst, showed excellent H_2O_2 catalytic activation (to produce more $^\bullet$OH) via changing surface electronic structure, inducing the formation of highly active electron-rich Cu(I) species, and providing additional active sites by OVs. The hollow structure grasped and enriched organic molecules, while $^\bullet$OH made them contact each other fully, ultimately accelerating pollutant degradation.[304] The incorporation of nonreducible metal oxides MxOy (M = Mg, Zn, Ca, Ba, Al) onto CuO hybrid magnetic nano-ferric oxide (Cu@Fe_3O_4) can change the persulfate activation mechanism pathway to increase the acetaminophen degradation rate. Added M led to surface OV formation and raised the zero-point charge (pHpzc) of CuM@Fe_3O_4 for enhanced PMS adsorption and activation. Also, it enhanced the surface formation of a new Cu species (Cu^{3+}) on CuM@Fe_3O_4, which then participated in the singlet oxygen generation.[305]

It has been confirmed that OVs in a magnesium-doped hematite (Mg/Fe_2O_3) catalyst are activated (PMS) for remediating organic pollutants. Incorporated Mg critically increased the OV content and specific surface area of 5% Mg/Fe_2O_3, causing increase activity in the degradation of RhB with vital roles of $^1O_2$ and $^\bullet O_2^-$ instead of $SO_4^{\bullet-}$ and $^\bullet$OH.[196] OV-enriched α-Fe_2O_3 was prepared from thermally treated goethite (α-FeOOH) by Qin et al. and used as a PMS activator for the oxidation of sulfamethoxazole (SMX). The extraordinary SMX degradation rate depended on the OV concentration.[306]

5.1.6. Oxygen Vacancy-Mediated Photocatalysis of Other Metal Oxides. 5.1.6.1. CeO_2. The defective Sm-doped CeO_2 nanorods (OV−Sm−CeO_2) were used by Yang et al. in visible light MB photodegradation of methyl blue, with a boosted effect compared to CeO_2 nanorods and Sm−CeO_2. The essential reactive species were $^\bullet$OH, $^\bullet O_2^-$, and h^+, confirmed via electron spin resonance spectroscopy.[307] Recently, in an enriched OVs AgI/CeO_2 heterojunction, the promoted e/h separation and transfer led to efficient photocatalytic O_2 activation. The TC photodegradation rate constant of AgI (5%)/CeO_2 was about 3× and 47× higher than those of CeO_2 and AgI, respectively (the mechanism in Figure 8a and b).[308] The enhanced photoactivity of the precipitation−sonication-prepared BiOI/CeO_2 nanocomposite series has also been related to excess surface OVs of the nanocomposite compared t CeO_2 and better e/h separation through the Z-scheme a mechanism.[309]

The presence of surface OVs in the defected CeO_2−AgI was confirmed by XPS, which extended the e/h lifetime and resulted in a boosted photocatalytic activity for the degradation of organic dyes, such as RhB, based on Z-scheme phenomena.[310]

5.1.6.2. Co_3O_4. The oxygen-deficient Co_3O_4/WO_3 nanocomposite showed excellent activity toward sodium diclofenac (DFC) degradation by photoinduced hydroxyl radicals. Formation of a monoclinic WO_3 phase and a p-n heterojunction (maximizes the generation of hydroxyl radicals), high e/h separation, strong visible light harvesting, and a strong catalyst−pollutant interaction in basic media are the main factors for this boosted photocatalytic activity. Figure 8c and d show the metal oxide semiconductor interaction (an important factor in decreasing Co_3O_4 NPs leaching in the solution), the improved CW_2 nanocomposite activity, and the charge transfer in the nanocomposite.[311]

5.1.6.3. SnO_{2-x}. Efficient OV defect engineering was done into the hydrothermally etched synthesized Zn_2SnO_4 (ZSO) NPs in a dilute acetic acid solution to obtain the ultrafine particle size SnO_{2-x} NPs. The synergistic RhB photodegradation effect is related to the increased active sites, intensified visible light harvesting, and the e/h separation rate induced by the OV defect engineering.[312] Among some one-step hydrothermally synthesized enriched OV tin dioxide (SnO_{2-x}) nanocrystals, the highest MO photodegradation efficiency was observed for SnO_{2-x} prepared at 80 °C under UV−visible light due to its high OV concentration (Figure 8e). The active $^\bullet O_2^-$ radical as the main reactive species that governed the SnO_{2-x} nanocrystals activity was produced by the electron-trapping and O_2 -adsorbing roles of OVs (Figure 8f).[313] The sol−gel-synthesized single-phase undoped and Sr-doped SnO_2 NPs ($Sn_{1-x}Sr_xO_2$ NPs) were tested for MB and Dinoseb photodegradation under UV light. Based on the XPS, SXAS, and PL data, the highest activity of $Sn_{0.95}Sr_{0.05}O_2$ was related to the presence of OVs, which led to the reduced band gap (Figure 8g).[314]

5.1.6.4. WO_3. WO_3 ultrathin surface-engineered nanosheets were fabricated solvothermally via low-temperature surface hydrogenation reduction. Their bandgap decreased to 2.48 eV because the induced surface OVs enhanced the visible light harvesting toward the photocatalytic degradation of the highly toxic metribuzin herbicide (100%). Suitable surface OVs promoted the e/h separation, accompanied by the two-dimensional ultrathin structure, facilitating the engineering of surfaces and furnishing many surface-active sites (Figure 8h).[315]

https://doi.org/10.1021/acsomega.3c07560
ACS Omega 2024, 9, 6093−6127

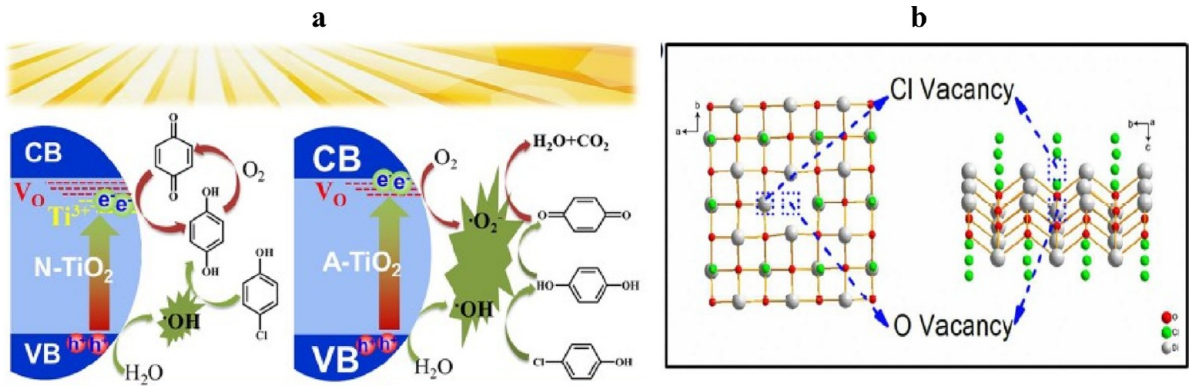

Figure 9. (a) Proposed mechanism of visible-light-irradiated A-TiO_2 and N-TiO_2.[325] Reprinted with permission from ref 325. Copyright 2018 American Chemical Society. (b) $BiO_{1-x}Cl_{1-y}$ crystal structures[326] Reprinted with permission from ref 326. Copyright 2018 American Chemical Society.

5.1.6.5. In_2O_3. In the work reported by Wan et al., the photocatalytic dehalogenation of decabromodiphenyl ether and hexabromobenzene by In_2O_3 strongly depended on the proton trapping enhanced by the induced OVs. The enhanced OV concentration critically trapped photoinduced electrons and protons, improved their transfer efficiency, accelerated the e/h separation, and enhanced the In_2O_3 photocatalytic activity in the PCET reactions.[316] An electrospinning and thermal treatment method under an NH_3 atmosphere was used to fabricate the nitrogen-doped In_2O_3 ($N-In_2O_3$) nanofibers. Its improved the visible light RhB photodegradation rate compared with that of pure In_2O_3 nanofibers can be attributed to the nitrogen atom introduced at interstitial sites and the generated surface OVs.[317]

A novel shape-controlled Cu_2O/reduced graphene oxide/In_2O_3 (Cu_2O/RGO/In_2O_3) OV-enriched hybrid was synthesized by Liu et al., via a facile, surfactant-free procedure with an excellent activity toward water oxidation and MB degradation compared with pure In_2O_3 and Cu_2O. As shown in Figure 8i, the In_2O_3/ Cu_2O heterojunction and induced OVs induce extra diffusive electronic states above the VB edge and reduce the hybrid band gap. Other reasons for this boosted activity are the alignment of band edge due to the different Fermi levels between In_2O_3 and Cu_2O and the charge transfer and distribution onto the graphene sheets, resulting in the downshift of VB of In_2O_3 and its critical enhanced oxidation potential.[318] A fabricated 2D/2D NiFe-LDH/Ti_3C_2Tx MXene heterojunction synthesized through a one-step hydrothermal method was obtained from the Ni/Fe molar ratio of 4:1 and an MXene loading amount of 40 mg of photodegraded 98% norfloxacin (NOR) in 4 h, with a 3.8× faster rate than bare NiFe-LDH nanosheets. The NiFe-LDH OVs facilitate the e/h separation, where the NiFe-LDH electrons are transferred to Ti_3C_2Tx s-MXene, forming a Schottky barrier at the interface of the two components.[319] A series of carbon-based defect-rich bimetallic oxides with OVs derived from peroxymonosulfate (PMS) were used for PMS activation to degrade 4-aminobenzoic acid ethyl ester (ABEE). Fe1Mn1−Fe NC showed higher catalytic degradation by generating sulfate, hydroxyl radicals, superoxide radicals, and singlet oxygen.[320]

Room temperature ferromagnetic (RTFM) ZrO_2 nanostructures with tetragonal (t-ZrO_2) and monoclinic (m-ZrO_2) phases were synthesized via a sol−gel procedure by Kumar et al. The saturation magnetization and calcination temperature variations changed the emission band intensity in the same trend. The presence of RTFM and decrease in emission band intensity is caused by density change of the OVs with the calcination temperature. OVs are the main factor for the ZrO_2 nanostructures' enhanced photocatalytic activity.[321]

A $SrTiO_3$ surface modified by ethanol quenching with enhanced visible light photocatalytic performance toward RhB was prepared by preheating $SrTiO_3$ nanocrystals to 800 °C and immediately quenching them by submersion in ethanol. Upon this rapid ethanol quenching, a high level of surface OVs were induced due to the interaction between hot $SrTiO_3$ and ethanol. The induced localized states in the modified $SrTiO_3$ band gap due to OVs acted as photoinduced charge traps to promote photocatalytic activity.[322] The prepared surface OV-rich $ZnFe_{0.8}Co_{0.4}O_{2.4}$ NPs with high activity for degrading refractory pollutants by PMS activation ($[O_3SO_IO_{II}H]^-$) could be adsorbed and trapped by the surface OVs in the form of O_I-OV or O_{II}-OV. Metal Co sites adsorbed pollutant molecules predominantly, in which metal species captured their electrons and then transferred them to the surface OVs, achieving efficient electron recycling in the aqueous suspensions.[323]

A summary of the roles of defects in different photocatalysts is shown in Table 1.

6. SYNERGETIC EFFECT OF DUAL DEFECTS

In some cases, outstanding photocatalytic performances were achieved due to the coexistence of dual-defect heterojunction photocatalysts. For instance, the OV-enriched TiO_2 hierarchical microspheres were modified with ultrathin sulfur vacancy-enriched MoS_{2-x} nanosheets to fabricate MoS_{2-x}@TiO_{2-OV} as a dual-defect heterojunction photocatalyst. It could mineralize some refractory pollutants in a simulated pharmaceutical wastewater sample. This unique interface modulates synergistic structural and distribution of defect sites with energy recovery. Based on the computational studies, this dual defect favors the adsorption of H* and •OH production and boosts the e/h separation and transfer efficiencies.[324]

Under various calcination atmospheres, defective anatase TiO_2 nanocrystals were fabricated by Xu et al. via a simple controllable chemical deposition procedure, where the presence of both OVs and Ti^{3+} defects in TiO_2 after N_2 treatment (N-TiO_2) were proven by XPS and ESR analysis, while only the OVs were present in air-calcined TiO_2 (A-TiO_2). ESR spectra confirmed the efficient activation of oxygen molecules to $^{\bullet}O_2^-$ species under visible light for A-TiO_2, hindering the accumulation of intermediates in *p*-chlorophenol (4-CP) photodegradation critically. A-TiO_2 obtained a higher e/h

https://doi.org/10.1021/acsomega.3c07560
ACS Omega 2024, 9, 6093−6127

separation than N-TiO_2, proving the vital role of suitable concentration of OVs in e/h transfer (Figure 9a).[325]

An in situ oxygen and chlorine dual-vacancy in BiOCl ($BiO_{1-x}Cl_{1-y}$) has been reported by Li et al. as a cost-effective green and scalable nature-derived reduction strategy with the extracted solution of green tea and spinach. These induced defects critically ameliorated the crystal and electronic band structure and surface state, enhanced photoabsorption, and improved surface charge transfer efficiency (11-fold enhancement). Profiting from these merits, it revealed excellent photocatalytic oxidation ability for selective CO_2 reduction into CO. The continuous adjustable photoresponse and defect level of $BiO_{1-x}Cl_{1-y}$ were regulated by extract concentration adjustment, which balances photoabsorption and photoredox driving force (Figure 9b).[326] Both theoretical calculations and experimental observations confirmed the high density of the high energy surface (100) in Bi_2WO_6 nano-bipyramid because of its induced defects, i.e., "Bi−O" vacancy pairs, as a critical factor for its increase in solar-light harvesting. Thus, Bi_2WO_6's chemical and electronic structures, the e/h separation efficiency, and solar light harvesting via its narrowed band gap energy were improved due to the presence of vacancy pairs. The findings give us insights into achieving more suitable photoactivity mechanisms by elucidating the reactive surface-enhanced photochemical reactivity relationship for designing and fabricating sensitive catalysts.[327]

7. CONCLUSION OR SUMMARY AND OUTLOOK

In recent years, a promising method to enhance the photocatalytic activity of semiconducting materials in energy-related applications is inducing and engineering anionic vacancies in the proposed photocatalyst. This Review illustrates the fundamental roles of anionic vacancies in the photocatalytic process. Further, the rational design of anionic vacancies of photocatalysts was also summarized. Then, we focused on the effects of oxygen vacancyies, and the effects of various OV factors, such as their distribution, concentrations, and the bulk and surface OVs, were illustrated on the multiple characteristics of photocatalysts, including electronic configuration, e/h transport characteristics, optical absorbance, and the appearance of ferromagnetic response. Progress in this field can enhance the understanding of OV defects, help us better design the related materials, secure clean energy, and lead to critical progress in environmental applications.

In general, the stability of the catalysts is of great importance from a practical application point of view. Thus, some high-cost, large E_g, and low-activity effective area common photocatalysts may not be beneficial practically. Accordingly, constructing vacancy-defected photocatalysts, especially the engineered ones, with excellent stability and cost-effective systems is promising for widespread application in large-scale wastewater treatment processes. Some requirements of the perfect material for vacancy engineering are visible light harvesting with high conversion of solar-conversion energy, suitable E_g structure for redox processes, high photostability for elongated applications, and commercial scalability.

The decisive impact of OVs on molecular activation and subsequent reaction pathways is because of their direct interactions with molecules. Beyond modulating the semiconductor's electronic structure, OVs give an effective strategy for maneuvering molecular adsorption/activation in the photodegradation reaction. The anionic/cationic vacancies can shape the band structure by forming intraband gap states and acting as e/h trapping sites.[328] Thus, from a theoretical and technological point of view, understanding the vacancy's roles in charge transport is of great importance to designing practical advanced materials.[329]

Despite the various reported works on the OVs engineering photocatalysis, it still comes with multiple challenges and is in an infant stage. The first challenge is the poor stability of OVs under the reaction conditions. For example, under prolonged air exposure, an OV is rapidly occupied by oxygen or water molecules, losing its activity. This emphasizes the importance of constructing catalysts with stable or recyclable defects for practical photodegradation applications. Another open question is the pathways in which the defects affect the photophysical features (e.g., carrier lifetime and diffusion length, and photoluminescence intensity) and photocatalytic performance and selectivity. Thus, deep DFT calculations have been aimed at the experimental results to facilitate the design of defective compounds with better activity.

Further, the relaxation dynamics of the polarons bound to OV with a key role in defect engineering have not been fundamentally investigated yet. So far, more works focused on the direct roles of OVs as active sites to improve photocatalytic efficiency with no essential characterizations, and no detailed attention has been paid to the effects of OVs at the atomic or molecular level and constructing the structure−activity relationship. A critical step for photocatalytic application is the large-scale construction of defective metal oxides. In general, a cheaper, simpler, and industrial OV introduction strategy is urgently needed due to most existing defect engineering methods being complex, unsafe, and unsuitable for mass production.

■ ASSOCIATED CONTENT

Supporting Information

The Supporting Information is available free of charge at https://pubs.acs.org/doi/10.1021/acsomega.3c07560.

A literature survey of oxygen vacancy research between 2015 and 2024 from Scopus (PDF)

■ AUTHOR INFORMATION

Corresponding Authors

Alireza Nezamzadeh-Ejhieh − *Department of Chemistry, Shahreza Branch, Islamic Azad University, Shahreza, Isfahan 86139-74183, Iran; Department of Chemistry, Isfahan (Khorasgan) Branch, Islamic Azad University, Isfahan, Isfahan 81551-39998, Iran;* orcid.org/0000-0002-8123-6968; Email: arnezamzadeh@iaush.ac.ir

Ahmad Reza Massah − *Department of Chemistry, Shahreza Branch, Islamic Azad University, Shahreza, Isfahan 86139-74183, Iran; Department of Chemistry, Isfahan (Khorasgan) Branch, Islamic Azad University, Isfahan, Isfahan 81551-39998, Iran*; Email: massah@iaush.ac.ir

Mahdieh Rezaei − *Department of Chemistry, Shahreza Branch, Islamic Azad University, Shahreza, Isfahan 86139-74183, Iran*; Email: m.rezayi1397@gmail.com

Complete contact information is available at: https://pubs.acs.org/10.1021/acsomega.3c07560

Notes

The authors declare no competing financial interest.

https://doi.org/10.1021/acsomega.3c07560
ACS Omega 2024, 9, 6093−6127

■ ACKNOWLEDGMENTS

The authors thank for Shareza Branch and Isfahan (Khorasgan) Branch, Islamic Azad University, Isfahan, Iran. The authors also thank for the publishers that permitted us to use corresponding graphics adopted from their published papers.

■ ABBREVIATIONS

AOP	Advanced oxidation process
A-TiO_2	Anatase TiO_2
ABEE	4-Aminobenzoic acid ethyl ester
BP	Black phosphorus
BB	BiOBr
BBI	$BiOBr_xI_{1-x}$
BOC	BiOCl
PDS	Peroxydisulfate
BBZSN	$Bi_2O_3-B_2O_3-ZnO-SrO-Na_2O$
BPA	Bisphenol A
BT	Brookite TiO_2
B-TiO_2	Black TiO_2
DFT	Density functional theory
4-CP	4-Chlorophenol
CC	Conductive carbon
CBM	Conduction band minimum
RDC	Dual reaction center
BDE	Decabromo diphenyl ether
ERS	Electron spin resonance
ZnO−F	Fructose-regulated ZnO
g-C_3N_4	Graphitic carbon nitride
IFCT	Interfacial charge transfer
MB	Methylene blue
MO	Methyl orange
NCs	Nanocrystals
NPs	Nanoparticles
N−In_2O_3	Nitrogen-doped In_2O_3
NOR	Norfloxacin
OV	Oxygen vacancy
PEC	Photoelectrochemcial
PS	Persulfate
PMS	Peroxymonosulfate
PCPNa	Pentachlorophenol sodium
PR	Phenol red
ROS	Reactive oxygen species
RGO	Reduced graphene oxide
RGO	Rhodamine B
RTFM	Room temperature ferromagnetic
R-TiO_2	Rutile TiO_2
$^1O_2$	Singlet oxygen
SOSs	Strong oxidizing species
SMX	Sulfamethoxazole
TC	Tetracycline
V_{Ti}	Ti vacancy
TOC	Total organic carbon
V	Vacancy
VBM	Valence band maximum
VOCs	Volatile organic compounds
W- TiO_2	White TiO_2
pHpzc	Zero-point charge
Zn_i	Zinc interstitial
ZSO	Zn_2SnO_4

■ REFERENCES

(1) Zafiu, C.; Part, F.; Ehmoser, E.-K.; Kähkönen, M. A. Investigations on inhibitory effects of nickel and cobalt salts on the decolorization of textile dyes by the white rot fungus Phanerochaete velutina. *Ecotoxicology and Environmental Safety* **2021**, *215*, No. 112093.

(2) Ghattavi, S.; Nezamzadeh-Ejhieh, A. A mechanistic study of the photocatalytic activity of AgI−WO3 in an experimentally designed approach toward methylene blue photodegradation. *Catalysis Science & Technology* **2023**, *13*, 737−749.

(3) Ghattavi, S.; Nezamzadeh-Ejhieh, A. Nanoscale AgI-WO3 binary photocatalyst: Synthesis, brief characterization, and investigation of its photocatalytic activity. *Mater. Res. Bull.* **2023**, *158*, No. 112085.

(4) Ellouzi, I.; Regraguy, B.; El hajjaji, S.; Harir, M.; Schmitt-Kopplin, P.; Lachheb, H.; Laânab, L. Synthesis of Fe-doped TiO2 with improved photocatalytic properties under Vis-L irradiation. *Iran. J. Catal.* **2022**, *12*, 283−293.

(5) Wang, H.; Zhang, L.; Chen, Z.; Hu, J.; Li, S.; Wang, Z.; Liu, J.; Wang, X. Semiconductor heterojunction photocatalysts: design, construction, and photocatalytic performances. *Chem. Soc. Rev.* **2014**, *43*, 5234−5244.

(6) Mirsalari, S. A.; Nezamzadeh-Ejhieh, A.; Massah, A. R. A Z-scheme CdS/Ag3PO4 catalyst: Characterization, experimental design and mechanism consideration for methylene blue. *Spectrochimica Acta Part A: Molecular and Biomolecular Spectroscopy* **2023**, *288*, No. 122139.

(7) Rezaei, M.; Nezamzadeh-Ejhieha, A. The ZnO-NiO nanocomposite: A brief characterization, kinetic and thermodynamic study and study the Arrhenius model on the sulfasalazine photodegradation. *Int. J. Hydrogen Energy* **2020**, *45*, 24749−24764.

(8) Zhao, L.; Chen, X.; Wang, X.; Zhang, Y.; Wei, W.; Sun, Y.; Antonietti, M.; Titirici, M.-M. One-Step Solvothermal Synthesis of a Carbon@TiO2 Dyade Structure Effectively Promoting Visible-Light Photocatalysis. *Adv. Mater.* **2010**, *22*, 3317−3321.

(9) Liu, G.; Wang, L.; Yang, H. G.; Cheng, H.-M.; Lu, G. Q. Titania-based photocatalysts—crystal growth, doping and heterostructuring. *J. Mater. Chem.* **2010**, *20*, 831−843.

(10) Li, J.; Li, X.; Wu, G.; Guo, J.; Yin, X.; Mu, M. Construction of 2D Co-TCPP MOF decorated on B-TiO2−X nanosheets: Oxygen vacancy and 2D−2D heterojunctions for enhancing visible light-driven photocatalytic degradation of bisphenol A. *Journal of Environmental Chemical Engineering* **2021**, *9*, No. 106723.

(11) Saeidi, S.; Rezaei, B.; Ensafi, A. A. Energy Band Engineering by CdTe/Si Codoped TiO2 Nanoarrays for Enhanced Photoelectrochemical Water Splitting. *ACS Applied Energy Materials* **2022**, *5*, 2795−2804.

(12) Saeidi, S.; Rezaei, B.; Ensafi, A. A. Fabrication and characterization of upconversion N-doped graphene quantum dots for improving photoelectrocatalytic performance of rutile hierarchical TiO_2 nanowires under visible and near-infrared light irradiations. *Materials Today Chemistry* **2022**, *23*, No. 100742.

(13) Li, X.; Yu, J.; Low, J.; Fang, Y.; Xiao, J.; Chen, X. Engineering heterogeneous semiconductors for solar water splitting. *Journal of Materials Chemistry A* **2015**, *3*, 2485−2534.

(14) Wang, S.; Pan, L.; Song, J.-J.; Mi, W.; Zou, J.-J.; Wang, L.; Zhang, X. Titanium-Defected Undoped Anatase TiO2 with p-Type Conductivity, Room-Temperature Ferromagnetism, and Remarkable Photocatalytic Performance. *J. Am. Chem. Soc.* **2015**, *137*, 2975−2983.

(15) Li, H.; Li, J.; Ai, Z.; Jia, F.; Zhang, L. Oxygen vacancy-mediated photocatalysis of BiOCl: reactivity, selectivity, and perspectives. *Angew. Chem., Int. Ed.* **2018**, *57*, 122−138.

(16) Pan, L.; Wang, S.; Xie, J.; Wang, L.; Zhang, X.; Zou, J.-J. Constructing TiO2 p-n homojunction for photoelectrochemical and photocatalytic hydrogen generation. *Nano Energy* **2016**, *28*, 296−303.

(17) Chen, X.; Liu, L.; Yu, P. Y.; Mao, S. S. Increasing solar absorption for photocatalysis with black hydrogenated titanium dioxide nanocrystals. *Science* **2011**, *331*, 746−750.

(18) Zhang, Y. C.; Afzal, N.; Pan, L.; Zhang, X.; Zou, J. J. Structure-activity relationship of defective metal-based photocatalysts for water splitting: experimental and theoretical perspectives. *Adv. Sci.* **2019**, *6*, No. 1900053.

https://doi.org/10.1021/acsomega.3c07560
ACS Omega 2024, 9, 6093−6127

(19) Vu, N.-N.; Kaliaguine, S.; Do, T.-O. Critical Aspects and Recent Advances in Structural Engineering of Photocatalysts for Sunlight-Driven Photocatalytic Reduction of CO2 into Fuels. *Adv. Funct. Mater.* **2019**, *29*, No. 1901825.
(20) Zhang, Y.-C.; Afzal, N.; Pan, L.; Zhang, X.; Zou, J.-J. Structure-Activity Relationship of Defective Metal-Based Photocatalysts for Water Splitting: Experimental and Theoretical Perspectives. *Adv. Sci.* **2019**, *6*, No. 1900053.
(21) Xiong, J.; Di, J.; Xia, J.; Zhu, W.; Li, H. Surface Defect Engineering in 2D Nanomaterials for Photocatalysis. *Adv. Funct. Mater.* **2018**, *28*, No. 1801983.
(22) Zhang, W.; Tian, Y.; He, H.; Xu, L.; Li, W.; Zhao, D. Recent advances in the synthesis of hierarchically mesoporous TiO2 materials for energy and environmental applications. *National Science Review* **2020**, *7*, 1702−1725.
(23) Wu, S.; Wang, J.; Li, Q.; Huang, Z.; Rao, Z.; Zhou, Y. Bi/BiOCl nanosheets enriched with oxygen vacancies to enhance photocatalytic CO 2 reduction. *Transactions of Tianjin University* **2021**, *27*, 155−164.
(24) Pan, Y.; Qian, Y.; Zheng, X.; Chu, S.-Q.; Yang, Y.; Ding, C.; Wang, X.; Yu, S.-H.; Jiang, H.-L. Precise fabrication of single-atom alloy co-catalyst with optimal charge state for enhanced photocatalysis. *Nat. Sci. Rev.* **2021**, *8*, No. nwaa224.
(25) Ye, D.; Liu, L.; Peng, Q.; Qiu, J.; Gong, H.; Zhong, A.; Liu, S. Effect of Controlling Thiophene Rings on D-A Polymer Photocatalysts Accessed via Direct Arylation for Hydrogen Production. *Molecules* **2023**, *28*, 4507.
(26) Cao, L.; Chen, D.; Li, W.; Caruso, R. A. Hierarchically Porous Titania Networks with Tunable Anatase:Rutile Ratios and Their Enhanced Photocatalytic Activities. *ACS Appl. Mater. Interfaces* **2014**, *6*, 13129−13137.
(27) Tan, J. Z. Y.; Nursam, N. M.; Xia, F.; Sani, M.-A.; Li, W.; Wang, X.; Caruso, R. A. High-Performance Coral Reef-like Carbon Nitrides: Synthesis and Application in Photocatalysis and Heavy Metal Ion Adsorption. *ACS Appl. Mater. Interfaces* **2017**, *9*, 4540−4547.
(28) Raizada, P.; Sudhaik, A.; Patial, S.; Hasija, V.; Parwaz Khan, A. A.; Singh, P.; Gautam, S.; Kaur, M.; Nguyen, V.-H. Engineering nanostructures of CuO-based photocatalysts for water treatment: Current progress and future challenges. *Arabian Journal of Chemistry* **2020**, *13*, 8424−8457.
(29) Yu, Y.; Cao, C.; Li, W.; Li, P.; Qu, J.; Song, W. Low-cost synthesis of robust anatase polyhedral structures with a preponderance of exposed {001} facets for enhanced photoactivities. *Nano Research* **2012**, *5*, 434−442.
(30) Zhao, Y.; Zhang, S.; Shi, R.; Waterhouse, G. I. N.; Tang, J.; Zhang, T. Two-dimensional photocatalyst design: A critical review of recent experimental and computational advances. *Mater. Today* **2020**, *34*, 78−91.
(31) Sun, S.; Wang, W.; Li, D.; Zhang, L.; Jiang, D. Solar Light Driven Pure Water Splitting on Quantum Sized BiVO4 without any Cocatalyst. *ACS Catal.* **2014**, *4*, 3498−3503.
(32) Low, J.; Yu, J.; Jaroniec, M.; Wageh, S.; Al-Ghamdi, A. A. Heterojunction Photocatalysts. *Adv. Mater.* **2017**, *29*, No. 1601694.
(33) Li, R.; Zhang, F.; Wang, D.; Yang, J.; Li, M.; Zhu, J.; Zhou, X.; Han, H.; Li, C. Spatial separation of photogenerated electrons and holes among {010} and {110} crystal facets of BiVO4. *Nat. Commun.* **2013**, *4*, 1432.
(34) Liu, X.; Gao, S.; Xu, H.; Lou, Z.; Wang, W.; Huang, B.; Dai, Y. Green synthetic approach for Ti3+ self-doped TiO2−x nanoparticles with efficient visible light photocatalytic activity. *Nanoscale* **2013**, *5*, 1870−1875.
(35) Zhang, X.; Zhang, L. Electronic and Band Structure Tuning of Ternary Semiconductor Photocatalysts by Self Doping: The Case of BiOI. *J. Phys. Chem. C* **2010**, *114*, 18198−18206.
(36) Huang, H.; Li, X.; Wang, J.; Dong, F.; Chu, P. K.; Zhang, T.; Zhang, Y. Anionic Group Self-Doping as a Promising Strategy: Band-Gap Engineering and Multi-Functional Applications of High-Performance CO32−-Doped Bi2O2CO3. *ACS Catal.* **2015**, *5*, 4094−4103.
(37) Wang, J.; Xia, Y.; Dong, Y.; Chen, R.; Xiang, L.; Komarneni, S. Defect-rich ZnO nanosheets of high surface area as an efficient visible-light photocatalyst. *Applied Catalysis B: Environmental* **2016**, *192*, 8−16.
(38) Bai, S.; Zhang, N.; Gao, C.; Xiong, Y. Defect engineering in photocatalytic materials. *Nano Energy* **2018**, *53*, 296−336.
(39) Zheng, Y.; Fu, K.; Yu, Z.; Su, Y.; Han, R.; Liu, Q. Oxygen vacancies in a catalyst for VOCs oxidation: synthesis, characterization, and catalytic effects. *Journal of Materials Chemistry A* **2022**, *10*, 14171−14186.
(40) Yu, H.; Shi, R.; Zhao, Y.; Bian, T.; Zhao, Y.; Zhou, C.; Waterhouse, G. I. N.; Wu, L.-Z.; Tung, C.-H.; Zhang, T. Alkali-Assisted Synthesis of Nitrogen Deficient Graphitic Carbon Nitride with Tunable Band Structures for Efficient Visible-Light-Driven Hydrogen Evolution. *Adv. Mater.* **2017**, *29*, No. 1605148.
(41) Liu, J.; Wei, Z.; Shangguan, W. Defects Engineering in Photocatalytic Water Splitting Materials. *ChemCatChem.* **2019**, *11*, 6177−6189.
(42) Wang, Y.; Zhang, J.; Balogun, M. S.; Tong, Y.; Huang, Y. Oxygen vacancy−based metal oxides photoanodes in photoelectrochemical water splitting. *Materials Today Sustainability* **2022**, *18*, No. 100118.
(43) Zhang, Y.-C.; Li, Z.; Zhang, L.; Pan, L.; Zhang, X.; Wang, L.; Fazal-e-Aleem; Zou, J.-J. Role of oxygen vacancies in photocatalytic water oxidation on ceria oxide: Experiment and DFT studies. *Appl. Catal. B: Environ.* **2018**, *224*, 101−108.
(44) Gurylev, V.; Perng, T. P. Defect engineering of ZnO: Review on oxygen and zinc vacancies. *Journal of the European Ceramic Society* **2021**, *41*, 4977−4996.
(45) Huang, Y.; Yu, Y.; Yu, Y.; Zhang, B. Oxygen Vacancy Engineering in Photocatalysis. *Solar RRL* **2020**, *4*, No. 2000037.
(46) Kumar, A.; Krishnan, V. Vacancy Engineering in Semiconductor Photocatalysts: Implications in Hydrogen Evolution and Nitrogen Fixation Applications. *Adv. Funct. Mater.* **2021**, *31*, No. 2009807.
(47) Zhuang, G.; Chen, Y.; Zhuang, Z.; Yu, Y.; Yu, J. Oxygen vacancies in metal oxides: recent progress towards advanced catalyst design. *Science China Materials* **2020**, *63*, 2089−2118.
(48) Zhao, S.; Yang, Y.; Bi, F.; Chen, Y.; Wu, M.; Zhang, X.; Wang, G. Oxygen vacancies in the catalyst: Efficient degradation of gaseous pollutants. *Chemical Engineering Journal* **2023**, *454*, No. 140376.
(49) Li, H.; Li, J.; Ai, Z.; Jia, F.; Zhang, L. Oxygen Vacancy-Mediated Photocatalysis of BiOCl: Reactivity, Selectivity, and Perspectives. *Angew. Chem., Int. Ed.* **2018**, *57*, 122−138.
(50) Dong, X.; Li, Y.; Li, D.; Liao, D.; Qin, T.; Prakash, O.; Kumar, A.; Liu, J. A new 3D 8-connected Cd(ii) MOF as a potent photocatalyst for oxytetracycline antibiotic degradation. *CrystEngComm* **2022**, *24*, 6933−6943.
(51) Khalaf, H. A.-F.; El-Baki, R. F. A. Effectiveness of Ceria and Stania Nanoparticles in Photodegradation Tenoxicam Antibiotics Using UV-H2O2. *Iran. J. Catal.* **2023**, *13*, 285−297.
(52) Aghdasi, S.; Shokri, M. Photocatalytic degradation of ciprofloxacin in the presence of synthesized ZnO nanocatalyst: The effect of operational parameters. *Iran. J. Catal.* **2016**, *6*, 481−487.
(53) Montalvo, C.; Gines, R. S.; Cantu, D.; Ruiz, A.; Aguilar, C. A.; Perez, I.; Ceron, R. M. Fluidized bed photoreactor for the removal of acetaminophen and pyridine using Al-doped TiO2 supported on alumina. *Iran. J. Catal.* **2022**, *12*, 295−313.
(54) El Bekkali, C.; Bouyarmane, H.; Laasri, S.; Laghzizil, A.; Saoiabi, A. Effects of metal oxide catalysts on the photodegradation of antibiotics effluent. *Iran. J. Catal.* **2018**, *8*, 241−247.
(55) Rao, C.; Zhou, L.; Pan, Y.; Lu, C.; Qin, X.; Sakiyama, H.; Muddassir, M.; Liu, J. The extra-large calixarene-based MOFs-derived hierarchical composites for photocatalysis of dye: Facile syntheses and contribution of carbon species. *J. Alloys Compd.* **2022**, *897*, No. 163178.
(56) Wang, J.; Rao, C.; Lu, L.; Zhang, S.; Muddassir, M.; Liu, J. Efficient photocatalytic degradation of methyl violet using two new 3D MOFs directed by different carboxylate spacers. *CrystEngComm* **2021**, *23*, 741−747.
(57) Allawi Abdul Sajad, F.; Egzar, H. K.; Mahdi, M. A. Preparation and Characterization of WO3 Nanosheets and Au/WO3 Nano-

https://doi.org/10.1021/acsomega.3c07560
ACS Omega 2024, 9, 6093−6127

composite for Rabid Photocatalytic degradation of methylene blue dye. *Iran. J. Catal.* **2023**, *13*, 319−330.
(58) Jasni, N.; Iqbal, A.; Abu Bakar, N. H. H.; Yuli Yanto, D. H.; Jia Yi, H.; Mohd Kaus, N. H.; Ahmad, M. N.; Mulijani, S. Highly Porous Bi(III) Modified Rice Husk Silica Photocatalyst for the Photocatalytic Removal of Cationic Methylene Blue. *Iran. J. Catal.* **2023**, *13*, 359−372.
(59) Wahyuni, E. T.; Wahyuni, S.; Nora, M.; Lestari, N. D.; Suherman, S. Doping TiO2 by Cr from tannery wastewater for improving its activity under visible light in the dye degradation. *Iran. J. Catal.* **2023**, *13*, 169−176.
(60) Zhang, Y.; Wang, T.; Zheng, B.; Shi, J.; Cai, C.; Mao, L.; Cheng, C.; Zong, S.; Guo, X.; Chen, Q. EDTA-dominated hollow tube-like porous graphitic carbon nitride towards enhanced photocatalytic hydrogen evolution. *J. Colloid Interface Sci.* **2022**, *619*, 289−297.
(61) Lin, S.; Zhao, Y.; Yun, Y.-S. Highly Effective Removal of Nonsteroidal Anti-inflammatory Pharmaceuticals from Water by Zr(IV)-Based Metal−Organic Framework: Adsorption Performance and Mechanisms. *ACS Appl. Mater. Interfaces* **2018**, *10*, 28076−28085.
(62) Li, L.; Zou, J.; Han, Y.; Liao, Z.; Lu, P.; Nezamzadeh-Ejhieh, A.; Liu, J.; Peng, Y. Recent advances in Al(iii)/In(iii)-based MOFs for the detection of pollutants. *New J. Chem.* **2022**, *46*, 19577−19592.
(63) Ghiaci, M.; Sedaghat, M. E.; Aghaei, H.; Gil, A. Synthesis of CdS- and ZnS-modified bentonite nanoparticles and their applications to the degradation of eosin B. *J. Chem. Technol. Biotechnol.* **2009**, *84*, 1908−1915.
(64) Thaninki, L. V.; Samson Nesaraj, A.; Arunkumar, M. Facile wet chemical synthesis and characterization of zinc doped gadolinium oxide nanoparticles for enhanced photodegradation of Rhodamine B dye under illumination of UV light. *Iran. J. Catal.* **2022**, *12*, 315−336.
(65) Wei, L.; Li, H.; Lu, J. Algae-induced photodegradation of antibiotics: A review. *Environ. Pollut.* **2021**, *272*, No. 115589.
(66) Selmi, A.; Teymourinia, H.; Zarei, A.; Timoumi, M.; Ramazani, A. CMCFO-Cr0.1 Nanoferrites: Sol-gel Synthesis, Structural, and Magnetic Studies: Applications for Photodegradation of Congo Red Dye. *Iran. J. Catal.* **2022**, *12*, 97−106.
(67) Seyedi-Chokanlou, T.; Aghabeygi, S.; Molahasani, N.; Abrinaei, F. Applying Taguchi method to optimize the synthesis conditions of ZrO2/TiO2/ZnO nanocomposite for high-performance photodegradation of Congo red. *Iran. J. Catal.* **2021**, *11*, 49−58.
(68) Gičević, A.; Hindija, L.; Karačić, A. Toxicity of azo dyes in pharmaceutical industry. *IFMBE Proc.* **2020**, *73*, 581−587.
(69) Benaouda, S.N.; Chaker, H.; Abidallah, F.; Bachir, C.; Tawheed, H.; Weidler, P.G.; Bengueddach, A.; Canales-Vázquez, J.; Hamacha, R. Heterogeneous photocatalytic degradation of anionic dye on polyaniline/microcrystalline cellulose composite. *J. Porous Mater.* **2023**, *30*, 327−341.
(70) Chaker, H.; Attar, A. E.; Djennas, M.; Fourmentin, S. A statistical modeling-optimization approach for efficiency photocatalytic degradation of textile azo dye using cerium-doped mesoporous ZnO: A central composite design in response surface methodology. *Chem. Eng. Res. Des.* **2021**, *171*, 198−212.
(71) Rehman, F. U.; Zahra, M.; Qayyum, I.; Raza, A.; Waseem, A. Optimization of Photo Catalytic Activity of ZnO Nano Composites by Surface Modification with Cu metal using Facile Hydrothermal Approach. *Iran J. Catal.* **2022**, *12*, 25−44.
(72) Wang, J. L.; Xu, L. J. Advanced Oxidation Processes for Wastewater Treatment: Formation of Hydroxyl Radical and Application. *Critical Reviews in Environmental Science and Technology* **2012**, *42*, 251−325.
(73) Rehman, F.; Sayed, M.; Khan, J. A.; Shah, N. S.; Khan, H. M.; Dionysiou, D. D. Oxidative removal of brilliant green by UV/S2O82−, UV/HSO5− and UV/H2O2 processes in aqueous media: A comparative study. *Journal of Hazardous Materials* **2018**, *357*, 506−514.
(74) Ren, W.; Nie, G.; Zhou, P.; Zhang, H.; Duan, X.; Wang, S. The Intrinsic Nature of Persulfate Activation and N-Doping in Carbocatalysis. *Environ. Sci. Technol.* **2020**, *54*, 6438−6447.
(75) Pourshirband, N.; Nezamzadeh-Ejhieh, A. The boosted activity of AgI/BiOI nanocatalyst: a RSM study towards Eriochrome Black T photodegradation. *Environmental Science and Pollution Research* **2022**, *29*, 45276−45291.
(76) Nouhad, R.; Nazir, R.; Djaballah, Y.; Mir, A.; Ameur, I.; Beldjebli, O. Synthesis of a thin film of CuO/MgO/PVC nanocomposites for Photocatalytic applications. *Iran. J. Catal.* **2023**, *13*, 23−34.
(77) Yaghoubi-berijani, M.; bahramian, b.; Zargari, S. The Study of Photocatalytic Degradation Mechanism under Visible Light Irradiation on BiOBr/Ag Nanocomposite. *Iran. J. Catal.* **2020**, *10*, 307−317.
(78) Sanakousar, F. M.; Vidyasagar, C. C.; Swapna, S. C.; Jiménez-Pérez, V. M.; Viswanath, C. C.; Prakash, K.; Sridhara, M. B. Effect of surfactant on structural and optical properties of V2O5 nanocrystals as a potential catalyst for photodegradation. *Iran. J. Catal.* **2023**, *13*, 57−72.
(79) Rafiq, A.; Ikram, M.; Ali, S.; Niaz, F.; Khan, M.U.; Khan, Q.S.; Maqbool, M. Photocatalytic degradation of dyes using semiconductor photocatalysts to clean industrial water pollution. *J. Ind. Eng. Chem.* **2021**, *97*, 111−128.
(80) Hemmatpour, P.; Nezamzadeh-Ejhieh, A. A Z-scheme CdS/BiVO4 photocatalysis towards Eriochrome black T: An experimental design and mechanism study. *Chemosphere* **2022**, *307*, No. 135925.
(81) Tran, Q. T. B.; Pham, D. H.; Ngo, M. N. T.; Pham, T. D.; Doan, T. V. H.; Luong, T. H. V. Cuprous oxide nanocubes functionalized with graphene quantum dots and its application for methylene blue degradation. *Iran. J. Catal.* **2022**, *12*, 85−95.
(82) Oliver, B.G.; Carey, J.H., Photodegradation of Wastes and Pollutants in Aquatic Environment. In *Homogeneous and Heterogeneous Photocatalysis*; Pelizzetti, E., Serpone, N., Eds.; Springer Netherlands: Dordrecht, Netherlands, 1986; pp 629−650.
(83) Yousefi, A.; Nezamzadeh-Ejhieh, A. Preparation and characterization of SnO2-BiVO4-CuO catalyst and kinetics of phenazopyridine photodegradation. *Iran. J. Catal.* **2021**, *11*, 247−259.
(84) Alikhani, M. R.; Saviz, S.; Sari, A. H. Synthesis and Characterization ZnO-Fe2O3 Nanocomposite with Thermal Plasma Method. *Iran. J. Catal.* **2022**, *12*, 181−188.
(85) Kangralkar, M. V.; Jayappa, M. Green synthesis of iron nanoparticles by Terminalia arjuna bark extract and photodegradation of rose bengal. *Iran. J. Catal.* **2020**, *10*, 181−188.
(86) Parul; Kaur, K.; Badru, R.; Singh, P. P.; Kaushal, S. Photodegradation of organic pollutants using heterojunctions: A review. *J. Environ. Chem. Eng.* **2020**, *8*, No. 103666.
(87) Ajmal, A.; Majeed, I.; Malik, R. N.; Idriss, H.; Nadeem, M. A. Principles and mechanisms of photocatalytic dye degradation on TiO2 based photocatalysts: a comparative overview. *RSC Adv.* **2014**, *4*, 37003−37026.
(88) Rezaei, B.; Soleimany, R.; Ensafi, A. A.; Irannejad, N. Photocatalytic degradation enhancements of dyes with bi-functionalized zones of modified nanoflower like TiO2 with Pt-C3N4 under sunlight irradiation. *Journal of Environmental Chemical Engineering* **2018**, *6*, 7010−7020.
(89) Khayyami, D.; Ensafi, A. A.; Kazemifard, N.; Rezaei, B. The investigation of Amido black 10B adsorption-photocatalytic degradation using the synergistic effect of Cr-doped ZnO/CDs nanocomposite under solar light. *Environmental Science and Pollution Research* **2020**, *27*, 8759−8771.
(90) Touati, A.; Hammedi, T.; Najjar, W.; Ksibi, Z.; Sayadi, S. Photocatalytic degradation of textile wastewater in presence of hydrogen peroxide: Effect of cerium doping titania. *Journal of Industrial and Engineering Chemistry* **2016**, *35*, 36−44.
(91) Gómez-Pastora, J.; Dominguez, S.; Bringas, E.; Rivero, M. J.; Ortiz, I.; Dionysiou, D. D. Review and perspectives on the use of magnetic nanophotocatalysts (MNPCs) in water treatment. *Chemical Engineering Journal* **2017**, *310*, 407−427.
(92) Pouretedal, H. R.; Fallahgar, M.; Sotoudeh Pourhasan, F.; Nasiri, M. Taguchi optimization of photodegradation of yellow water of trinitrotoluene production catalyzed by nanoparticles TiO2/N under visible light. *Iran. J. Catal.* **2017**, *7*, 317−326.
(93) Arunkumar, M.; Nesaraj, A. S. Photocatalytic degradation of malachite green dye using NiAl2O4 and Co doped NiAl2O4

https://doi.org/10.1021/acsomega.3c07560
ACS Omega 2024, 9, 6093−6127

nanophotocatalysts prepared by simple one pot wet chemical synthetic route. *Iran. J. Catal.* **2020**, *10*, 235−245.
(94) Pouretedal, H. R.; Ahmadi, M. Preparation, characterization and determination of photocatalytic activity of MCM-41/ZnO and MCM-48/ZnO nanocomposites. *Iran. J. Catal.* **2013**, *3*, 149−155.
(95) Bahranifard, A. Application of TiO2−zeolite as photocatalyst for photodegradation of some organic pollutants. *Iran. J. Catal.* **2011**, *1*, 45−50.
(96) Pouretedal, H. R.; Basati, S. Synthesis, characterization and photocatalytic activity of CeO2-SBA-15. *Iran. J. Catal.* **2012**, *2*, 51−55.
(97) Bagheri Ghomi, A.; Ashayeri, V. Photocatalytic efficiency of CuFe2O4 by supporting on clinoptilolite in the decolorization of acid red 206 aqueous solutions. *Iran. J. Catal.* **2012**, *2*, 135−140.
(98) Nezamzadeh-Ejhieh, A.; Banan, Z. Kinetic investigation of photocatalytic degradation of dimethyldisulfide by zeolite A containing nano CdS. *Iran. J. Catal.* **2012**, *2*, 79−83.
(99) Mahadadalkar, M. A.; Gosavi, S. W.; Kale, B. B. Interstitial charge transfer pathways in a TiO2/CdIn2S4 heterojunction photocatalyst for direct conversion of sunlight into fuel. *Journal of Materials Chemistry A* **2018**, *6*, 16064−16073.
(100) Shabanian-Boroujeni, E.; Nezamzadeh-Ejhieh, A. The coupled WO3-AgBr nanocatalyst, part I: Experimental design, kinetics and mechanism studies of the boosted photocatalytic activity towards metronidazole in an aqueous solution. *J. Photochem. Photobiol., A* **2024**, *446*, No. 115148.
(101) Xu, J.; Wang, Y.; Weng, C.; Bai, W.; Jiao, Y.; Kaegi, R.; Lowry, G. V. Reactivity, Selectivity, and Long-Term Performance of Sulfidized Nanoscale Zerovalent Iron with Different Properties. *Environ. Sci. Technol.* **2019**, *53*, 5936−5945.
(102) Zhu, M.; Tang, Y.; Chen, X.; Liao, B.; Yu, Y.; Hou, S.; Fan, X. Internal electric field and oxygen vacancies synergistically optimized Ba2+ doped SrBi2B2O7 for photocatalytic tetracycline degradation from water. *Chemical Engineering Journal* **2022**, *433*, No. 134580.
(103) Yang, J.-X.; Yu, W.-B.; Li, C.-F.; Dong, W.-D.; Jiang, L.-Q.; Zhou, N.; Zhuang, Z.-P.; Liu, J.; Hu, Z.-Y.; Zhao, H.; et al. PtO nanodots promoting Ti3C2MXene in-situ converted Ti3C2/TiO2 composites for photocatalytic hydrogen production. *Chem. Eng. J.* **2021**, *420*, No. 129695.
(104) Zhao, H.; Li, C.-F.; Hu, Z.-Y.; Liu, J.; Li, Y.; Hu, J.; Van Tendeloo, G.; Chen, L.-H.; Su, B.-L. Size effect of bifunctional gold in hierarchical titanium oxide-gold-cadmium sulfide with slow photon effect for unprecedented visible-light hydrogen production. *J. Colloid Interface Sci.* **2021**, *604*, 131−140.
(105) Deng, X.; Chen, Y.; Wen, J.; Xu, Y.; Zhu, J.; Bian, Z. Polyaniline-TiO2 composite photocatalysts for light-driven hexavalent chromium ions reduction. *Science bulletin* **2020**, *65* (2), 105−112.
(106) Ida, S.; Kim, N.; Ertekin, E.; Takenaka, S.; Ishihara, T. Photocatalytic Reaction Centers in Two-Dimensional Titanium Oxide Crystals. *J. Am. Chem. Soc.* **2015**, *137*, 239−244.
(107) Ren, P.; Song, M.; Lee, J.; Zheng, J.; Lu, Z.; Engelhard, M.; Yang, X.; Li, X.; Kisailus, D.; Li, D. Edge dislocations induce improved photocatalytic efficiency of colored TiO2. *Adv. Mater. Int.* **2019**, *6*, No. 1901121.
(108) Liu, M.; Jing, D.; Zhou, Z.; Guo, L. Twin-induced one-dimensional homojunctions yield high quantum efficiency for solar hydrogen generation. *Nat. Commun.* **2013**, *4*, 2278.
(109) Liu, F.; Shi, R.; Wang, Z.; Weng, Y.; Che, C. M.; Chen, Y. Direct Z-scheme hetero-phase junction of black/red phosphorus for photocatalytic water splitting. *Angew. Chem.* **2019**, *131*, 11917−11921.
(110) Wang, Y.; Cai, J.; Wu, M.; Chen, J.; Zhao, W.; Tian, Y.; Ding, T.; Zhang, J.; Jiang, Z.; Li, X. Rational construction of oxygen vacancies onto tungsten trioxide to improve visible light photocatalytic water oxidation reaction. *Applied Catalysis B: Environmental* **2018**, *239*, 398−407.
(111) He, Y.; Lei, Q.; Li, C.; Han, Y.; Shi, Z.; Feng, S. Defect engineering of photocatalysts for solar-driven conversion of CO2 into valuable fuels. *Mater. Today* **2021**, *50*, 358−384.
(112) Kudo, A.; Miseki, Y. Heterogeneous photocatalyst materials for water splitting. *Chem. Soc. Rev.* **2009**, *38*, 253−278.
(113) Zhang, K.; Zhou, W.; Chi, L.; Zhang, X.; Hu, W.; Jiang, B.; Pan, K.; Tian, G.; Jiang, Z. Black N/H-TiO2 Nanoplates with a Flower-Like Hierarchical Architecture for Photocatalytic Hydrogen Evolution. *ChemSusChem* **2016**, *9*, 2841−2848.
(114) Liu, Y.; Xiao, C.; Li, Z.; Xie, Y. Vacancy Engineering for Tuning Electron and Phonon Structures of Two-Dimensional Materials. *Adv. Energy Mater.* **2016**, *6*, No. 1600436.
(115) Kato, K.; Uemura, Y.; Asakura, K.; Yamakata, A. Role of Oxygen Vacancy in the Photocarrier Dynamics of WO3 Photocatalysts: The Case of Recombination Centers. *J. Phys. Chem. C* **2022**, *126*, 9257−9263.
(116) Wu, P.; Wang, J.; Zhao, J.; Guo, L.; Osterloh, F. E. Structure defects in g-C3N4 limit visible light driven hydrogen evolution and photovoltage. *Journal of Materials Chemistry A* **2014**, *2*, 20338−20344.
(117) Jiang, W.; Loh, H.; Low, B. Q. L.; Zhu, H.; Low, J.; Heng, J. Z. X.; Tang, K. Y.; Li, Z.; Loh, X. J.; Ye, E.; Xiong, Y. Role of oxygen vacancy in metal oxides for photocatalytic CO2 reduction. *Applied Catalysis B: Environmental* **2023**, *321*, No. 122079.
(118) Gan, J.; Lu, X.; Wu, J.; Xie, S.; Zhai, T.; Yu, M.; Zhang, Z.; Mao, Y.; Wang, S. C. I.; Shen, Y.; Tong, Y. Oxygen vacancies promoting photoelectrochemical performance of In2O3 nanocubes. *Sci. Rep* **2013**, *3*, 1021.
(119) Jia, S.; Gao, J.; Shen, Q.; Xue, J.; Zhang, Z.; Liu, X.; Jia, H. Effect of Oxygen Vacancy Concentration on the Photocatalytic Hydrogen Evolution Performance of Anatase TiO2: DFT and Experimental Studies. *J. Mater. Sci.: Mater. Electron.* **2021**, *32*, 13369−13381.
(120) Yu, H.; Li, J.; Zhang, Y.; Yang, S.; Han, K.; Dong, F.; Ma, T.; Huang, H. Three-in-One Oxygen Vacancies: Whole Visible-Spectrum Absorption, Efficient Charge Separation, and Surface Site Activation for Robust CO2 Photoreduction. *Angew. Chem., Int. Ed.* **2019**, *58*, 3880−3884.
(121) Kong, M.; Li, Y.; Chen, X.; Tian, T.; Fang, P.; Zheng, F.; Zhao, X. Tuning the Relative Concentration Ratio of Bulk Defects to Surface Defects in TiO2 Nanocrystals Leads to High Photocatalytic Efficiency. *J. Am. Chem. Soc.* **2011**, *133*, 16414−16417.
(122) Yan, J.; Wu, G.; Guan, N.; Li, L.; Li, Z.; Cao, X. Understanding the effect of surface/bulk defects on the photocatalytic activity of TiO2: anatase versus rutile. *Phys. Chem. Chem. Phys.* **2013**, *15*, 10978−10988.
(123) Pei, Z.; Weng, S.; Liu, P. Enhanced photocatalytic activity by bulk trapping and spatial separation of charge carriers: A case study of defect and facet mediated TiO2. *Applied Catalysis B: Environmental* **2016**, *180*, 463−470.
(124) Li, Y.; Wu, X.; Ho, W.; Lv, K.; Li, Q.; Li, M.; Lee, S. C. Graphene-induced formation of visible-light-responsive SnO2-Zn2SnO4 Z-scheme photocatalyst with surface vacancy for the enhanced photoreactivity towards NO and acetone oxidation. *Chemical Engineering Journal* **2018**, *336*, 200−210.
(125) Pan, L.; Wang, S.; Mi, W.; Song, J.; Zou, J.-J.; Wang, L.; Zhang, X. Undoped ZnO abundant with metal vacancies. *Nano Energy* **2014**, *9*, 71−79.
(126) Di, J.; Chen, C.; Zhu, C.; Song, P.; Xiong, J.; Ji, M.; Zhou, J.; Fu, Q.; Xu, M.; Hao, W.; Xia, J.; Li, S.; Li, H.; Liu, Z. Bismuth Vacancy-Tuned Bismuth Oxybromide Ultrathin Nanosheets toward Photocatalytic CO2 Reduction. *ACS Appl. Mater. Interfaces* **2019**, *11*, 30786−30792.
(127) Yan, D.; Xia, C.; Zhang, W.; Hu, Q.; He, C.; Xia, B. Y.; Wang, S. Cation Defect Engineering of Transition Metal Electrocatalysts for Oxygen Evolution Reaction. *Adv. Energy Mater.* **2022**, *12*, No. 2202317.
(128) Guo, S.-q.; Hu, Z.; Zhen, M.; Gu, B.; Shen, B.; Dong, F. Insights for optimum cation defects in photocatalysis: A case study of hematite nanostructures. *Applied Catalysis B: Environmental* **2020**, *264*, No. 118506.
(129) Liu, B.; Wang, Y.; Peng, H.-Q.; Yang, R.; Jiang, Z.; Zhou, X.; Lee, C.-S.; Zhao, H.; Zhang, W. Iron Vacancies Induced Bifunctionality in Ultrathin Feroxyhyte Nanosheets for Overall Water Splitting. *Adv. Mater.* **2018**, *30*, No. 1803144.
(130) Bak, T.; Nowotny, M. K.; Sheppard, L. R.; Nowotny, J. Effect of Prolonged Oxidation on Semiconducting Properties of Titanium Dioxide. *J. Phys. Chem. C* **2008**, *112*, 13248−13257.

https://doi.org/10.1021/acsomega.3c07560
ACS Omega 2024, 9, 6093−6127

(131) Sun, C.; Liao, T.; Lu, G. Q.; Smith, S. C. The Role of Atomic Vacancy on Water Dissociation over Titanium Dioxide Nanosheet: A Density Functional Theory Study. *J. Phys. Chem. C* **2012**, *116*, 2477−2482.
(132) Gao, S.; Gu, B.; Jiao, X.; Sun, Y.; Zu, X.; Yang, F.; Zhu, W.; Wang, C.; Feng, Z.; Ye, B.; Xie, Y. Highly Efficient and Exceptionally Durable CO2 Photoreduction to Methanol over Freestanding Defective Single-Unit-Cell Bismuth Vanadate Layers. *J. Am. Chem. Soc.* **2017**, *139*, 3438−3445.
(133) Li, J.; Wu, X.; Pan, W.; Zhang, G.; Chen, H. Vacancy-Rich Monolayer BiO2−x as a Highly Efficient UV, Visible, and Near-Infrared Responsive Photocatalyst. *Angew. Chem., Int. Ed.* **2018**, *57*, 491−495.
(134) Yan, D.; Li, Y.; Huo, J.; Chen, R.; Dai, L.; Wang, S. Defect Chemistry of Nonprecious-Metal Electrocatalysts for Oxygen Reactions. *Adv. Mater.* **2017**, *29*, No. 1606459.
(135) Mao, C.; Wang, J.; Zou, Y.; Li, H.; Zhan, G.; Li, J.; Zhao, J.; Zhang, L. Anion (O, N, C, and S) vacancies promoted photocatalytic nitrogen fixation. *Green Chem.* **2019**, *21*, 2852−2867.
(136) Long, M.; Zheng, L. Engineering vacancies for solar photocatalytic applications. *Chinese Journal of Catalysis* **2017**, *38*, 617−624.
(137) Liu, Y.; Cheng, H.; Lyu, M.; Fan, S.; Liu, Q.; Zhang, W.; Zhi, Y.; Wang, C.; Xiao, C.; Wei, S.; Ye, B.; Xie, Y. Low Overpotential in Vacancy-Rich Ultrathin CoSe2 Nanosheets for Water Oxidation. *J. Am. Chem. Soc.* **2014**, *136*, 15670−15675.
(138) Hu, Y. H. A Highly Efficient Photocatalyst—Hydrogenated Black TiO2 for the Photocatalytic Splitting of Water. *Angew. Chem., Int. Ed.* **2012**, *51*, 12410−12412.
(139) Li, L.; Yan, J.; Wang, T.; Zhao, Z.-J.; Zhang, J.; Gong, J.; Guan, N. Sub-10 nm rutile titanium dioxide nanoparticles for efficient visible-light-driven photocatalytic hydrogen production. *Nat. Commun.* **2015**, *6*, 5881.
(140) Zhang, H.; Cai, J.; Wang, Y.; Wu, M.; Meng, M.; Tian, Y.; Li, X.; Zhang, J.; Zheng, L.; Jiang, Z.; Gong, J. Insights into the effects of surface/bulk defects on photocatalytic hydrogen evolution over TiO2 with exposed {001} facets. *Applied Catalysis B: Environmental* **2018**, *220*, 126−136.
(141) Zhang, N.; Li, X.; Ye, H.; Chen, S.; Ju, H.; Liu, D.; Lin, Y.; Ye, W.; Wang, C.; Xu, Q.; Zhu, J.; Song, L.; Jiang, J.; Xiong, Y. Oxide Defect Engineering Enables to Couple Solar Energy into Oxygen Activation. *J. Am. Chem. Soc.* **2016**, *138*, 8928−8935.
(142) Liu, F.; Leung, Y. H.; Djurisic, A. B.; Ng, A. M. C.; Chan, W. K. Native defects in ZnO: effect on dye adsorption and photocatalytic degradation. *J. Phys. Chem. C* **2013**, *117*, 12218−12228.
(143) Pan, Y.; Liu, C.-j.; Ge, Q. Adsorption and Protonation of CO2 on Partially Hydroxylated γ-Al2O3 Surfaces: A Density Functional Theory Study. *Langmuir* **2008**, *24*, 12410−12419.
(144) Dimitrijevic, N. M.; Vijayan, B. K.; Poluektov, O. G.; Rajh, T.; Gray, K. A.; He, H.; Zapol, P. Role of Water and Carbonates in Photocatalytic Transformation of CO2 to CH4 on Titania. *J. Am. Chem. Soc.* **2011**, *133*, 3964−3971.
(145) Jiang, J.; Zhao, K.; Xiao, X.; Zhang, L. Synthesis and Facet-Dependent Photoreactivity of BiOCl Single-Crystalline Nanosheets. *J. Am. Chem. Soc.* **2012**, *134*, 4473−4476.
(146) Zhu, Y.; Ling, Q.; Liu, Y.; Wang, H.; Zhu, Y. Photocatalytic performance of BiPO4 nanorods adjusted via defects. *Applied Catalysis B: Environmental* **2016**, *187*, 204−211.
(147) Zhang, J.; Chang, X.; Li, C.; Li, A.; Liu, S.; Wang, T.; Gong, J. WO3 photoanodes with controllable bulk and surface oxygen vacancies for photoelectrochemical water oxidation. *Journal of Materials Chemistry A* **2018**, *6*, 3350−3354.
(148) Zhang, K.; Park, J. H. Surface Localization of Defects in Black TiO2: Enhancing Photoactivity or Reactivity. *J. Phys. Chem. Lett.* **2017**, *8*, 199−207.
(149) Liu, Q.; Wang, F.; Lin, H.; Xie, Y.; Tong, N.; Lin, J.; Zhang, X.; Zhang, Z.; Wang, X. Surface oxygen vacancy and defect engineering of WO3 for improved visible light photocatalytic performance. *Catalysis Science & Technology* **2018**, *8*, 4399−4406.
(150) Yu, X.; Kim, B.; Kim, Y. K. Highly Enhanced Photoactivity of Anatase TiO2 Nanocrystals by Controlled Hydrogenation-Induced Surface Defects. *ACS Catal.* **2013**, *3*, 2479−2486.
(151) Wu, Z.; Cao, S.; Zhang, C.; Piao, L. Effects of bulk and surface defects on the photocatalytic performance of size-controlled TiO2 nanoparticles. *Nanotechnology* **2017**, *28*, No. 275706.
(152) Zhang, X.; Zhao, Z.; Zhang, W.; Zhang, G.; Qu, D.; Miao, X.; Sun, S.; Sun, Z. Surface Defects Enhanced Visible Light Photocatalytic H2 Production for Zn-Cd-S Solid Solution. *Small* **2016**, *12*, 793−801.
(153) Jiang, D.; Wang, W.; Zhang, L.; Zheng, Y.; Wang, Z. Insights into the Surface-Defect Dependence of Photoreactivity over CeO2 Nanocrystals with Well-Defined Crystal Facets. *ACS Catal.* **2015**, *5*, 4851−4858.
(154) Shen, Z.; Zhou, Y.; Guo, Y.; Zhao, J.; Song, J.; Xie, Y.; Ling, Y.; Zhang, W. Tuning the concentration of surface/bulk oxygen vacancies in CeO2 nanorods to promote highly efficient photodegradation of organic dyes. *Chin. Chem. Lett.* **2021**, *32*, 2524−2528.
(155) Li, F.; Jiang, X.; Zhao, J.; Zhang, S. Graphene oxide: A promising nanomaterial for energy and environmental applications. *Nano Energy* **2015**, *16*, 488−515.
(156) Tompkins, F. C. Superficial Chemistry and Solid Imperfections. *Nature* **1960**, *186*, 3−6.
(157) Over, H.; Kim, Y. D.; Seitsonen, A.; Wendt, S.; Lundgren, E.; Schmid, M.; Varga, P.; Morgante, A.; Ertl, G. Atomic-scale structure and catalytic reactivity of the RuO2 (110) surface. *Science* **2000**, *287*, 1474−1476.
(158) Jiang, Y.; Wang, S.; Zhang, Y.; Yan, J.; Li, W. Kinetic study of the formation of oxygen vacancy on lanthanum Manganite electrodes. *J. Electrochem. Soc.* **1998**, *145*, 373.
(159) Selim, S.; Pastor, E.; García-Tecedor, M.; Morris, M. R.; Francàs, L.; Sachs, M.; Moss, B.; Corby, S.; Mesa, C. A.; Gimenez, S.; Kafizas, A.; Bakulin, A. A.; Durrant, J. R. Impact of Oxygen Vacancy Occupancy on Charge Carrier Dynamics in BiVO4 Photoanodes. *J. Am. Chem. Soc.* **2019**, *141*, 18791−18798.
(160) Yang, Y.; Yin, L.-C.; Gong, Y.; Niu, P.; Wang, J.-Q.; Gu, L.; Chen, X.; Liu, G.; Wang, L.; Cheng, H.-M. An Unusual Strong Visible-Light Absorption Band in Red Anatase TiO2 Photocatalyst Induced by Atomic Hydrogen-Occupied Oxygen Vacancies. *Adv. Mater.* **2018**, *30*, No. 1704479.
(161) Feng, S.; Wang, T.; Liu, B.; Hu, C.; Li, L.; Zhao, Z. J.; Gong, J. Enriched surface oxygen vacancies of photoanodes by photoetching with enhanced charge separation. *Angew. Chem.* **2020**, *132*, 2060−2064.
(162) An, X.; Zhang, L.; Wen, B.; Gu, Z.; Liu, L.-M.; Qu, J.; Liu, H. Boosting photoelectrochemical activities of heterostructured photoanodes through interfacial modulation of oxygen vacancies. *Nano Energy* **2017**, *35*, 290−298.
(163) Zhang, B.; Liu, P.; Li, Z.; Song, X. Synthesis of Two-Dimensional Sr-Doped LaNiO3 Nanosheets with Improved Electrochemical Performance for Energy Storage. *Nanomaterials* **2021**, *11* (1), 155.
(164) Xu, L.; Jiang, Q.; Xiao, Z.; Li, X.; Huo, J.; Wang, S.; Dai, L. Plasma-engraved Co3O4 nanosheets with oxygen vacancies and high surface area for the oxygen evolution reaction. *Angew. Chem.* **2016**, *128*, 5363−5367.
(165) Wang, G.; Ling, Y.; Li, Y. Oxygen-deficient metal oxide nanostructures for photoelectrochemical water oxidation and other applications. *Nanoscale* **2012**, *4*, 6682−6691.
(166) Bonke, S. A.; Wiechen, M.; MacFarlane, D. R.; Spiccia, L. Renewable fuels from concentrated solar power: towards practical artificial photosynthesis. *Energy Environ. Sci.* **2015**, *8*, 2791−2796.
(167) Badmus, K. O.; Wewers, F.; Al-Abri, M.; Shahbaaz, M.; Petrik, L. F. Synthesis of oxygen deficient TiO2 for improved photocatalytic efficiency in solar radiation. *Catalysts* **2021**, *11*, 904.
(168) Bhardwaj, A.; Kaur, J.; Wuest, M.; Wuest, F. In situ click chemistry generation of cyclooxygenase-2 inhibitors. *Nat. Commun.* **2017**, *8*, 1.

https://doi.org/10.1021/acsomega.3c07560
ACS Omega 2024, 9, 6093−6127

(169) Dou, S.; Tao, L.; Wang, R.; El Hankari, S.; Chen, R.; Wang, S. Plasma-Assisted Synthesis and Surface Modification of Electrode Materials for Renewable Energy. *Adv. Mater.* **2018**, *30*, No. 1705850.
(170) Liang, H.; Gandi, A. N.; Anjum, D. H.; Wang, X.; Schwingenschlögl, U.; Alshareef, H. N. Plasma-Assisted Synthesis of NiCoP for Efficient Overall Water Splitting. *Nano Lett.* **2016**, *16*, 7718−7725.
(171) Osorio-Vargas, P. A.; Pulgarin, C.; Sienkiewicz, A.; Pizzio, L. R.; Blanco, M. N.; Torres-Palma, R. A.; Pétrier, C.; Rengifo-Herrera, J. A. Low-frequency ultrasound induces oxygen vacancies formation and visible light absorption in TiO2 P-25 nanoparticles. *Ultrasonics Sonochemistry* **2012**, *19*, 383−386.
(172) Di Valentin, C.; Pacchioni, G.; Selloni, A.; Livraghi, S.; Giamello, E. Characterization of Paramagnetic Species in N-Doped TiO2 Powders by EPR Spectroscopy and DFT Calculations. *J. Phys. Chem. B* **2005**, *109*, 11414−11419.
(173) Guan, M.; Xiao, C.; Zhang, J.; Fan, S.; An, R.; Cheng, Q.; Xie, J.; Zhou, M.; Ye, B.; Xie, Y. Vacancy Associates Promoting Solar-Driven Photocatalytic Activity of Ultrathin Bismuth Oxychloride Nanosheets. *J. Am. Chem. Soc.* **2013**, *135*, 10411−10417.
(174) Tan, H.; Zhao, Z.; Niu, M.; Mao, C.; Cao, D.; Cheng, D.; Feng, P.; Sun, Z. A facile and versatile method for preparation of colored TiO2 with enhanced solar-driven photocatalytic activity. *Nanoscale* **2014**, *6*, 10216−10223.
(175) Chen, Y.; Yang, W.; Gao, S.; Sun, C.; Li, Q. Synthesis of Bi2MoO6 Nanosheets with Rich Oxygen Vacancies by Postsynthesis Etching Treatment for Enhanced Photocatalytic Performance. *ACS Applied Nano Materials* **2018**, *1*, 3565−3578.
(176) Meng, L.; Ren, Z.; Zhou, W.; Qu, Y.; Wang, G. MgTiO 3/MgTi 2 O 5/TiO 2 heterogeneous belt-junctions with high photocatalytic hydrogen production activity. *Nano Research* **2017**, *10*, 295−304.
(177) Nakamura, I.; Negishi, N.; Kutsuna, S.; Ihara, T.; Sugihara, S.; Takeuchi, K. Role of oxygen vacancy in the plasma-treated TiO2 photocatalyst with visible light activity for NO removal. *J. Mol. Catal. A: Chem.* **2000**, *161*, 205−212.
(178) Wang, X.-j.; Zhao, Y.; Li, F.-t.; Dou, L.-j.; Li, Y.-p.; Zhao, J.; Hao, Y.-j. A chelation strategy for in-situ constructing surface oxygen vacancy on {001} facets exposed BiOBr nanosheets. *Sci. Rep.* **2016**, *6*, 24918.
(179) Xue, J.; Ma, S.; Zhou, Y.; Zhang, Z. Facile synthesis of ZnO−C nanocomposites with enhanced photocatalytic activity. *New J. Chem.* **2015**, *39*, 1852−1857.
(180) Pan, J.-B.; Wang, B.-H.; Wang, J.-B.; Ding, H.-Z.; Zhou, W.; Liu, X.; Zhang, J.-R.; Shen, S.; Guo, J.-K.; Chen, L.; Au, C.-T.; Jiang, L.-L.; Yin, S.-F. Activity and Stability Boosting of an Oxygen-Vacancy-Rich BiVO4 Photoanode by NiFe-MOFs Thin Layer for Water Oxidation. *Angew. Chem., Int. Ed.* **2021**, *60*, 1433−1440.
(181) Yang, J.; Xie, N.; Zhang, J.; Fan, W.; Huang, Y.; Tong, Y. Defect Engineering Enhances the Charge Separation of CeO2 Nanorods toward Photocatalytic Methyl Blue Oxidation. *Nanomaterials* **2020**, *10*, 2307.
(182) Fan, X.; Balogun, M.-S.; Huang, Y.; Tong, Y. Oxygen-Deficient Three-Dimensional Porous Co3O4 Nanowires as an Electrode Material for Water Oxidation and Energy Storage. *ChemElectroChem.* **2017**, *4*, 2453−2459.
(183) Qi, Y.; Song, L.; Ouyang, S.; Liang, X.; Ning, S.; Zhang, Q.; Ye, J. Photoinduced Defect Engineering: Enhanced Photothermal Catalytic Performance of 2D Black In2O3−x Nanosheets with Bifunctional Oxygen Vacancies. *Adv. Mater.* **2020**, *32*, No. 1903915.
(184) Wang, G.; Wang, H.; Ling, Y.; Tang, Y.; Yang, X.; Fitzmorris, R. C.; Wang, C.; Zhang, J. Z.; Li, Y. Hydrogen-treated TiO2 nanowire arrays for photoelectrochemical water splitting. *Nano Lett.* **2011**, *11*, 3026−3033.
(185) Li, P.; Cao, W.; Zhu, Y.; Teng, Q.; Peng, L.; Jiang, C.; Feng, C.; Wang, Y. NaOH-induced formation of 3D flower-sphere BiOBr/Bi4O5Br2 with proper-oxygen vacancies via in-situ self-template phase transformation method for antibiotic photodegradation. *Science of The Total Environment* **2020**, *715*, No. 136809.
(186) Zhang, X.; Wang, C.; Chen, J.; Zhu, W.; Liao, A.; Li, Y.; Wang, J.; Ma, L. Enhancement of the Field Emission from the TiO2 Nanotube Arrays by Reducing in a NaBH4 Solution. *ACS Appl. Mater. Interfaces* **2014**, *6*, 20625−20633.
(187) Zhang, H.-X.; Zhao, M.; Jiang, Q. Effect of oxygen vacancies on electronic structures and field emission properties of TiO2 nanotubes: A density-functional theory investigation. *Appl. Phys. Lett.* **2013**, *103*, No. 023111.
(188) Xing, M.; Fang, W.; Nasir, M.; Ma, Y.; Zhang, J.; Anpo, M. Self-doped Ti3+-enhanced TiO2 nanoparticles with a high-performance photocatalysis. *J. Catal.* **2013**, *297*, 236−243.
(189) Jeon, I.-Y.; Choi, H.-J.; Jung, S.-M.; Seo, J.-M.; Kim, M.-J.; Dai, L.; Baek, J.-B. Large-Scale Production of Edge-Selectively Functionalized Graphene Nanoplatelets via Ball Milling and Their Use as Metal-Free Electrocatalysts for Oxygen Reduction Reaction. *J. Am. Chem. Soc.* **2013**, *135*, 1386−1393.
(190) Wu, J.; Li, X.; Shi, W.; Ling, P.; Sun, Y.; Jiao, X.; Gao, S.; Liang, L.; Xu, J.; Yan, W.; Wang, C.; Xie, Y. Efficient Visible-Light-Driven CO2 Reduction Mediated by Defect-Engineered BiOBr Atomic Layers. *Angew. Chem., Int. Ed.* **2018**, *57*, 8719−8723.
(191) Huang, Y.; Li, K.; Li, S.; Lin, Y.; Liu, H.; Tong, Y. Ultrathin Bi2MoO6 Nanosheets for Photocatalysis: Performance Enhancement by Atomic Interfacial Engineering. *ChemistrySelect* **2018**, *3*, 7423−7428.
(192) Lei, W.; Yu, Y.; Zhang, H.; Jia, Q.; Zhang, S. Defect engineering of nanostructures: Insights into photoelectrochemical water splitting. *Mater. Today* **2022**, *52*, 133−160.
(193) Khazaee, Z.; Mahjoub, A. R.; Cheshme Khavar, A. H.; Srivastava, V.; Sillanpää, M. Synthesis of layered perovskite Ag,F-Bi2MoO6/rGO: A surface plasmon resonance and oxygen vacancy promoted nanocomposite as a visible-light photocatalyst. *J. Photochem. Photobiol., A* **2019**, *379*, 130−143.
(194) Maarisetty, D.; Baral, S. S. Defect engineering in photocatalysis: formation, chemistry, optoelectronics, and interface studies. *Journal of Materials Chemistry A* **2020**, *8*, 18560−18604.
(195) Huang, Y.; Li, H.; Fan, W.; Zhao, F.; Qiu, W.; Ji, H.; Tong, Y. Defect Engineering of Bismuth Oxyiodide by IO3− Doping for Increasing Charge Transport in Photocatalysis. *ACS Appl. Mater. Interfaces* **2016**, *8*, 27859−27867.
(196) Guo, S.; Liu, M.; You, L.; Cheng, G.; Li, J.; Zhou, K. Oxygen vacancy induced peroxymonosulfate activation by Mg-doped Fe2O3 composites for advanced oxidation of organic pollutants. *Chemosphere* **2021**, *279*, No. 130482.
(197) Xu, K.; Xu, D.; Li, Z.; Zhang, S.; Tong, L.; Peng, J.; Zhang, S.; Shen, J.; Chen, X. Enhanced visible-light photocatalytic degradation of ciprofloxacin hydrochloride by bulk iodine doped BiOCl with rich oxygen vacancy. *Appl. Surf. Sci.* **2022**, *578*, No. 152083.
(198) Zhang, Q.; Nie, W.; Hou, T.; Shen, H.; Li, Q.; Guan, C.; Duan, L.; Zhao, X. Optical and Photocatalytic Properties of Br-Doped BiOCl Nanosheets with Rich Oxygen Vacancies and Dominating {001} Facets. *Nanomaterials* **2022**, *12*, 2423.
(199) Takata, T.; Domen, K. Defect engineering of photocatalysts by doping of aliovalent metal cations for efficient water splitting. *J. Phys. Chem. C* **2009**, *113*, 19386−19388.
(200) Li, J.-h.; Ren, J.; Liu, Y.; Mu, H.-y.; Liu, R.-h.; Zhao, J.; Chen, L.-j.; Li, F.-t. In situ synthesis of Cl-doped Bi2O2CO3 and its enhancement of photocatalytic activity by inducing generation of oxygen vacancies. *Inorganic Chemistry Frontiers* **2020**, *7*, 2969−2978.
(201) Zhang, M.; Wang, J.; Xue, H.; Zhang, J.; Peng, S.; Han, X.; Deng, Y.; Hu, W. Acceptor-Doping Accelerated Charge Separation in Cu2O Photocathode for Photoelectrochemical Water Splitting: Theoretical and Experimental Studies. *Angew. Chem., Int. Ed.* **2020**, *59*, 18463−18467.
(202) Shyamal, S.; Hajra, P.; Mandal, H.; Bera, A.; Sariket, D.; Satpati, A. K.; Malashchonak, M. V.; Mazanik, A. V.; Korolik, O. V.; Kulak, A. I.; Skorb, E. V.; Maity, A.; Streltsov, E. A.; Bhattacharya, C. Eu modified Cu2O thin films: Significant enhancement in efficiency of photoelectrochemical processes through suppression of charge carrier recombination. *Chemical Engineering Journal* **2018**, *335*, 676−684.
(203) Brandt, I. S.; Tumelero, M. A.; Martins, C. A.; Plá Cid, C. C.; Faccio, R.; Pasa, A. A. Defects controlling electrical and optical

https://doi.org/10.1021/acsomega.3c07560
ACS Omega 2024, 9, 6093−6127

properties of electrodeposited Bi doped Cu2O. *J. Appl. Phys.* **2018**, *123*, No. 161412.
(204) Ganesan, K. P.; Anandhan, N.; Gopu, G.; Amaliroselin, A.; Marimuthu, T.; Paneerselvam, R. An enhancement of ferromagnetic, structural, morphological, and optical properties of Mn-doped Cu2O thin films by an electrodeposition technique. *Journal of Materials Science: Materials in Electronics* **2019**, *30*, 19524−19535.
(205) Zhou, W.; Fu, H. Defect-mediated electron−hole separation in semiconductor photocatalysis. *Inorganic Chemistry Frontiers* **2018**, *5*, 1240−1254.
(206) Shi, R.; Ye, H.-F.; Liang, F.; Wang, Z.; Li, K.; Weng, Y.; Lin, Z.; Fu, W.-F.; Che, C.-M.; Chen, Y. Interstitial P-Doped CdS with Long-Lived Photogenerated Electrons for Photocatalytic Water Splitting without Sacrificial Agents. *Adv. Mater.* **2018**, *30*, No. 1705941.
(207) Zhang, L.; Wang, W.; Jiang, D.; Gao, E.; Sun, S. Photoreduction of CO2 on BiOCl nanoplates with the assistance of photoinduced oxygen vacancies. *Nano Research* **2015**, *8*, 821−831.
(208) Li, J.; Li, H.; Zhan, G.; Zhang, L. Solar Water Splitting and Nitrogen Fixation with Layered Bismuth Oxyhalides. *Acc. Chem. Res.* **2017**, *50*, 112−121.
(209) Bora, T.; Sathe, P.; Laxman, K.; Dobretsov, S.; Dutta, J. Defect engineered visible light active ZnO nanorods for photocatalytic treatment of water. *Catal. Today* **2017**, *284*, 11−18.
(210) Zhao, Y.; Zhao, Y.; Shi, R.; Wang, B.; Waterhouse, G. I. N.; Wu, L.-Z.; Tung, C.-H.; Zhang, T. Tuning Oxygen Vacancies in Ultrathin TiO2 Nanosheets to Boost Photocatalytic Nitrogen Fixation up to 700 nm. *Adv. Mater.* **2019**, *31*, No. 1806482.
(211) Chen, S.; Xiao, Y.; Wang, Y.; Hu, Z.; Zhao, H.; Xie, W. A Facile Approach to Prepare Black TiO2 with Oxygen Vacancy for Enhancing Photocatalytic Activity. *Nanomaterials* **2018**, *8*, 245.
(212) Park, S.; Baek, S.; Kim, D.-W.; Lee, S. Oxygen-vacancy-modified brookite TiO2 nanorods as visible-light-responsive photocatalysts. *Mater. Lett.* **2018**, *232*, 146−149.
(213) Wu, S.; Li, X.; Tian, Y.; Lin, Y.; Hu, Y. H. Excellent photocatalytic degradation of tetracycline over black anatase-TiO2 under visible light. *Chemical Engineering Journal* **2021**, *406*, No. 126747.
(214) Rahman, K. H.; Kar, A. K. Role of Bridging Oxygen Vacancy on Reduced Anatase TiO2 (101) for Photodegradation of Rhodamine-B. *ECS Journal of Solid State Science and Technology* **2021**, *10*, No. 116004.
(215) Li, D.; Xu, K.; Niu, Z.; Zhang, C. Annealing and Plasma Effects on the Structural and Photocatalytic Properties of TiO2 Fibers Produced by Electrospinning. *Catalysts* **2022**, *12*, 1441.
(216) Arenas-Hernandez, A.; Zuñiga Islas, C.; Moreno, M.; Calleja Arriaga, W.; Mendoza-Cervantes, J. C.; Carlos, N.; Ascencio-Hurtado, C. R.; Heredia Jiménez, A. Study of Oxygen Vacancies in TiO2 Nanostructures and Their Relationship with Photocatalytic Activity. *Appl. Sci.* **2022**, *12*, 3690.
(217) Zou, Y.; Yang, K.; Chen, Q.; Wang, H.; Meng, X. Molten salt construction of stable oxygen vacancies on TiO2 for enhancement of visible light photocatalytic activity. *RSC Adv.* **2018**, *8*, 36819−36825.
(218) Zhang, K.; Zhou, W.; Zhang, X.; Sun, B.; Wang, L.; Pan, K.; Jiang, B.; Tian, G.; Fu, H. Self-floating amphiphilic black TiO2 foams with 3D macro-mesoporous architectures as efficient solar-driven photocatalysts. *Applied Catalysis B: Environmental* **2017**, *206*, 336−343.
(219) Li, W.; Liang, R.; Hu, A.; Huang, Z.; Zhou, Y. N. Generation of oxygen vacancies in visible light activated one-dimensional iodine TiO2 photocatalysts. *RSC Adv.* **2014**, *4*, 36959−36966.
(220) Wang, M.; Nie, B.; Yee, K.-K.; Bian, H.; Lee, C.; Lee, H. K.; Zheng, B.; Lu, J.; Luo, L.; Li, Y. Y. Low-temperature fabrication of brown TiO2 with enhanced photocatalytic activities under visible light. *Chem. Commun.* **2016**, *52*, 2988−2991.
(221) Badmus, K.O.; Wewers, F.; Al-Abri, M.; Shahbaaz, M.; Petrik, L.F. Synthesis of Oxygen Deficient TiO2 for Improved Photocatalytic Efficiency in Solar Radiation. *Catalysts* **2021**, *11*, 904.
(222) Xie, H.; Li, N.; Chen, X.; Jiang, J.; Zhao, X. Surface oxygen vacancies promoted photodegradation of benzene on TiO2 film. *Appl. Surf. Sci.* **2020**, *511*, No. 145597.
(223) Cao, Y.; Xing, Z.; Shen, Y.; Li, Z.; Wu, X.; Yan, X.; Zou, J.; Yang, S.; Zhou, W. Mesoporous black Ti3+/N-TiO2 spheres for efficient visible-light-driven photocatalytic performance. *Chemical Engineering Journal* **2017**, *325*, 199−207.
(224) Xie, Y.; Hu, D.; Liu, L.; Zhou, P.; Xu, J.; Ling, Y. Oxygen vacancy induced fast lithium storage and efficient organics photodegradation over ultrathin TiO2 nanolayers grafted graphene sheets. *Journal of Hazardous Materials* **2016**, *318*, 551−560.
(225) Alyami, M. Ultra-Violet-Assisted Scalable Method to Fabricate Oxygen-Vacancy-Rich Titanium-Dioxide Semiconductor Film for Water Decontamination under Natural Sunlight Irradiation. *Nanomaterials* **2023**, *13*, 703.
(226) Ni, J.; Wang, W.; Liu, D.; Zhu, Q.; Jia, J.; Tian, J.; Li, Z.; Wang, X.; Xing, Z. Oxygen vacancy-mediated sandwich-structural TiO2−x /ultrathin g-C3N4/TiO2−x direct Z-scheme heterojunction visible-light-driven photocatalyst for efficient removal of high toxic tetracycline antibiotics. *Journal of Hazardous Materials* **2021**, *408*, No. 124432.
(227) Qi, W.; Zhang, F.; An, X.; Liu, H.; Qu, J. Oxygen vacancy modulation of {010}-dominated TiO2 for enhanced photodegradation of Sulfamethoxazole. *Catal. Commun.* **2019**, *118*, 35−38.
(228) Miao, Z.; Wang, G.; Zhang, X.; Dong, X. Oxygen vacancies modified TiO2/Ti3C2 derived from MXenes for enhanced photocatalytic degradation of organic pollutants: The crucial role of oxygen vacancy to schottky junction. *Appl. Surf. Sci.* **2020**, *528*, No. 146929.
(229) Liu, X.; Xing, Z.; Zhang, Y.; Li, Z.; Wu, X.; Tan, S.; Yu, X.; Zhu, Q.; Zhou, W. Fabrication of 3D flower-like black N-TiO2-x@MoS2 for unprecedented-high visible-light-driven photocatalytic performance. *Applied Catalysis B: Environmental* **2017**, *201*, 119−127.
(230) Liu, C.; Xu, C.; Wang, W.; Chen, L.; Li, X.; Wu, Y. Oxygen Vacancy Mediated Band-Gap Engineering via B-Doping for Enhancing Z-Scheme A-TiO2/R-TiO2 Heterojunction Photocatalytic Performance. *Nanomaterials* **2023**, *13*, 794.
(231) Fang, W.; Dappozze, F.; Guillard, C.; Zhou, Y.; Xing, M.; Mishra, S.; Daniele, S.; Zhang, J. Zn-Assisted TiO2−x Photocatalyst with Efficient Charge Separation for Enhanced Photocatalytic Activities. *J. Phys. Chem. C* **2017**, *121*, 17068−17076.
(232) Cushing, S. K.; Meng, F.; Zhang, J.; Ding, B.; Chen, C. K.; Chen, C.-J.; Liu, R.-S.; Bristow, A. D.; Bright, J.; Zheng, P.; Wu, N. Effects of Defects on Photocatalytic Activity of Hydrogen-Treated Titanium Oxide Nanobelts. *ACS Catal.* **2017**, *7*, 1742−1748.
(233) Verma, R.; Samdarshi, S. K. Correlating oxygen vacancies and phase ratio/interface with efficient photocatalytic activity in mixed phase TiO2. *J. Alloys Compd.* **2015**, *629*, 105−112.
(234) Kim, M.; Lee, B.; Ju, H.; Kim, J. Y.; Kim, J.; Lee, S. W. Oxygen-Vacancy-Introduced BaSnO3−δ Photoanodes with Tunable Band Structures for Efficient Solar-Driven Water Splitting. *Adv. Mater.* **2019**, *31*, No. 1903316.
(235) Liu, Y.; Kong, X.; Guo, X.; Li, Q.; Ke, J.; Wang, R.; Li, Q.; Geng, Z.; Zeng, J. Enhanced N2 Electroreduction over LaCoO3 by Introducing Oxygen Vacancies. *ACS Catal.* **2020**, *10*, 1077−1085.
(236) Chen, L.-l.; Zhai, B.-g.; Huang, Y. M. Rendering visible-light photocatalytic activity to undoped ZnO via intrinsic defects engineering. *Catalysts* **2020**, *10*, 1163.
(237) Zhang, Q.; Xu, M.; You, B.; Zhang, Q.; Yuan, H.; Ostrikov, K. Oxygen vacancy-mediated ZnO nanoparticle photocatalyst for degradation of methylene blue. *Applied Sciences* **2018**, *8*, 353.
(238) Liu, D.; Lv, Y.; Zhang, M.; Liu, Y.; Zhu, Y.; Zong, R.; Zhu, Y. Defect-related photoluminescence and photocatalytic properties of porous ZnO nanosheets. *Journal of Materials Chemistry A* **2014**, *2*, 15377−15388.
(239) Lakshmi Prasanna, V.; Vijayaraghavan, R. Insight into the Mechanism of Antibacterial Activity of ZnO: Surface Defects Mediated Reactive Oxygen Species Even in the Dark. *Langmuir* **2015**, *31*, 9155−9162.
(240) Hamdy, M. S.; Yahia, I. S.; Knoff, W.; Story, T. Oxygen-defected ZnO: Facial Synthesis and high photocatalytic performance under visible light. *Optik* **2018**, *158*, 1123−1130.
(241) Guo, H.-L.; Zhu, Q.; Wu, X.-L.; Jiang, Y.-F.; Xie, X.; Xu, A.-W. Oxygen deficient ZnO1−x nanosheets with high visible light photocatalytic activity. *Nanoscale* **2015**, *7*, 7216−7223.

https://doi.org/10.1021/acsomega.3c07560
ACS Omega 2024, 9, 6093−6127

(242) Fang, J.; Fan, H.; Ma, Y.; Wang, Z.; Chang, Q. Surface defects control for ZnO nanorods synthesized by quenching and their anti-recombination in photocatalysis. *Appl. Surf. Sci.* **2015**, *332*, 47−54.
(243) Xia, T.; Wallenmeyer, P.; Anderson, A.; Murowchick, J.; Liu, L.; Chen, X. Hydrogenated black ZnO nanoparticles with enhanced photocatalytic performance. *RSC Adv.* **2014**, *4*, 41654−41658.
(244) Lv, Y.; Yao, W.; Ma, X.; Pan, C.; Zong, R.; Zhu, Y. The surface oxygen vacancy induced visible activity and enhanced UV activity of a ZnO1−x photocatalyst. *Catalysis Science & Technology* **2013**, *3*, 3136−3146.
(245) Xu, Y.; Li, H.; Sun, B.; Qiao, P.; Ren, L.; Tian, G.; Jiang, B.; Pan, K.; Zhou, W. Surface oxygen vacancy defect-promoted electron-hole separation for porous defective ZnO hexagonal plates and enhanced solar-driven photocatalytic performance. *Chemical Engineering Journal* **2020**, *379*, No. 122295.
(246) Zhan, S.; Zhang, H.; Mi, X.; Zhao, Y.; Hu, C.; Lyu, L. Efficient Fenton-like Process for Pollutant Removal in Electron-Rich/Poor Reaction Sites Induced by Surface Oxygen Vacancy over Cobalt−Zinc Oxides. *Environ. Sci. Technol.* **2020**, *54*, 8333−8343.
(247) Zhang, Q.; Zhao, X.; Duan, L.; Shen, H.; Liu, R. Controlling oxygen vacancies and enhanced visible light photocatalysis of CeO2/ZnO nanocomposites. *J. Photochem. Photobiol., A* **2020**, *392*, No. 112156.
(248) Sun, D.; Chi, D.; Yang, Z.; Xing, Z.; Chen, P.; Li, Z.; Pan, K.; Zhou, W. CdS quantum dots modified surface oxygen vacancy defect ZnO1-x-TiO2-x solid solution sphere as Z-Scheme heterojunctions for efficient visible light-driven photothermal-photocatalytic performance. *J. Alloys Compd.* **2020**, *826*, No. 154218.
(249) You, J.; Sun, W.; Su, S.; Ao, Z.; Liu, C.; Yao, G.; Lai, B. Degradation of bisphenol A by peroxymonosulfate activated with oxygen vacancy modified nano-NiO-ZnO composite oxides: A typical surface-bound radical system. *Chemical Engineering Journal* **2020**, *400*, No. 125915.
(250) Lin, L.; Huang, J.; Li, X.; Abass, M. A.; Zhang, S. Effective surface disorder engineering of metal oxide nanocrystals for improved photocatalysis. *Applied Catalysis B: Environmental* **2017**, *203*, 615−624.
(251) Liu, Y.; Wang, R.; Yang, Z.; Du, H.; Jiang, Y.; Shen, C.; Liang, K.; Xu, A. Enhanced visible-light photocatalytic activity of Z-scheme graphitic carbon nitride/oxygen vacancy-rich zinc oxide hybrid photocatalysts. *Chinese Journal of Catalysis* **2015**, *36*, 2135−2144.
(252) Wang, X.; Xu, H.; Zhang, Y.; Ji, X.; Zhang, R. Fructose-regulated ZnO single-crystal nanosheets with oxygen vacancies for photo-degradation of high concentration pollutants and photocatalytic hydrogen evolution. *Ceram. Int.* **2021**, *47*, 16170−16177.
(253) He, W.; Wang, Y.; Fan, C.; Wang, Y.; Zhang, X.; Liu, J.; Li, R. Enhanced charge separation and increased oxygen vacancies of h-BN/OV-BiOCl for improved visible-light photocatalytic performance. *RSC Adv.* **2019**, *9*, 14286−14295.
(254) Jiang, S.; Wang, L.; Hao, W.; Li, W.; Xin, H.; Wang, W.; Wang, T. Visible-Light Photocatalytic Activity of S-Doped α-Bi2O3. *J. Phys. Chem. C* **2015**, *119*, 14094−14101.
(255) Niu, M.; Zhu, R.; Tian, F.; Song, K.; Cao, G.; Ouyang, F. The effects of precursors and loading of carbon on the photocatalytic activity of C−BiVO4 for the degradation of high concentrations of phenol under visible light irradiation. *Catal. Today* **2015**, *258*, 585−594.
(256) Liu, Y.; Lv, Y.; Zhu, Y.; Liu, D.; Zong, R.; Zhu, Y. Fluorine mediated photocatalytic activity of BiPO4. *Applied Catalysis B: Environmental* **2014**, *147*, 851−857.
(257) Phuruangrat, A.; Maneechote, A.; Dumrongrojthanath, P.; Ekthammathat, N.; Thongtem, S.; Thongtem, T. Visible-light driven photocatalytic degradation of rhodamine B by Ag/Bi2WO6 hetero-structures. *Mater. Lett.* **2015**, *159*, 289−292.
(258) Meng, X.; Zhang, Z. Bi2MoO6 co-modified by reduced graphene oxide and palladium (Pd2+ and Pd0) with enhanced photocatalytic decomposition of phenol. *Applied Catalysis B: Environmental* **2017**, *209*, 383−393.
(259) Wang, Q.; Wang, W.; Zhong, L.; Liu, D.; Cao, X.; Cui, F. Oxygen vacancy-rich 2D/2D BiOCl-g-C3N4 ultrathin heterostructure nanosheets for enhanced visible-light-driven photocatalytic activity in environmental remediation. *Applied Catalysis B: Environmental* **2018**, *220*, 290−302.
(260) Wu, S.; Xiong, J.; Sun, J.; Hood, Z. D.; Zeng, W.; Yang, Z.; Gu, L.; Zhang, X.; Yang, S.-Z. Hydroxyl-Dependent Evolution of Oxygen Vacancies Enables the Regeneration of BiOCl Photocatalyst. *ACS Appl. Mater. Interfaces* **2017**, *9*, 16620−16626.
(261) Ge, S.; Li, D.; Cui, Z.; Zhang, Y.; Zhang, S.; Zhang, T.; Jia, G.; He, W.; Zheng, Z. Regulating the relative content of O2− and OH for PCPNa degradation on BiOCl plates with controllable exposed crystal faces and surface oxygen vacancies. *Sep. Purif. Technol.* **2019**, *228*, No. 115743.
(262) Xu, T.; Yang, M.; Chen, C.; Duan, R.; Shen, Q.; Sun, C. Photocatalytic activation of C-Br bond on facet-dependent BiOCl with oxygen vacancies. *Appl. Surf. Sci.* **2021**, *548*, No. 149243.
(263) Song, Z.; Dong, X.; Fang, J.; Xiong, C.; Wang, N.; Tang, X. Improved photocatalytic degradation of perfluorooctanoic acid on oxygen vacancies-tunable bismuth oxychloride nanosheets prepared by a facile hydrolysis. *Journal of Hazardous Materials* **2019**, *377*, 371−380.
(264) Li, H.; Tang, X.; Zhong, J.; Li, J.; Chen, G.; Chen, C. Carbon nanofibers induced tunable oxygen vacancies on BiOCl for high efficient destruction of decontaminants. *Surfaces and Interfaces* **2021**, *25*, No. 101247.
(265) Li, H.; Zhang, L. Oxygen vacancy induced selective silver deposition on the {001} facets of BiOCl single-crystalline nanosheets for enhanced Cr(vi) and sodium pentachlorophenate removal under visible light. *Nanoscale* **2014**, *6*, 7805−7810.
(266) Li, H.; Shi, J. G.; Zhao, K.; Zhang, L. Z. Sustainable Molecular Oxygen Activation with Oxygen Vacancies on the {001} Facets of BiOCl Nanosheets under Solar Light. *Nanoscale* **2014**, *6*, 14168.
(267) Dong, W.; Xie, T.; Wu, Z.; Peng, H.; Ren, H.; Meng, F.; Lin, H. Oxygen-vacancy-rich BiOCl materials with ultrahigh photocatalytic efficiency by etching bismuth glass. *RSC Adv.* **2021**, *11*, 38894−38906.
(268) Lyu, J.; Hu, Z.; Li, Z.; Ge, M. Removal of tetracycline by BiOBr microspheres with oxygen vacancies: Combination of adsorption and photocatalysis. *J. Phys. Chem. Solids* **2019**, *129*, 61−70.
(269) Song, M.; Du, M.; Liu, Q.; Xing, F.; Huang, C.; Qiu, X. Enhancement of photocatalytic activities in hierarchical BiOBr microflowers induced by oxygen vacancies. *Catal. Today* **2019**, *335*, 193−199.
(270) Wang, H.; Yong, D.; Chen, S.; Jiang, S.; Zhang, X.; Shao, W.; Zhang, Q.; Yan, W.; Pan, B.; Xie, Y. Oxygen-Vacancy-Mediated Exciton Dissociation in BiOBr for Boosting Charge-Carrier-Involved Molecular Oxygen Activation. *J. Am. Chem. Soc.* **2018**, *140*, 1760−1766.
(271) Cai, Z.; Zhong, J.; Li, J.; Jin, H. Oxygen vacancies enriched BiOBr with boosted photocatalytic behaviors. *Inorg. Chem. Commun.* **2021**, *126*, No. 108450.
(272) Wang, Q.; Liu, Z.; Liu, D.; Wang, W.; Zhao, Z.; Cui, F.; Li, G. Oxygen vacancy-rich ultrathin sulfur-doped bismuth oxybromide nanosheet as a highly efficient visible-light responsive photocatalyst for environmental remediation. *Chemical Engineering Journal* **2019**, *360*, 838−847.
(273) Zhang, D.; Liu, H.; Su, C.; Li, H.; Geng, Y. Combustion synthesis of highly efficient Bi/BiOBr visible light photocatalyst with synergetic effects of oxygen vacancies and surface plasma resonance. *Sep. Purif. Technol.* **2019**, *218*, 1−7.
(274) Wang, Q.; Liu, Z.; Liu, D.; Liu, G.; Yang, M.; Cui, F.; Wang, W. Ultrathin two-dimensional BiOBrxI1-x solid solution with rich oxygen vacancies for enhanced visible-light-driven photoactivity in environmental remediation. *Applied Catalysis B: Environmental* **2018**, *236*, 222−232.
(275) Li, X.; Xiong, J.; Gao, X.; Ma, J.; Chen, Z.; Kang, B.; Liu, J.; Li, H.; Feng, Z.; Huang, J. Novel BP/BiOBr S-scheme nano-heterojunction for enhanced visible-light photocatalytic tetracycline removal and oxygen evolution activity. *Journal of Hazardous Materials* **2020**, *387*, No. 121690.
(276) Hua, C.; Dong, X.; Wang, Y.; Zheng, N.; Ma, H.; Zhang, X. Bi-modified 3D BiOBr microsphere with oxygen vacancies for efficient visible-light photocatalytic performance. *J. Mater. Sci.* **2019**, *54*, 9397−9413.

https://doi.org/10.1021/acsomega.3c07560
ACS Omega 2024, 9, 6093−6127

(277) Shi, X.; Wang, P.; Wang, L.; Bai, Y.; Xie, H.; Zhou, Y.; Wang, J. A.; Li, Z.; Qu, L.; Shi, M.; Ye, L. Few Layered BiOBr with Expanded Interlayer Spacing and Oxygen Vacancies for Efficient Decomposition of Real Oil Field Produced Wastewater. *ACS Sustainable Chem. Eng.* **2018**, *6*, 13739−13746.
(278) Xu, H.; Hu, Y.; Huang, D.; Lin, Y.; Zhao, W.; Huang, Y.; Zhang, S.; Tong, Y. Glucose-Induced Formation of Oxygen Vacancy and Bi-Metal Comodified Bi5O7Br Nanotubes for Efficient Performance Photocatalysis. *ACS Sustainable Chem. Eng.* **2019**, *7*, 5784−5791.
(279) Huang, Y.; Li, H.; Balogun, M. S.; Liu, W.; Tong, Y.; Lu, X.; Ji, H. Oxygen Vacancy Induced Bismuth Oxyiodide with Remarkably Increased Visible-Light Absorption and Superior Photocatalytic Performance. *ACS Appl. Mater. Interfaces* **2014**, *6*, 22920.
(280) Ji, M.; Chen, R.; Di, J.; Liu, Y.; Li, K.; Chen, Z.; Xia, J.; Li, H. Oxygen vacancies modulated Bi-rich bismuth oxyiodide microspheres with tunable valence band position to boost the photocatalytic activity. *J. Colloid Interface Sci.* **2019**, *533*, 612−620.
(281) Liu, X.; Xiong, X.; Ding, S.; Jiang, Q.; Hu, J. Bi metal-modified Bi4O5I2 hierarchical microspheres with oxygen vacancies for improved photocatalytic performance and mechanism insights. *Catalysis Science & Technology* **2017**, *7*, 3580−3590.
(282) Jahurul Islam, M.; Amaranatha Reddy, D.; Han, N. S.; Choi, J.; Song, J. K.; Kim, T. K. An oxygen-vacancy rich 3D novel hierarchical MoS2/BiOI/AgI ternary nanocomposite: enhanced photocatalytic activity through photogenerated electron shuttling in a Z-scheme manner. *Phys. Chem. Chem. Phys.* **2016**, *18*, 24984−24993.
(283) Wang, D.; Shen, H.; Guo, L.; Wang, C.; Fu, F.; Liang, Y. Ag/Bi2MoO6-x with enhanced visible-light-responsive photocatalytic activities via the synergistic effect of surface oxygen vacancies and surface plasmon. *Appl. Surf. Sci.* **2018**, *436*, 536−547.
(284) Fu, F.; Shen, H.; Sun, X.; Xue, W.; Shoneye, A.; Ma, J.; Luo, L.; Wang, D.; Wang, J.; Tang, J. Synergistic effect of surface oxygen vacancies and interfacial charge transfer on Fe(III)/Bi2MoO6 for efficient photocatalysis. *Applied Catalysis B: Environmental* **2019**, *247*, 150−162.
(285) Xu, J.; Bian, Z.; Xin, X.; Chen, A.; Wang, H. Size dependence of nanosheet BiVO4 with oxygen vacancies and exposed {0 0 1} facets on the photodegradation of oxytetracycline. *Chemical Engineering Journal* **2018**, *337*, 684−696.
(286) Mansour, S.; Akkari, R.; Ben Chaabene, S.; Saïd Zina, M. Effect of surface site defects on photocatalytic properties of BiVO4/TiO2 heterojunction for enhanced methylene blue degradation. *Advances in Materials Science and Engineering* **2020**, *2020*, 1−16.
(287) Yang, M.; Xu, T.; Jin, X.; Shen, Q.; Sun, C. Oxygen vacancies enriched Bi2WO6 for enhanced decabromodiphenyl ether photodegradation via C-Br bond activation. *Appl. Surf. Sci.* **2022**, *581*, No. 152439.
(288) Lv, Y.; Yao, W.; Zong, R.; Zhu, Y. Fabrication of Wide−Range−Visible Photocatalyst Bi2WO6−x nanoplates via Surface Oxygen Vacancies. *Sci. Rep* **2016**, *6*, 19347.
(289) Huang, T.; Tian, F.; Wen, Z.; Li, G.; Liang, Y.; Chen, R. Synergistic mediation of metallic bismuth and oxygen vacancy in Bi/Bi2WO6-x to promote 1O2 production for the photodegradation of bisphenol A and its analogues in water matrix. *Journal of Hazardous Materials* **2021**, *403*, No. 123661.
(290) Ding, J.; Dai, Z.; Qin, F.; Zhao, H.; Zhao, S.; Chen, R. Z-scheme BiO1-xBr/Bi2O2CO3 photocatalyst with rich oxygen vacancy as electron mediator for highly efficient degradation of antibiotics. *Applied Catalysis B: Environmental* **2017**, *205*, 281−291.
(291) Di, J.; Xia, J.; Chen, X.; Ji, M.; Yin, S.; Zhang, Q.; Li, H. Tunable oxygen activation induced by oxygen defects in nitrogen doped carbon quantum dots for sustainable boosting photocatalysis. *Carbon* **2017**, *114*, 601−607.
(292) Wei, Z.; Liu, Y.; Wang, J.; Zong, R.; Yao, W.; Wang, J.; Zhu, Y. Controlled synthesis of a highly dispersed BiPO4 photocatalyst with surface oxygen vacancies. *Nanoscale* **2015**, *7*, 13943−13950.
(293) Zou, X.; Mei, Z.; Jiang, J.; Guo, H. MOFs-derived Bi2O3@C with rich oxygen vacancies through rapid thermal annealing technology for photodegradation of tetracycline hydrochloride. *Appl. Surf. Sci.* **2022**, *586*, No. 152813.
(294) Wang, L.-r.; Hou, T.-t.; Xin, Y.; Zhu, W.-k.; Yu, S.-y.; Xie, Z.-c.; Liang, S.-q.; Wang, L.-b. Large-scale synthesis of porous Bi2O3 with oxygen vacancies for efficient photodegradation of methylene blue. *Chinese Journal of Chemical Physics* **2020**, *33*, 500.
(295) Chen, D.; Wu, S.; Fang, J.; Lu, S.; Zhou, G.; Feng, W.; Yang, F.; Chen, Y.; Fang, Z. A nanosheet-like α-Bi2O3/g-C3N4 heterostructure modified by plasmonic metallic Bi and oxygen vacancies with high photodegradation activity of organic pollutants. *Sep. Purif. Technol.* **2018**, *193*, 232−241.
(296) Goud, B. S.; Koyyada, G.; Jung, J. H.; Reddy, G. R.; Shim, J.; Nam, N. D.; Vattikuti, S. V. P. Surface oxygen vacancy facilitated Z-scheme MoS2/Bi2O3 heterojunction for enhanced visible-light driven photocatalysis-pollutant degradation and hydrogen production. *Int. J. Hydrogen Energy* **2020**, *45*, 18961−18975.
(297) Vattikuti, S. V. P.; Police, A. K. R.; Shim, J.; Byon, C. In situ fabrication of the Bi2O3−V2O5 hybrid embedded with graphitic carbon nitride nanosheets: Oxygen vacancies mediated enhanced visible-light−driven photocatalytic degradation of organic pollutants and hydrogen evolution. *Appl. Surf. Sci.* **2018**, *447*, 740−756.
(298) Yang, C.; Gao, G.; Zhang, J.; Liu, R.; Fan, R.; Zhao, M.; Wang, Y.; Gan, S. Surface oxygen vacancy induced solar light activity enhancement of a CdWO4/Bi2O2CO3 core−shell heterostructure photocatalyst. *Phys. Chem. Chem. Phys.* **2017**, *19*, 14431−14441.
(299) Tang, Q.; Wu, J.; Chen, X.-Z.; Sanchis-Gual, R.; Veciana, A.; Franco, C.; Kim, D.; Surin, I.; Pérez-Ramírez, J.; Mattera, M.; Terzopoulou, A.; Qin, N.; Vukomanovic, M.; Nelson, B. J.; Puigmartí-Luis, J.; Pané, S. Tuning oxygen vacancies in Bi4Ti3O12 nanosheets to boost piezo-photocatalytic activity. *Nano Energy* **2023**, *108*, No. 108202.
(300) Guo, S.; Wang, H.; Yang, W.; Fida, H.; You, L.; Zhou, K. Scalable synthesis of Ca-doped α-Fe2O3 with abundant oxygen vacancies for enhanced degradation of organic pollutants through peroxymonosulfate activation. *Applied Catalysis B: Environmental* **2020**, *262*, No. 118250.
(301) Ren, L.; Zhou, W.; Sun, B.; Li, H.; Qiao, P.; Xu, Y.; Wu, J.; Lin, K.; Fu, H. Defects-engineering of magnetic γ-Fe2O3 ultrathin nanosheets/mesoporous black TiO2 hollow sphere heterojunctions for efficient charge separation and the solar-driven photocatalytic mechanism of tetracycline degradation. *Applied Catalysis B: Environmental* **2019**, *240*, 319−328.
(302) Long, X.; Feng, C.; Ding, D.; Chen, N.; Yang, S.; Chen, H.; Wang, X.; Chen, R. Oxygen vacancies-enriched CoFe2O4 for peroxymonosulfate activation: The reactivity between radical-non-radical coupling way and bisphenol A. *Journal of Hazardous Materials* **2021**, *418*, No. 126357.
(303) Wu, L.; Zhang, Q.; Hong, J.; Dong, Z.; Wang, J. Degradation of bisphenol A by persulfate activation via oxygen vacancy-rich CoFe2O4−x. *Chemosphere* **2019**, *221*, 412−422.
(304) Ding, R.-R.; Li, W.-Q.; He, C.-S.; Wang, Y.-R.; Liu, X.-C.; Zhou, G.-N.; Mu, Y. Oxygen vacancy on hollow sphere CuFe2O4 as an efficient Fenton-like catalysis for organic pollutant degradation over a wide pH range. *Applied Catalysis B: Environmental* **2021**, *291*, No. 120069.
(305) Zhou, X.; Jawad, A.; Luo, M.; Luo, C.; Zhang, T.; Wang, H.; Wang, J.; Wang, S.; Chen, Z.; Chen, Z. Regulating activation pathway of Cu/persulfate through the incorporation of unreducible metal oxides: Pivotal role of surface oxygen vacancies. *Applied Catalysis B: Environmental* **2021**, *286*, No. 119914.
(306) Qin, Q.; Liu, T.; Zhang, J.; Wei, R.; You, S.; Xu, Y. Facile synthesis of oxygen vacancies enriched α-Fe2O3 for peroxymonosulfate activation: A non-radical process for sulfamethoxazole degradation. *Journal of Hazardous Materials* **2021**, *419*, No. 126447.
(307) Yang, J.; Xie, N.; Zhang, J.; Fan, W.; Huang, Y.; Tong, Y. Defect engineering enhances the charge separation of CeO2 nanorods toward photocatalytic methyl blue oxidation. *Nanomaterials* **2020**, *10*, 2307.
(308) Li, M.; Wang, P.; Ji, Z.; Zhou, Z.; Xia, Y.; Li, Y.; Zhan, S. Efficient photocatalytic oxygen activation by oxygen-vacancy-rich

https://doi.org/10.1021/acsomega.3c07560
ACS Omega 2024, 9, 6093−6127

CeO2-based heterojunctions: Synergistic effect of photoexcited electrons transfer and oxygen chemisorption. *Applied Catalysis B: Environmental* **2021**, *289*, No. 120020.
(309) Sultana, S.; Mansingh, S.; Parida, K. Facile synthesis of CeO2 nanosheets decorated upon BiOI microplate: A surface oxygen vacancy promoted z-scheme-based 2D-2D nanocomposite photocatalyst with enhanced photocatalytic activity. *J. Phys. Chem. C* **2018**, *122*, 808−819.
(310) Islam, M. J.; Reddy, D. A.; Choi, J.; Kim, T. K. Surface oxygen vacancy assisted electron transfer and shuttling for enhanced photocatalytic activity of a Z-scheme CeO2−AgI nanocomposite. *RSC Adv.* **2016**, *6*, 19341−19350.
(311) Malefane, M. E.; Feleni, U.; Kuvarega, A. T. Cobalt (II/III) oxide and tungsten (VI) oxide p-n heterojunction photocatalyst for photodegradation of diclofenac sodium under visible light. *Journal of Environmental Chemical Engineering* **2020**, *8*, No. 103560.
(312) Jia, T.; Sun, C.; Shi, N.; Yu, D.; Long, F.; Hu, J.; Wang, J.; Dong, B.; Li, J.; Fu, F.; Hu, S.; Lee, J.H. Efficient Oxygen Vacancy Defect Engineering for Enhancing Visible-Light Photocatalytic Performance over SnO2-x Ultrafine Nanocrystals. *Nanomaterials* **2022**, *12*, 3342.
(313) Anuchai, S.; Phanichphant, S.; Tantraviwat, D.; Pluengphon, P.; Bovornratanaraks, T.; Inceesungvorn, B. Low temperature preparation of oxygen-deficient tin dioxide nanocrystals and a role of oxygen vacancy in photocatalytic activity improvement. *J. Colloid Interface Sci.* **2018**, *512*, 105−114.
(314) Ahmed, A.; Siddique, M. N.; Alam, U.; Ali, T.; Tripathi, P. Improved photocatalytic activity of Sr doped SnO2 nanoparticles: a role of oxygen vacancy. *Appl. Surf. Sci.* **2019**, *463*, 976−985.
(315) Wu, J.; Qiao, P.; Li, H.; Ren, L.; Xu, Y.; Tian, G.; Li, M.; Pan, K.; Zhou, W. Surface-oxygen vacancy defect-promoted electron-hole separation of defective tungsten trioxide ultrathin nanosheets and their enhanced solar-driven photocatalytic performance. *J. Colloid Interface Sci.* **2019**, *557*, 18−27.
(316) Wan, Z.; Mao, Q.; Chen, Q. Proton-dependent photocatalytic dehalogenation activities caused by oxygen vacancies of In2O3. *Chemical Engineering Journal* **2021**, *403*, No. 126389.
(317) Lu, N.; Shao, C.; Li, X.; Miao, F.; Wang, K.; Liu, Y. A facile fabrication of nitrogen-doped electrospun In2O3 nanofibers with improved visible-light photocatalytic activity. *Appl. Surf. Sci.* **2017**, *391*, 668−676.
(318) Liu, J.; Ke, J.; Li, D.; Sun, H.; Liang, P.; Duan, X.; Tian, W.; Tadé, M. O.; Liu, S.; Wang, S. Oxygen Vacancies in Shape Controlled Cu2O/Reduced Graphene Oxide/In2O3 Hybrid for Promoted Photocatalytic Water Oxidation and Degradation of Environmental Pollutants. *ACS Appl. Mater. Interfaces* **2017**, *9*, 11678−11688.
(319) Ma, Y.; Xu, D.; Chen, W.; Tang, Y.; Wang, X.; Li, L.; Wang, J. Oxygen-vacancy-embedded 2D/2D NiFe-LDH/MXene Schottky heterojunction for boosted photodegradation of norfloxacin. *Appl. Surf. Sci.* **2022**, *572*, No. 151432.
(320) Huang, Z.; Wu, P.; Liu, J.; Yang, S.; Chen, M.; Li, Y.; Niu, W.; Ye, Q. Defect-rich carbon based bimetallic oxides with abundant oxygen vacancies as highly active catalysts for enhanced 4-aminobenzoic acid ethyl ester (ABEE) degradation toward peroxymonosulfate activation. *Chemical Engineering Journal* **2020**, *395*, No. 124936.
(321) Kumar, S.; Ojha, A. K. Oxygen vacancy induced photoluminescence properties and enhanced photocatalytic activity of ferromagnetic ZrO2 nanostructures on methylene blue dye under ultra-violet radiation. *J. Alloys Compd.* **2015**, *644*, 654−662.
(322) Xiao, Y.; Chen, S.; Wang, Y.; Hu, Z.; Zhao, H.; Xie, W. Ethanol-quenching introduced oxygen vacancies in strontium titanate surface and the enhanced photocatalytic activity. *Nanomaterials* **2019**, *9*, 883.
(323) Zhang, H.; Li, C.; Lyu, L.; Hu, C. Surface oxygen vacancy inducing peroxymonosulfate activation through electron donation of pollutants over cobalt-zinc ferrite for water purification. *Applied Catalysis B: Environmental* **2020**, *270*, No. 118874.
(324) Wu, Y.; Chen, X.; Cao, J.; Zhu, Y.; Yuan, W.; Hu, Z.; Ao, Z.; Brudvig, G. W.; Tian, F.; Yu, J. C.; Li, C. Photocatalytically recovering hydrogen energy from wastewater treatment using MoS2 @TiO2 with sulfur/oxygen dual-defect. *Applied Catalysis B: Environmental* **2022**, *303*, No. 120878.
(325) Xu, M.; Chen, Y.; Qin, J.; Feng, Y.; Li, W.; Chen, W.; Zhu, J.; Li, H.; Bian, Z. Unveiling the Role of Defects on Oxygen Activation and Photodegradation of Organic Pollutants. *Environ. Sci. Technol.* **2018**, *52*, 13879−13886.
(326) Li, M.; Zhang, Y.; Li, X.; Wang, Y.; Dong, F.; Ye, L.; Yu, S.; Huang, H. Nature-derived approach to oxygen and chlorine dual-vacancies for efficient photocatalysis and photoelectrochemistry. *ACS Sustainable Chem. Eng.* **2018**, *6*, 2395−2406.
(327) Zhang, G.; Hu, Z.; Sun, M.; Liu, Y.; Liu, L.; Liu, H.; Huang, C.-P.; Qu, J.; Li, J. Formation of Bi2WO6 Bipyramids with Vacancy Pairs for Enhanced Solar-Driven Photoactivity. *Adv. Funct. Mater.* **2015**, *25*, 3726−3734.
(328) Guo, Y.; Xu, K.; Wu, C.; Zhao, J.; Xie, Y. Surface chemical-modification for engineering the intrinsic physical properties of inorganic two-dimensional nanomaterials. *Chem. Soc. Rev.* **2015**, *44*, 637−646.
(329) Li, G.; Blake, G. R.; Palstra, T. T. M. Vacancies in functional materials for clean energy storage and harvesting: the perfect imperfection. *Chem. Soc. Rev.* **2017**, *46*, 1693−1706.

https://doi.org/10.1021/acsomega.3c07560
ACS Omega 2024, 9, 6093−6127